ABSTRACT

Title of Dissertation: SYNTHESIS OF NOVEL ALKALINE POLYMER ELECTROLYTE FOR ALKALINE FUEL CELL APPLICAITONS.

Yanting Luo, Doctor of Philosophy, 2013

Directed By: Professor Chunsheng Wang
Department of Chemical and Biomolecular Engineering

Development of the intrinsically OH^- conductive polymeric electrolyte (alkaline polymer electrolyte, APE) is the critical component to enable the wide application of alkaline fuel cell (AFC) technology. Alkaline polymer electrolyte fuel cell (APEFC) based on AFC technology has been revived recently for applications in transportation and portable electronic devices due to its advantages of using non-noble metal catalysts, faster oxygen reduction in alkaline medium, and compact design. The research described in this dissertation aims to synthesize a novel APE, with controlled ionic conductivity and mechanical strength to achieve high fuel cell power density and long durability.

Most APEs synthesized up to now use a modification of existing engineering polymer backbones, which are very difficult to balance its mechanical properties with its ionic conductivities. In this research, we copolymerized APE precursor polymers, namely poly (methyl methacrylate-co-butyl acrylate-co vinylbenzyl chloride) (PMBV) from three functional monomers, methyl methacrylate (MMA), butyl acrylate (BA) and vinylbenzyl chloride (VBC), where VBC was the functional group that was attached with trimethylamine (TMA) and was the OH^- carrier after ion-exchanging. MMA was used for mechanical support and BA was used to alleviate the brittleness coming from MMA and VBC. We synthesized alkaline polymer electrolytes from bottom-up polymerization of these selected functional monomers using free radical solution and miniemulsion copolymerization techniques. By miniemulsion copolymerization, the properties of the obtained APEs could be precisely controlled by tuning the (1) monomer ratio, (2) glass transition temperature (T_g), (3) molecular weight (MW), and (4) crosslinking the copolymer. The increase in T_g was realized by eliminating BA from monomers, which was a low T_g component. MW was optimized through investigating binary copolymerization kinetics factors (initiator and surfactant). For crosslinking, the newly obtained poly (methyl methacrylate-co-vinylbenzyl chloride) (PMV) was crosslinked as a semi-interpenetrating network (s-IPN) to reduce water uptake and thus enhanced the mechanical strength in a humidified environment for APEFCs. After the optimization, our best quaternized PMBV (QPMBV) series APE membranes could reach a maximum power density of 180 mW/cm^2 and the crosslinked QPMV APE could last 420 hours on APEFCs, which was among the best overall performance in APE technologies.

In the future, we propose to use fluorinated polymer monomers to redesign the polymer backbone. Another direction in the design of APEs is to reselect the possible functional OH^- carrier groups to make APEs more chemically and mechanically stable in a high pH environment. And last but not least, atomic force spectroscopy (AFM) is proposed to observe the APE nanostructure, the ionic conductive path, and the local mechanical strength by applying a small voltage between the tip and stage.

SYNTHESIS OF NOVEL ALKALINE POLYMER ELECTROLYTE FOR ALKALINE FUEL CELL APPLICAITONS.

By

Yanting Luo

Dissertation submitted to the Faculty of the Graduate School of the
University of Maryland, College Park, in partial fulfillment
of the requirements for the degree of
Doctoral of Philosophy
2013

Advisory Committee:
Professor Chunsheng Wang, Committee Chair
Professor Kyu Yong Choi
Professor Srinivasa R. Raghavan
Professor Dongxia Liu
Professor Teng Li, Dean's representative

Dedicated to my parents, Yi Luo and Kun Yao,

who love me much more than I can pay them back.

Acknowledgements

I am truly grateful to my advisor, Prof. Chunsheng Wang, who advised me during my PhD study. From 2007 to 2012, I learned from him not only the knowledge in energy research but also how to be a good researcher: diligent, foresighted and thinking critically. Also, he is more than a mentor. He cares not only about research but also his students' future. Tremendous thanks to my advisor again for everything. I would also like to thank Dr. Deryn Chu for the funding support from Army Research Lab from 2008 to 2012. He also provided me with valuable suggestion on this research. In addition, I want to thank Prof. Juchen Guo once in our group. In the past five years, we worked together, discussed about difficulties and direction on this particular project. Without his encouragement and support, I could not have achieved what I have done. I am also grateful to Prof. Kyu Yong Choi, Prof. Srinivasa R. Raghavan and Prof. Peter Kofinas for the technical support in their labs.

Also, I'd like to thank my lab mates, especially Dr. Xilin Chen, Dr. Yunhua Xu, Dr. Yujie Zhu, Yihang Liu, Yang Wen, Fangyu Cao, Dr. Qing Liu, Alex Langrock, Chao Luo and Ying Liu. You guys accompanied me through both hard and splendid days during the five years in lab. I would also like to thank my friends Dr. Zhao Zhang, Dr. Chao Hu, Jiayi Cao, Qiongyu Huang, Lvyuan Chen and Qiang Huang. We came to University of Maryland together and celebrated the arrival date every year. We shared the happiness and sorrow in life. I appreciate the friendship between us and I know wherever my friends are; they are always in my heart.

Table of Contents

List of Tables

List of Figures

Chapter 1 Introduction

1. 1 Fuel Cells

A fuel cell is an electrochemical device that transforms the chemical energy in a fuel into electrical energy. The energy crisis, mostly from the world's over-consumption of oil, has spurred the development of fuel cell technology as a possible solution to more efficient energy conversion. Also, the fuel cell is able to independently scale up from the small range like for cell phone applications to the giant megawatt range needed for power plants. Compared with rechargeable batteries, it offers higher energy densities and can be recharged faster by simply refueling. Therefore, fuel cell technology is expected to be a next generation power source to revolutionize the transportation industry, improve stationary power generation, and provide reliable portable power for our personal electronic devices.

1.1.1 Fuel Cell Types & Application

Fuel cells can be categorized by the different types of electrolytes they use. There are five major types of fuel cells: 1) Phosphoric acid fuel cell (PAFC), 2) Polymer electrolyte membrane fuel cell (PEMFC), 3) Alkaline fuel cell (AFC), 4) Molten carbonate fuel cell (MCFC) and 5) Solid-oxide fuel cell (SOFC). Some of them have already been applied in our daily life due to the suitable temperature regimens, cost, fuel tolerance and performance characteristics, as shown in Figure 1.1. PAFC and SOFC/MCFC have applications in stationary back-up power plants for buildings

because of their stable performance and scalable capacity [1-4]. In transportation, there have been some prototypes and demo models of fuel cell electric vehicles (FCEVs) released since 2009 [5]. The technology was typically based on PEMFC, which was an active research topic over the last decade and is still under intensive investigation to further improve the technology and to lower the cost, which is mostly due to the platinum catalyst and Nafion® electrolyte [6]. PEMFC is also promising for small electronic devices like cell phones, MP3 players, and laptops [7].

AFC was originally used in the aerospace industry because of their improved cathode performance, potential for non-precious metal catalyst, and low electrolyte material cost, and was applied successfully in Apollo missions in the 1960's. There are also a few applications of AFCs in space shuttle orbiters, submarines and naval aboard ships [8].

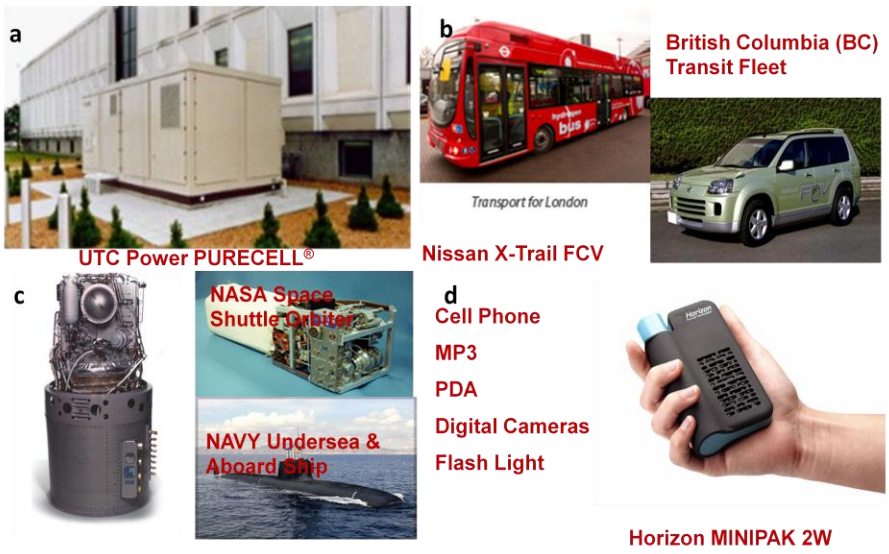

Figure 1.1 Fuel Cell applications a) PAFC/SOFC in building power back-up; b) PEMFC in transportation; c) AFC in aerospace engineering; d) PEMFC in small electronics [9].

1.1.2 Low Temperature Fuel Cells & Principles

PEMFC and AFC are low temperature fuel cells with operating temperature regimes limited to below 100 ^{o}C.

Over the last two decades, PEMFCs have been anticipated as a next generation power supply solution. In PEMFCs, the heart of the technology is the proton exchange membrane (PEM), which can conduct protons from anode to cathode, and thus complete the electrochemical reactions at both sides of the electrodes. The commercialized PEM is well known as Nafion (®DuPont). Nafion is made of hydrophobic polytetrafluoroethylene (PTFE) backbones with the hydrophilic attached sulphonated fluoroethylene pendant as the side chains [10], as shown in Figure 1.2.

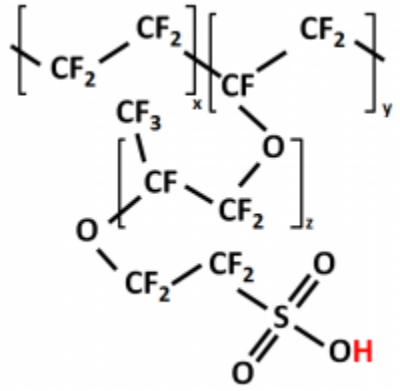

Figure 1.2 Structure of Nafion [10]

Nafion has features that make it suitable as an acid solid electrolyte. Firstly, the polymer is acidic and has great H^+ conductivity since the protons are attached to the pendant side chains. If they are well hydrated, the H^+ ions can move freely within the polymer matrix material [11]. Second, the mechanical strength is good due to the perfluorized polymer PTFE. So they could be made into very thin films and are basically chemical resistant.

However, the deep and thorough investigation of mature PEMFCs found that there are still many problems that prevent their use in broad application and commercialization. The high costs of Nafion and noble electrode catalysts [12] as well as the poor CO endurance [13] of the catalyst are all obstacles that need to be addressed. Nevertheless, the innovation to employ a solid membrane electrolyte to make the fuel cells compact and free of corrosion is still worthwhile.

Because of the downfall of PEMFCs, AFCs attracted revived attention again. In conventional AFCs, hydroxyl (OH^-) ions are available and mobile from cathode to anode through an alkaline electrolyte. The electrochemical reactions on both electrodes can be demonstrated in the following diagram Figure 1.3.

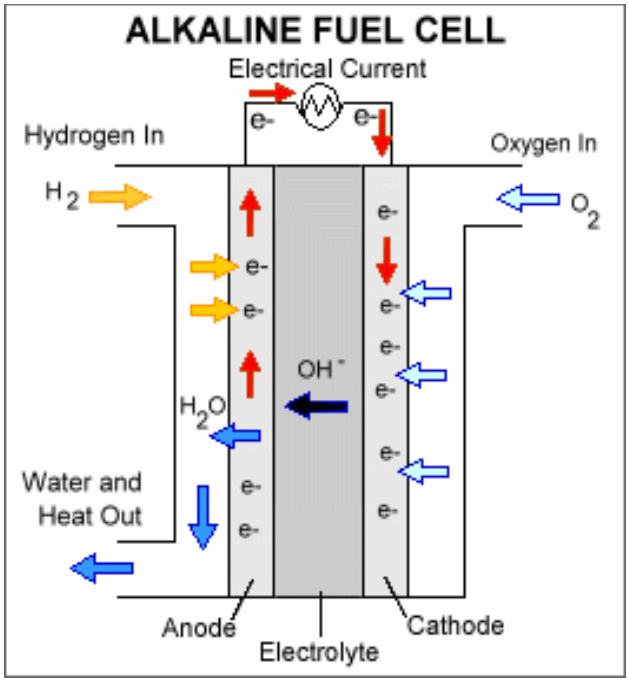

Figure 1.3 Diagram of a conventional AFC [14]

At the anode, OH^- reacts with hydrogen, releasing energy and electrons and producing water.

$$H_2 + 2OH^- \longrightarrow 2H_2O + 2e^- \quad [1.1]$$

The electrons released from the anode pass through the external circuit to the cathode, where they react with the oxidant to form new OH^- ions. The OH^- ions thus are then moved through the electrolyte solution to complete the AFC system.

$$O_2 + 2H_2O + 4e^- \longrightarrow 4OH^- \quad [1.2]$$

One important advantage of AFCs is the faster kinetics of oxidant reduction on the cathode. Hence, the activation overpotential at the cathode is generally less than that in PEMFCs. Moreover, AFCs are capable of using non-noble metal electrodes like nickel which is considerably cheaper than that of platinum used in PEMFCs. However, conventional AFCs have a serious problem with the KOH electrolyte solution. The carbon dioxide in the air will react with the KOH solution to form potassium carbonate:

$$2KOH+CO_2 \rightarrow K_2CO_3+H_2O \quad [1.3]$$

Potassium Carbonate ion will not only reduce the performance of the cell since less OH^- ions are available in the electrolyte [15], but also contaminate the electrode catalysts by deposition on the surface of the electrodes [16]. Therefore, widespread commercialization has been limited in the conventional AFC and only several applications, mostly in aerospace engineering, have been realized.

1.2 Motivation

1.2.1 Development of Alkaline Polymer Electrolyte Fuel Cells (APEFCs)

Recent breakthroughs in polymer science and technology have made it possible to replace the KOH solution electrolyte with a solid alkaline polymer electrolyte (APE). This is termed as alkaline polymer electrolyte fuel cells (APEFCs). The APEFCs possess all the particular advantages of a conventional AFC to surpass PEMFCs in terms of performance. Besides the superior performance, using intrinsic APE can prevent carbonate formation. It also can enable compact design, and eliminate the corrosion from KOH solution. All these advantages make APEFCs a very promising energy conversion technology.

1.2.2 Alkaline Polymer Electrolyte (APE)

The difference between the conventional AFC and APEFC is the employment of APE in APEFC. So, the solid membrane APE is a key component in APEFCs whose properties determine the ultimate performance of the APEFC.

For an APE, the theory to use a solid electrolyte was similar to Nafion, as depicted in Figure 1.4. The APEs are usually working in humidified condition. The strong and tough polymer backbones will be regarded as a stable hydrophobic matrix. The side chains are usually functionalized to have quaternized amine sites to ionically bond hydroxyl ions (OH^-). Structured in this way, the side chains are basically hydrophilic and can absorb the water vapor in APEFCs in humidified conditions. The hydrophilic side chains tend to cluster within the entire polymer hydrophobic matrix and are thus termed as the hydrophilic region. After absorbing of a large quantity of water, the

OH- is relatively less attracted by the quaternized amine group and able to move freely inside of the hydrophilic region while the hydrophobic polymer matrix region is kept as the mechanical support. This is the origin of the movement of OH^- in the solid electrolyte.

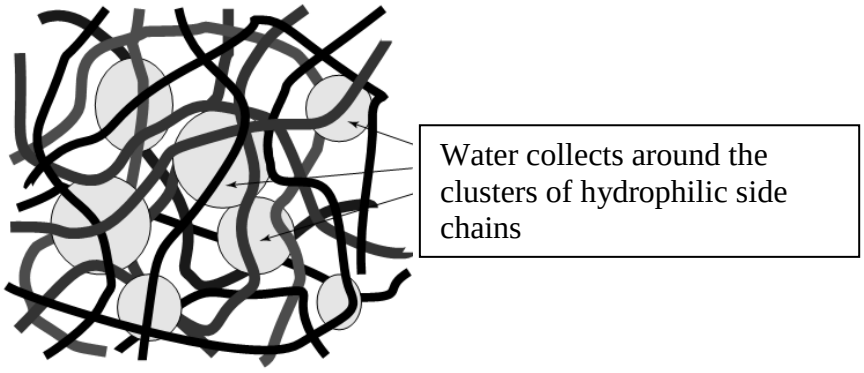

Figure 1.4 Structure of ideal APE working principles [15]

1.2.3 Criteria of APE

Several stringent requirements are needed for a standard APE to meet the demands of a compactly designed APEFC.

1) Anion conductivity higher than 10^{-2} S/cm at room temperature.

2) Good mechanical properties to satisfy fuel cell operation.

3) Low cost.

4) Metal-cation- and liquid-electrolyte-free to avoid the formation of carbonates.

1.3 Review of Previous Work Utilizing APEs in APEFCs

1.3.1 State-of-the-art of Available APEs

No ideal APEs have been developed up to this date. PEO based APE was one of the earliest APEs developed in the 1970s. Intrinsically, PEO polymer has no anion conductive functional groups, so it can only be the matrix to hold KOH solution [17]. Therefore, requirement 4) cannot be satisfied. Also, the membrane cannot work in the absence of KOH. Similar KOH included APEs were Chitosan based mixtures [18, 19], cross-linked PVA, PAA or PVA-co-PAA [20-21].

Another category of APE was the quaternized polymer with intrinsic anion conductive functional groups. Some were quaternized through a vinyl benzylchloride (VBC) functional group. Varcoe et.al grafted VBC to fluorinated polyethylene backbones through r-ray radiation [22-27]. This method is expensive and hard to process. A more common synthesis route is chloromethylation of polymers with phenyl structured backbones followed by quaternization. Many polymers have been used as the precursors to synthesize this type of APEs, including polysulfone [28-30], poly(arylene ether sulfone) (PAES) [31], polyetherketone [32], poly(ether imide)[33] polyethersulfone cardo [34], poly(phthalazinon ether sulfone ketone) [35], poly(dimethyl phenylene oxide)[36], and poly(phenylene) [37]. These precursor polymers share a merit that they are all excellent engineering polymers with great mechanical properties due to the rigid ring-structured backbones. However, this advantage can be seriously undermined by the chloromethylation-quaternization process, which changes the polymers from ionic insulator to ionomer thus from

hydrophobic to hydrophilic. As a result of the hydrophilicity, the mechanical property of the APEs in the humidified fuel cell working environment can be starkly different from that of the precursors. Due to the existence of phenyl groups in every repeating unit, these precursor polymers can be changed to extremely hydrophilic through chloromethylation-quaternization. In this case, the resulting APEs may have very high anionic conductivity, but very poor mechanical property in a humidified environment. Therefore, a shortcoming of the chloromethylation-quaternization process is that the degree of chloromethylation and quaternization is difficult to be precisely controlled [8], making it hard to balance conductivity with mechanical properties. Cost is also a concern, since the aforementioned APE precursors are high-cost polymers due to the sophisticated production process. There are also some other anion conductive polymers with different quaternized functional groups like PVP [38, 39] and polyepichlorydrin [40, 41], yet the intrinsic conductivities were rather low.

The crosslinking method also has long been used to synthesize APEs to enhance the mechanical strength. Current crosslinked APEs can be categorized as direct-crosslinking and indirect-crosslinking. A typical direct-crosslinking APE was performed by Yan's group [42], in which 1-vinyl-3-methylimidazolium iodide, styrene, acrylonitrile, and divinylbenzene (DVB) was photo-crosslinked directly into one membrane. Another example of direct-crosslinking APE came from the Friedel-Crafts reaction between chloroacetylated poly (2, 6-dimethyl-1, 4-phenylene oxide) (CPPO) and bromomethylated poly (2, 6-dimethyl-1, 4-phenylene oxide) (BPPO) [43]. The partial crosslinking of CPPO/BPPO polymer enhanced the mechanical properties of

the APE. However, there was neither a polarization curve nor durability performance shown with those direct-crosslinking APEs. For indirect-crosslinking APEs, a semi-interpenetrating network (s-IPN) was usually employed. In a typical s-IPN structure, one polymer is locked into another cross-linked polymer matrix. The cross-linked polymer matrix gives mechanical support to the whole structure, while the other polymer provides functionality. Two s-IPN APE systems have been widely investigated to this date. One was the chitosan based APEs which were crosslinked with different crosslinkers including glutaraldehyde (GA) [44, 45], glyoxal [46], and diethylene glycol diglycidyl ether [46, 47]. These s-IPNs prominently decreased water uptake of the APEs from the original unacceptable 500+ % [46]. The other s-IPN system is the poly (vinyl alcohol) (PVA) based APEs. In these AAEMs, crosslinked PVA by GA or dibromoethane formed the locking matrix, and the OH- conducting polymers included poly (vinyl pyrrolidone) [48], poly (N-ethyl-4-vinyl pyridinium bromide) [49, 50], poly (acrylamide-co-diallyldimethylammonium chloride) [51], and poly (dimethyl dimethylene piperidinium chloride) [52]. However, all the resulting APE membranes had relatively low conductivities around 10^{-3} S cm^{-1}. Recently, Zhou *et al* reported an s-IPN APE based on chloromethylated poly (arylene ether sulfone) (PAES) with thtraphenylolethane glycidyl ether as the crosslinker [53]. This obtained APE had low water uptake (20 to 60 wt. %), low swelling ratio (0 to 30 vol. %), and relatively high conductivity of 0.01 S cm^{-1}. Another s-IPN type APE was the work from Fauvarque *et al* [54]. Poly (epichlorhydrin) was employed as the locking matrix with allyl glycidyl ether as the crosslinker. Two cyclic diamines 1,4-diazabicyclo-[2, 2, 2]-octane and 1-azabicyclo-[2, 2, 2]-octane were incorporated into the matrix as the

conducting portion. The enhanced APEs could reach a tensile modulus around 2 GPa and the conductivity was 1.3×10^{-2} S cm^{-1} at room temperature.

1.3.2 State-of-the-art for the Performances of APEFCs

The performance of APEFCs using different APEs has also been extensively investigated. Agel *et al* investigated the feasibility of AFC application using their H55 APE early in 2001. The performance showed a peak power of 20mW/cm^2 at the current density of 50mA/cm^2 [40]. Later, J. R. Varcoe and R.C.T. Slade applied the APE of ETFE (Ethylene tetrafluoroethylene) with quaternary-ammonium grafted function to operate in AFC. Their elaborate work of AFC conditions and operation obtained a promising performance of 130mW/cm^2 [23]. Another category of potential APEs, with polysulfone (PS) included in their polymer backbones has also shown decent performance. L. Zhuang *et al* studied the quaternized ammonia polysulfone (QAPS) APE and achieved a peak power of 50 mW/cm^2 at a current density of 85mA/cm^2. They did not use the noble metal as the catalysts [30]. More recently, Y. Yan *et al* used a different P functional group showed more promising performance of APEFCs. Their best performance can reach 800 mA/cm^2 at the end of the voltage drop with a peak power delivery of 250 mW/cm^2 during the discharging process, though this performance was obtained with 3 atm back pressure [55].

However, the performance of those AFCs is still not satisfactory. There are two major challenges that impede the ultimate performance, which are the two stringent requirements for APE stated before, conductivity and mechanical property. For comparison, Nafion® can reach a conductivity of 0.1 S/cm at room temperature [13].

For all the possible APEs, the best conductivity that can be obtained is still one order of magnitude lower, which exhibits higher ohmic loss as shown in the performance polarization curve. Another issue is the mechanical support. The mechanism of OH^- transport in the APE is supposed to be similar to H^+ in Nafion®, yet there is still a difference between the two. The OH^- ion is much larger than H^+, which makes OH^- almost impossible to transfer smoothly through the micro-channels tangled out by polymer backbones. Therefore, the mechanism of OH^- transport is thought to be hopping from one cation site to another. Also, there is still a big concern of cation site stability from the nucleophilic attack by OH^-, and the over hydrated hydrophilic region is prone to make APE swell, deform and ultimately lose mechanical support.

1.4 Scope of This Research & Objectives

The aim of this project is to synthesize novel APEs, which balance high ionic conductivity and mechanical strength to sustain in AFCs. Specifically, free radical copolymerization is employed for the first time as a bottom-up approach to synthesize APE precursor polymers from intentionally selected functional monomers. Two free radical polymerization methods, solution polymerization and miniemulsion polymerization have been employed in this research. A crosslinking method is also used to further enhance the mechanical strength of the obtained APEs. The obtained precursor copolymers were fabricated by casting method into APEs. The mechanical properties and conductivities of the obtained APEs can be tuned from monomer ratio adjustment during the polymerization synthesis. After membrane fabrication, the obtained APEs will be processed into membrane electrode assembly (MEA) with a standard industry method to test the performance in APEFCs.

The broader impact of this research is to push forward the development of AFCs and enlighten its potential as a next generation power source. The uniqueness of this research is that the proposed APE is an attractive alternative to other APEs. It is also the first time using of a bottom-up copolymerization method to synthesis APEs in order to control both conductivity and mechanical strength while almost all the existing APEs can only modify the commercial engineering polymer backbones without further precise control of desired properties.

1. 5 Fuel Cell Performance testing and APE characterization

The research will focus on four processes related to APE:

1) Synthesis of APE precursor polymers;

2) Casting of the obtained polymers to APEs;

3) Fabrication of APEs into membrane electrode assembly (MEA);

4) APEs performance in APEFCs.

The ionic conductivity of APEs synthesized by different copolymerization approaches is measured using electrochemical impedance spectroscopy (EIS). The mechanical properties are obtained using tensile tests. The APE performances in AFC are tested in standard AFC operation conditions using an Arbin fuel cell test station. The detailed fuel cell test and APE characterization is described below.

1.5.1 Membrane Electrode Assembly (MEA)

Membrane Electrode assembly (MEA) is an assembled stack consisting of five layers; 1) gas diffusion layer on anode, 2) anode catalyst layer 3) membrane electrolyte, 4) cathode catalyst layer, and 5) gas diffusion layer on cathode. Therefore, the membrane electrolyte is sandwiched by electrodes through a hot-press. The most commonly used materials for 1) and 5) are carbon cloth or Toray carbon fiber paper. Also, the material for both anode and cathode catalysts in this research is still platinum.

MEA is fabricated in a method that is used as the standard in the PEMFCs industry [15]. The carbon paper (Toray, TGP-H-60) is first brushed with PTFE/carbon black (35/65 wt. %) slurry ($0.2 \pm 0.02 mg/cm^2$). The catalyst of Pt/C (60/40 wt. %) is dispersed in a dilute OH^- exchanged APE solution in ethanol/ water mixture (50/50 vol.) by sonication. This catalyst dispersion is sprayed onto the processed carbon paper with a Pt loading of 0.4 ± 0.05 mg/cm^2. The spraying process is demonstrated in Figure 1.5.

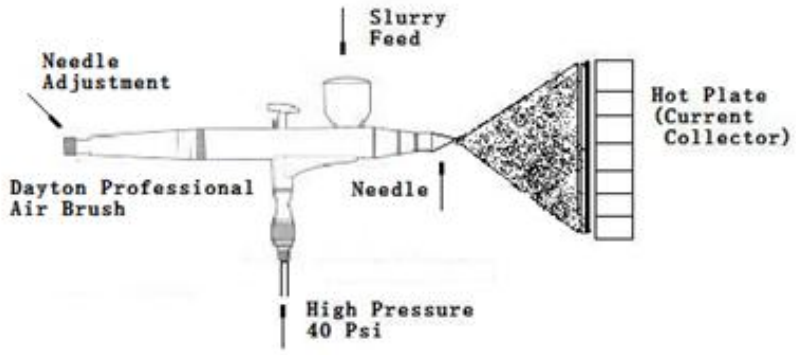

Figure 1.5 Spraying process using Dayton® air brush [56]

Then the APE membrane is sandwiched by two $5cm^2$ catalyst loaded carbon papers using a hot-press (Carver® 973214A) under 2atm of pressure at 60 ℃ for 10 min to obtain the MEA. Figure 1.6 shows a fabricated MEA using our APE.

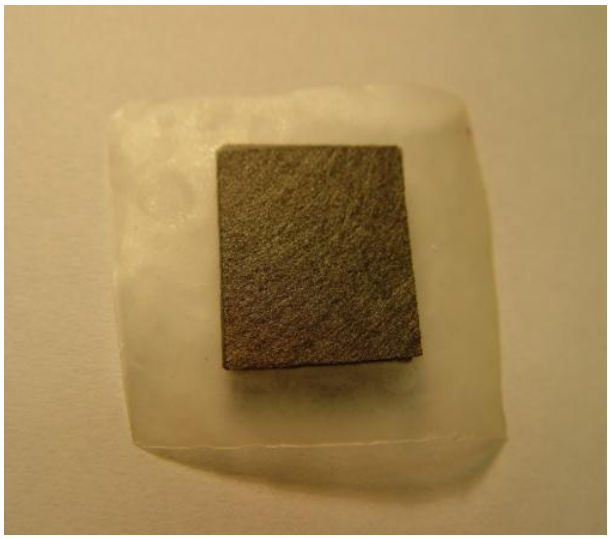

Figure 1.6 MEA fabrication

1.5.2 APEFC Architecture

A single APEFC is assembled as depicted in Figure 1.7. The MEA is sandwiched between two block pieces of graphite with silicone gaskets to ensure air tightness. The fuel (hydrogen) and oxidant (oxygen) flows through the serpentine channels in the graphite block in contact with the carbon paper in the MEA. Since the carbon paper is porous, gases go further to react at electrodes at both sides of the catalyst layers in MEA, where the chemical reactions give out the electrons.

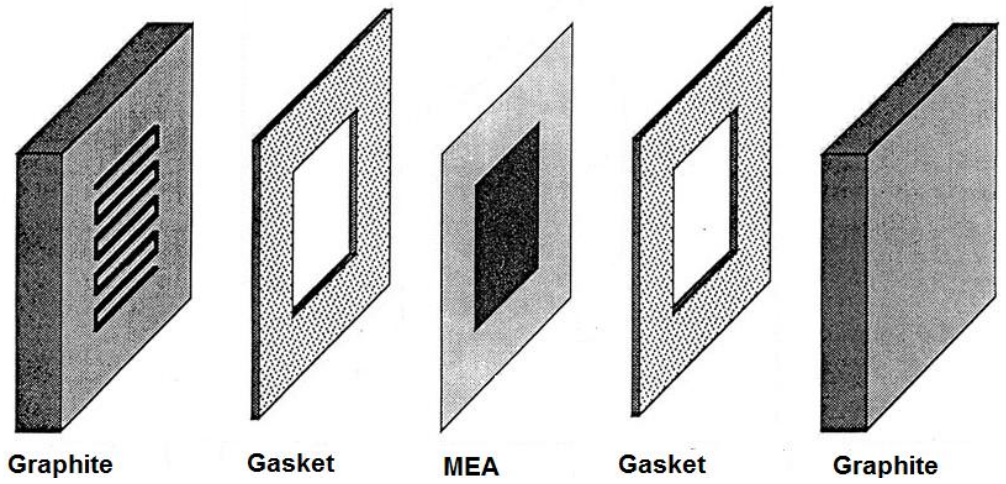

Figure 1.7 Single APEFC assembling structure [57]

1.5.3 Gas Line Humidity Control

The relative humidity (RH) in the APEFC is controlled by dew point temperature (DPT) and gas temperature (GT) through the dew point humidifier (DPH) with a bubbling method through the gas supply lines. The following DPH structure (Figure 1.8) illustrates the working principles of this method.

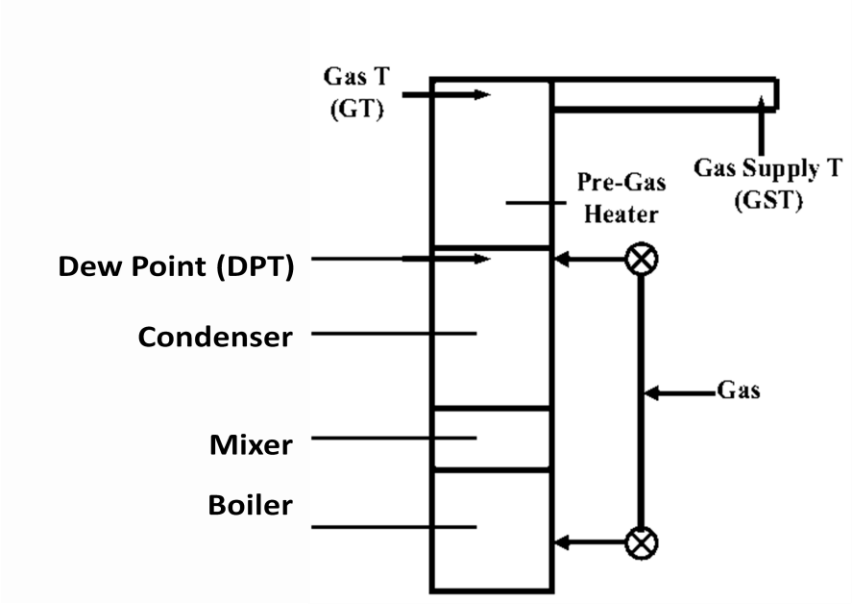

Figure 1.8 Structure of Humidifier [58]

After boiling, mixing, and condensing the humidifier has the saturated water vapor at the outlet at DPT. Hence, the volume mass density of the water vapor can be calculated by the following formula, if an ideal gas is assumed. The volume mass density is also called specific or absolute humidity (AH).

$$PV = RnT$$

$$AH = \frac{M_{water} \cdot n}{V} = \frac{M_{water} \cdot P}{RT}$$

$$\begin{aligned} AH &= \frac{P(Pa)}{T(K) \times R(Jmol^{-1}K^{-1}) / M_{water}(gmol^{-1})} \\ &= \frac{P_{sat}(Jm^{-3})}{(273.15+t)(K) \times 8.31(Jmol^{-1}K^{-1}) / 18(gmol^{-1})} \\ &= \frac{P_{sat}}{(273.15+t) \times 462}(g/L) \end{aligned} \qquad [1.4]$$

After the humidifier, the saturated water vapor will mix with the gas and is heated to a higher temperature (GT). The AH of saturated water vapor at GT can be calculated with the same equation 1.4. Hence, the RH is computed by dividing the AH of saturated water vapor in DPT by the AH of saturated water vapor in GT. That is

$$RH = \frac{AH_{DPT}}{AH_{GT}} = \frac{P_{sat,DPT}}{P_{sat,GT}} \cdot \frac{(273.15+DPT)}{(273.15+GT)} \times 100\% \qquad [1.5]$$

An engineering drawing of RH vs. GT is shown in Figure 1.9, where ΔT is the difference between GT and DPT.

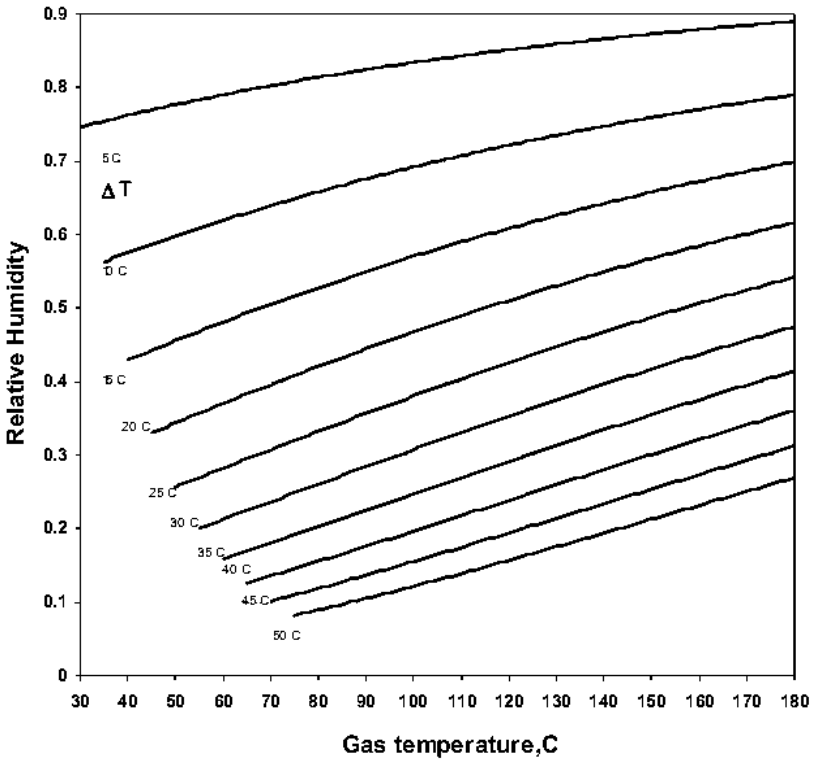

Figure 1.9 Engineering RH control graph [58]

1.5.4 Performance Test on APEFCs

There are two types of important electrochemical performance tests using the fuel cell test station. They are 1) the slow-scan potentiostatic technique for polarization performance and 2) the galvanostatic technique for durability performance. The most important characterization of the APEFC performance is the polarization curve. This curve is usually obtained by a potentiostatic technique, in which the voltage is controlled by the operator to measure the response of the output current. As shown in the fuel cell assembly picture in Figure 1.10, both current cables and voltage cables are attached to the outside copper current collectors. The hydrogen and oxygen lines are also connected onto the copper current collectors, where they can be channeled into the graphite. It also provides a place to put a thermal couple (TC) to control the

operation temperature of the fuel cell. The inside detail of this current collector has been discussed in section 1.5.2 APEFCs architecture.

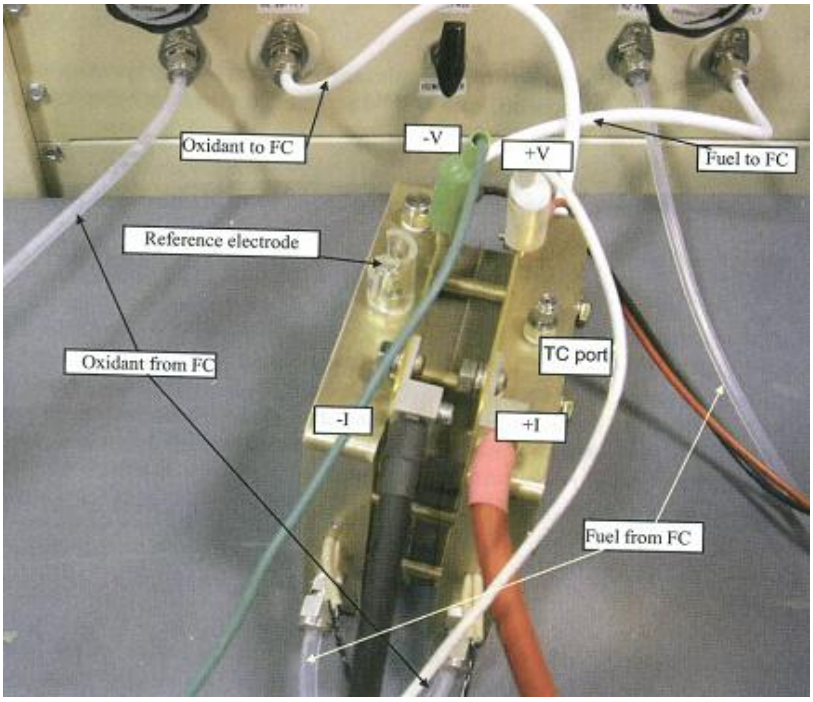

Figure 1.10 Fuel cell assembly with current/voltage cables attached [58]

In the performance test, the current density will be increased gradually. The output voltage will drop accordingly and be measured. A typical polarization curve is shown in Figure 1.11. Much information can be obtained from this polarization curve. Thermal theoretical potential can be calculated from the Nernst equation.

$$E = Er - \frac{RT}{2F} \ln \frac{P_{H_2O}}{P_{H_2} P_{O_2}^{1/2}} \qquad [1.6]$$

Where Er is the reversible standard potential for this reaction; R is the gas constant; T is the absolute temperature; F is the Faraday constant; and P_i is the portion pressure.

If it is in standard temperature and pressure (STP), the thermal theoretical potential can be calculated as:

$$E = 1.229 - \frac{8.314 \cdot 298.15}{2 \cdot 96485} \ln \frac{1}{1 \cdot 1^{1/2}} = 1.229V \qquad [1.7]$$

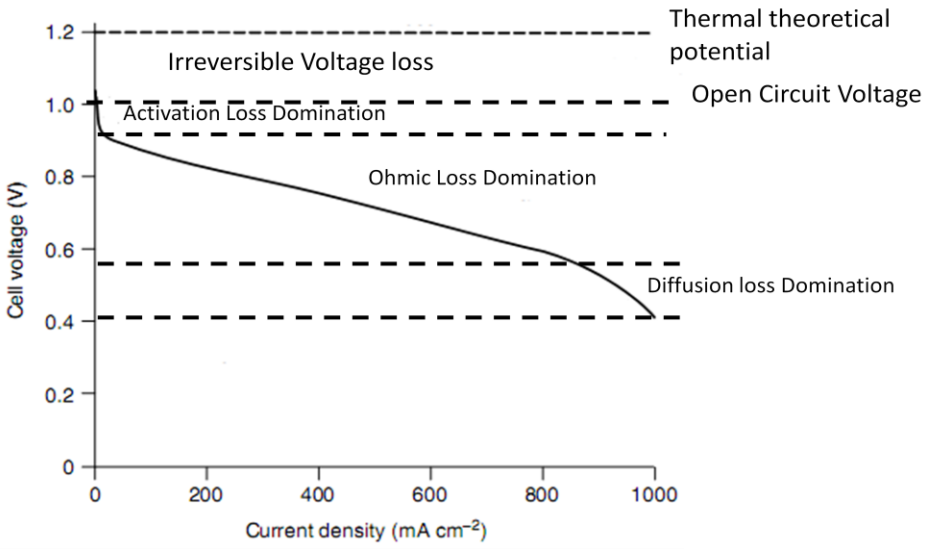

Figure 1.11 polarization curve for fuel cell performance test [15]

However, the open circuit voltage is always lower than the theoretical number because of several irreversible potential losses. As the current increases, the cell output voltage will drop due to the activation loss, ohmic loss, and diffusion loss. If the activation loss is more than 100 mV, the slope of the ohmic loss is steep and the diffusion loss comes very soon, and the voltage will drop very quickly along the scanned current density. This is regarded as a severe polarization for a fuel cell. A criteria for a commercialized PEMFC using Nafion as the electrolyte can reach more than 1A/cm^2 of the scanned current density with limited activation loss and ohmic loss. Another performance characterization is the power density.

$$P = VI \; mW / cm^2 \qquad [1.8]$$

Where V is the instant voltage value and I is the corresponding instant current. From the polarization curve with the correlation between the voltage and the current change profile, there is a power peak within the range of scanned current densities, showing the maximum power that the fuel cell can reach.

In this study, polarization performance will be carried out on the Arbin® fuel cell station at different temperatures with 80 % RH. Hydrogen and oxygen are used as the fuel and oxidant respectively at 100 ± 2 sccm (standard cm^3 min^{-1}). The fuel cell is discharged from the open circuit voltage (OCV=1.04 ± 0.02 V) using a current rate of 3 mA/s with 1 atm back pressure.

The durability performance is conducted using a galvanostatic technique, in which the current is controlled by the operator to measure the response of the output voltage. To date, little investigation on membrane durability has been conducted on APEFCs. However, this test is of great importance for the long term prospect of APEFCs. In this study, the current density chosen in tests is according to the peak power density's corresponding current density.

1.6 Characterization Techniques of APE Properties

1.6.1 Electrochemical Impedance Spectroscopy (EIS)

Electrochemical Impedance Spectroscopy (EIS) is another important electrochemical measurement to get information regarding the ohmic resistance as well as the conductivity of the APE. The diagram of fuel cell lines connection within an EIS test is shown in Figure 1.12.

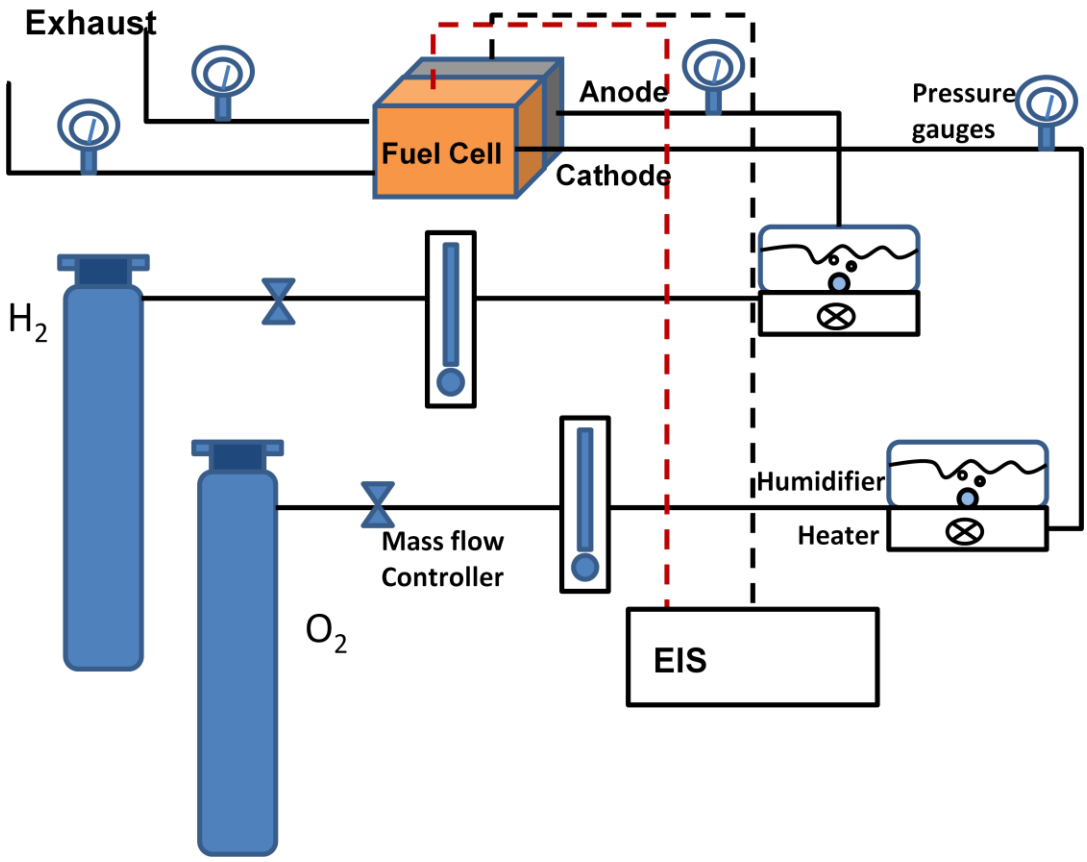

Figure 1.12 Attached EIS measurement to the fuel cell test station

For the APE properties investigation, EIS is employed to measure the ionic conductivity of the APE membrane. In the EIS technique, a sinusoidal wave perturbation of voltage is imposed on a system and the response of the current signal is received. Usually both the original perturbation of voltage and the response of current versus time can be plotted correspondingly. In Figure 1.13, it is found that the response of the current is slower than the voltage input, as the sine wave changes the phase between voltage curve and current curve. Furthermore, the amplitude is also changed for the current response. There are two parameters that can describe this phenomenon. One is the magnitude, defined as amplitude of voltage divided by the

amplitude of current (V/I). Another is the phase shift, as shown in Figure 12, and can be measured with the phase angle ϕ.

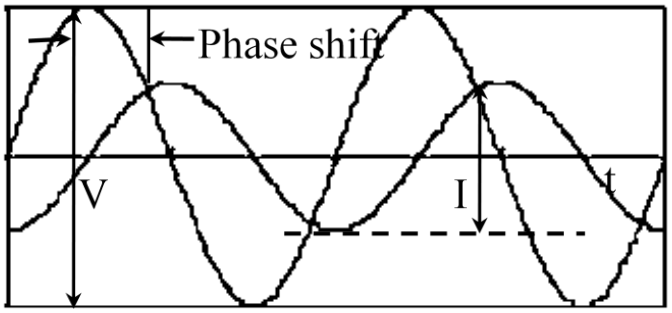

Figure 1.13 Perturbation of the voltage and the current response [59]

Here we define the impedance as Z in the following formula and write it with the two parameters,

$$Z = \frac{V(t)}{I(t)}$$

$$Z = \frac{V\cos(wt)}{I\cos(wt-\phi)} = \frac{Ve^{jwt}}{Ie^{(jwt-j\phi)}} = \frac{V}{I}(\cos\phi + j\sin\phi) \qquad [1.9]$$

Where *w* is the radial frequency in a unit of radians per second. If we sketch one impedance point in the complex plane, we can get the following information with the exact moment t as shown in Figure 1.14. Line up all the moments of the impedance and we get the EIS spectroscopy in Figure 1.15.

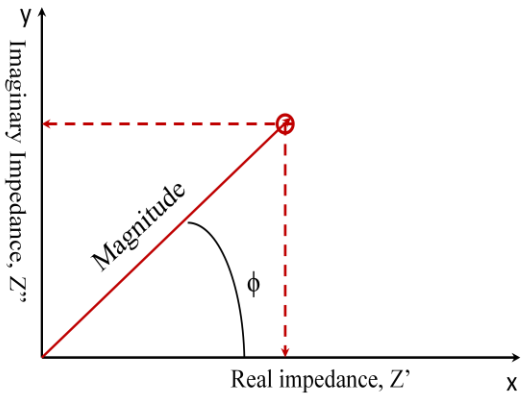

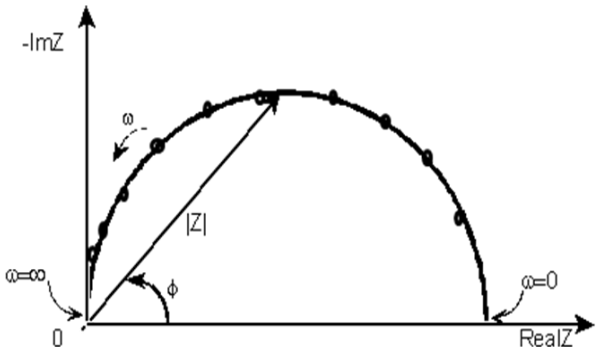

Figure 1.14 Impedance of moment t [59] Figure 1.15 Typical EIS spectroscopy [59]

The impedence of a pure APE membrane was measured four probe technique. Theoretically two semi-circles in series can be read from the EIS with the first real part impedance indicating the resistance of the membrane and the second one indicating the resistance of the interface between membrane and the probes.

In our lab, anion conductivities are measured using EIS (Gamry Instruments 3000, Potentiostat/ Galvanostat/ ZRA) with the fixture of conductivity cell (BekkTech, BT-112) (Figure 1.16).

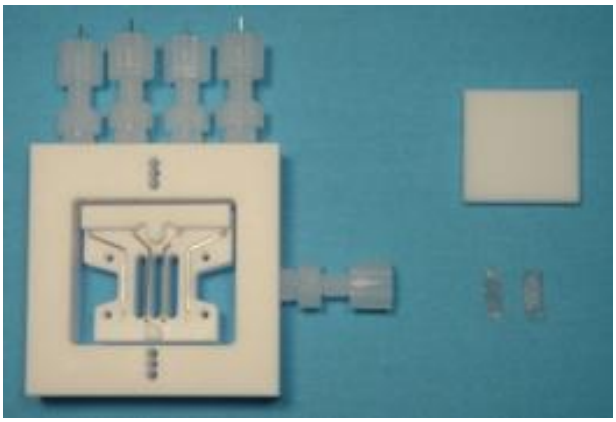

Figure 1.16 BekkTech® conductivity cell [60]

The temperature and humidity are also controlled using the Arbin fuel cell test station.

Conductivity is calculated by

$$\sigma = \frac{l}{Rab} \qquad [1.10]$$

Where l is the membrane thickness, a is the membrane width, b is the membrane length and R is the resistance obtained from EIS.

1.6.2 Mechanical Properties

1.6.2.1 Motivation

This research is focused on the polymeric derived materials used as the APE with balanced properties between electrochemical conductivity performance and mechanical strength on fuel cells. While the EIS was used to characterize the electrochemical conductivity properties, mechanical properties including Young's modulus, tensile strength also need to be characterized. The motivation to test the mechanical properties is to ensure that the obtained APE can operator on fuel cell without any assembling problems. If the APE is not tough, it will properly break down under the pressure enforced from gasket and graphite press. If that case takes place, the fuel cell will be short circuit internally and cannot use anymore. Also, the fuel cell is a power source that usually runs continuously under a humidified environment. In a humidified environment, the mechanical properties of APE will be partially lost due to the water-uptake within the APE. Therefore, water-uptake is also one of the criteria to characterize the mechanical properties.

1.6.2.2 Tensile Test

The mechanical properties are characterized by tensile tests. A tensile test is performed on the APEs to determine Young's modulus, tensile strength as well as the elongation at break. In the tensile test, the sample specimen is stretched by an increasing force. In this stretching process, the stress sustained by the specimen is measured and the elongation denoted as strain is recorded accordingly. The information of tensile test is provided by the stress-strain curve. Young's modulus is the initial slope of the stress-strain curve and demonstrates the stiffness of the material, while tensile strength is the ultimate stress before breaking. Elongation at break is the ultimate increase in the length of a test specimen produced by a tensile load. A long elongation indicates a ductile material, while a short elongation indicates a brittle material. A high tensile strength illustrates a rigid material, while a low tensile strength indicates soft. If a material has a high Young's modulus, high tensile strength and high elongation at break, we call this a tough material, and it will provide great mechanical support. APEs will be tested on DMA (dynamic mechanical analyzer, TA Instruments Q800) for the tensile tests at room temperature. The stretch rate will be 1N/min.

1.7 Overview

To address the research objectives outlined above, the rest of the dissertation is organized as follows.

In Chapter 2, successful synthesis of proof-of-concept AFC polyelectrolytes APE based on a ternary copolymer, namely poly (methyl methacrylate-co-butyl acrylate-co-vinylbenzyl chloride) (PMBV) is achieved by free radical solution polymerization. The purpose of this preliminary study is to demonstrate the feasibility of obtaining desired APE through specific monomer selections and a designed synthesis procedure. It is the foundation of both consequent optimization of polymerization synthesis and detailed investigation on the correlation between polymerization factors and membrane properties.

Chapter 3 optimizes the polymerization method from solution to miniemulsion copolymerization. In this chapter, the advantages of employing miniemulsion polymerization in APE material preparation have been discussed in detail. Moreover, a regular procedure from pristine polymer precursor preparation, membrane fabrication to MEA process and APEFC performance test has been reported. Therefore, this work facilitates the later research in its standardized way of membrane preparation and testing.

In Chapter 4, a series of QPMBV-APEs is synthesized with designed composition using miniemulsion copolymerization. This chapter qualitatively discusses the composition and molecular weight effects from QPMBV copolymers onto the membrane properties. Moreover, our membranes demonstrated one of the best overall performance including high deliverable power density and durability.

In Chapter 5, a more detailed quantitative control of the miniemulsion polymerization process is disclosed. A number of polymerization kinetics factors

including polymer composition drift, initiator effect and surfactant effect on molecular weight are investigated to precisely tailor the electrolyte properties including conductivity, mechanical strength and water mass-uptake. In this chapter, the monomers are reselected and butyl acrylate is removed to increase the glass transition temperature as well as facilitate the kinetics investigation in polymerization. This investigation demonstrated a quantitatively controllable polymerization procedure of poly (methyl methacrylate-co-vinylbenzyl chloride) (PMV) membrane with tunable and balanced properties.

Chapter 6 is focused on fuel cell durability enhancement by the crosslinking method. Crosslinking is used to reduce the water uptake and swelling ratio by locking the functionalized QPMV into a poly (divinylbenzene) (PDVB) polymer network. Crosslinking significantly enhanced the durability performance with only a minor sacrifice of power density.

Chapter 2

Free Radical Solution Polymerization of Poly (methyl methacrylate-co-butyl acrylate-co-vinylbenzyl chloride) Membrane Electrolyte for Alkaline Fuel Cells

The results presented in this chapter have been published in *J. Power Sources*:
Y. Luo, J. Guo, C. Wang, D. Chu, "Quaternized Poly(methyl methacrylate-co-butyl acrylate-co-vinylbenzyl chloride) Membrane as Solid Electrolyte for Alkaline Fuel Cell", *J. Power Sources*, 195 (**2010**) 3765.

2.1 Introduction

The current methods for preparation of the aforementioned APEs mainly focus on modifications of pre-existing polymers. A disadvantage of this method is that it is difficult to achieve a balance between OH^- conductivity and mechanical properties. For instance, every repeating unit on a polysulfone (PS) polymer chain can be chloromethylized so that the entire PS polymer chain is consequently quaternized. The degree of quaternization can only be coarsely controlled by reaction time with the tertiary amines. If the degree of quaternization is high, despite high OH^- conductivity, the obtained polymer may suffer poor mechanical properties in an aqueous environment due to the strong hydrophilicity from the high degree of

quaternization. Instead of modification of pre-existing polymers, a new route of preparation of polyelectrolyte OH^- conductive membranes via copolymerization of selected functional monomers was reported in this study. Using this procedure, OH^- conductivity and mechanical properties can be balanced by varying the ratio of supporting chain monomers to OH^- conducting monomers.

2.1.1 Free Radical Polymerization

Free radical polymerization is one of the most common and useful reaction for making polymers. It is a method of polymerization by which a polymer forms by the successive addition of vinyl monomers, that is, from small molecules containing carbon-carbon double bonds. Following its generation by initiator, the initiating free radical adds (non-radical) monomer units, thereby growing the polymer chain. The following reaction in 2.1 is the process for radical generation. The whole process starts off with a molecule called an initiator. In this Chapter, we use 2,2'-azo-bis-isobutyrylnitrile (AIBN) as the initiator.

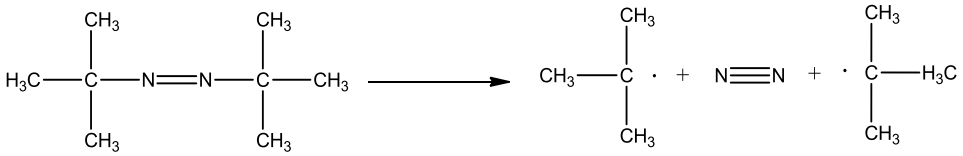

AIBN [2.1]

The initiator AIBN falls apart to three components. When this split happens, we are left with two fragments, each of which has one unpaired electron. These are the free radicals that can add monomer units.

Free radical polymerization is an important synthesis route for obtaining a wide variety of different polymers and material composites. It is one of the most versatile forms of polymerization available and allows facile reactions of polymeric free radical chain ends and other monomer chemicals. In 2001, 40 billion of the 110 billion pounds of polymers produced in the United States were produced by free radical polymerization [61].

2.1.2 Free Radical Solution Polymerization of PMBV

In this study, polymer APEs based on a copolymer of methyl methacrylate (MMA), butyl acrylate (BA) and vinylbenzyl chloride (VBC), namely poly(methyl methacrylate-*co*-butyl acrylate-*co*-vinylbenzyl chloride) (PMBV), was synthesized through free radical solution copolymerization. The benefit of solution polymerization is that it reduces the viscosity of the MMA included polymerization system, which usually causes the problem of self-acceleration [61]. Polymerized VBC can be quaternized to provide the OH^- conductivity because of its chloromethyl group. The quaternized VBC portion is expected to be hydrophilic [62] and lack mechanical strength in the aqueous environment. Therefore, polymer chain portion with good mechanical strength must be incorporated to balance the OH^- conductivity and mechanical properties. MMA was chosen to provide this function. Because both VBC and MMA polymers are in glassy state in ambient temperature, BA polymer, which is a rubbery polymer [63] in ambient temperature, was also used in the copolymer to alleviate the brittleness so that the PMBV copolymer can retain the toughness and flexibility even after quaternization, and in the aqueous environment. Three different

monomer ratios were used for the copolymerization to demonstrate the effect of monomer ratio on the OH^- conductivity and mechanical properties.

2. 2 Experimental

2.2.1 Copolymerization

***Materials*:** MMA (99%), BA (99%) and VBC (97%) were all purchased from Sigma-Aldrich. Monomers were passed through an inhibitor remover (Sigma-Aldrich) column before copolymerization. Initiator, 2,2'-Azobis(2-methylpropionitrile) (AIBN) was purchased from Sigma-Aldrich and used as received. Toluene was purchased from VWR and used as received as the solvent for the copolymerization.

***Synthesis*:** Three different molar ratios of monomers (MMA: BA: VBC = 50:40:10, 53:40:7 and 55:40:5) were used in copolymerization. A representative copolymerization process was as follows (for MMA: BA: VBC = 50:40:10): Monomers (MMA: 0.15 mole, BA: 0.12 mole, VBC: 0.03 mole) were blended in 50 mL of toluene and put into a three-neck round bottom flask. The reactants mixture was heated using an oil bath, and vigorous stirring was provided by a magnetic stir bar. 5×10^{-4} mole AIBN was added when the temperature reached 50 ℃ to start the copolymerization. The reactants were kept in a nitrogen environment throughout the reaction, and a condenser was used to prevent evaporation. The reaction lasted 36 hours and was stopped by quenching the flask in an ice water bath. After evaporation of solvent and unreacted monomers in the hood for 24 hours, the copolymer was dried in a vacuum oven at 50 ℃ for another 24 hours. Figure 2.1 demonstrated the synthesis methodology of PMBV.

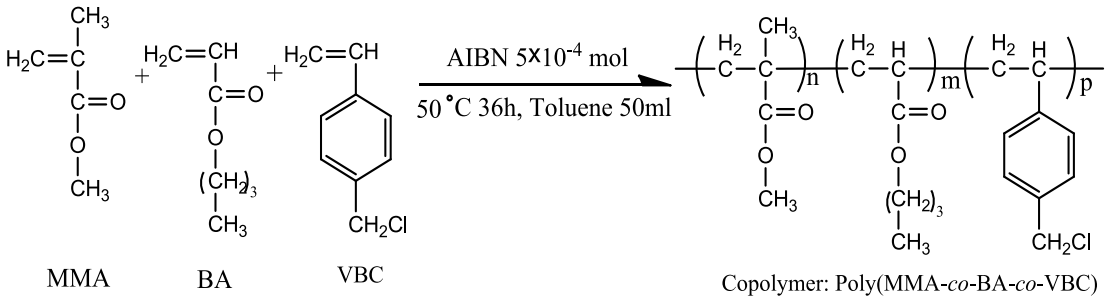

Figure 2.1 Synthesis of poly (MMA-*co*-BA-*co*-VBC) (PMBV)

***Characterization*:** Gel permeation chromatography (GPC), differential scanning calorimetry (DSC) and proton nuclear magnetic resonance (^{1}H-NMR) was performed to characterize the copolymers. GPC (Waters 2410 Refractive Index Detector, Polymer Labs mixed-bed columns) using tetrahydrofuran (THF) as the carrier was used to determine the molecular weight (MW) and molecular weight distribution (polydispersity index, PDI) of PMBV. ^{1}H-NMR (Bruker DRX-400 high resolution) was used to determine the composition of the obtained PMBV using D-chloroform as the solvent. The NMR results revealed the actual VBC composition in the copolymer rather than the monomer in the reactants mixture. DSC (TA Instruments Q100) was used to determine the glass transition temperature (T_g) of PMBV. The heat-cool-heat procedure was applied between 120 ℃ and -20 ℃ at a rate of 10 ℃/min.

2.2.2 APE preparation

The obtained PMBV was dissolved in dimethylformamide (DMF) and quaternized through reaction with trimethylamine (Me_3N, Sigma-Aldrich) for 8 hours at room temperature (Figure 2.2). The quaternized PMBV (QPMBV) solution was then casted into a membrane on a leveled smooth surface and dried in the fume hood for 24 hours

and then in the vacuum oven at 60 ℃ for an additional 24 hours. Figure 2.3 showed a picture of as-prepared QPMBV membrane. The obtained membrane was soaked in 6M KOH solution overnight to exchange Cl^- to OH^-. The OH^- exchanged QPMBV membrane was washed with de-ionized water until a pH of 7 was reached.

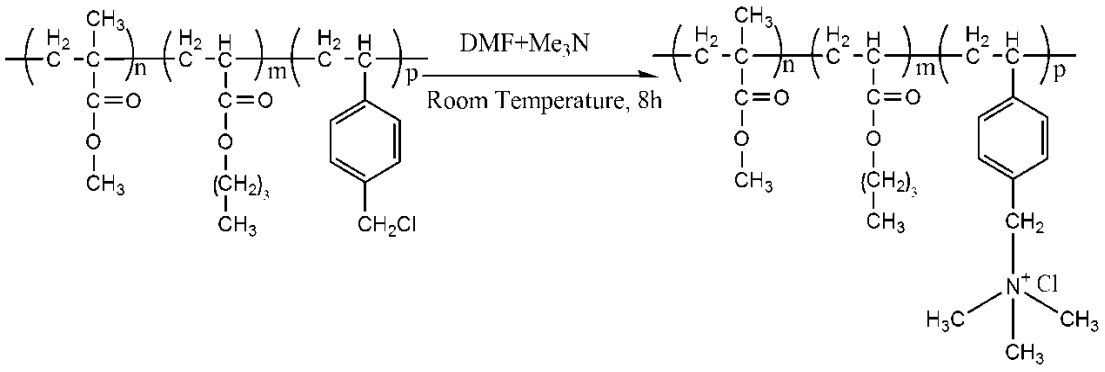

Figure 2.2 Quaternization by trimethylamine (TMA)

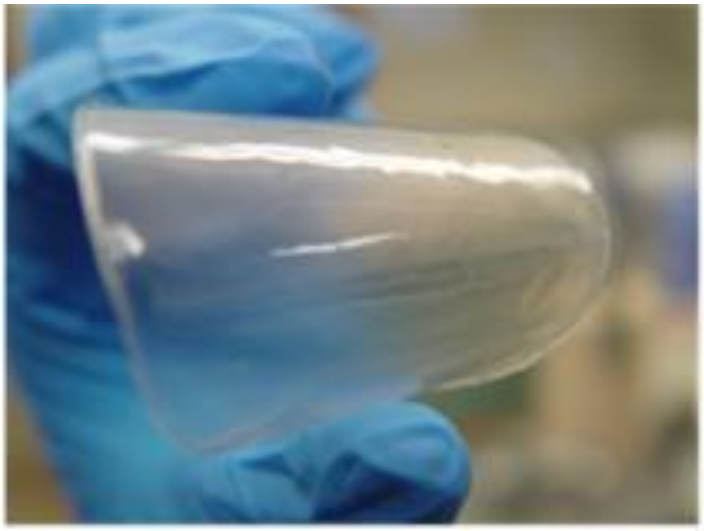

Figure 2.3 A representative QPMBV membrane.

***Water uptake*:** Water uptake percentage of the wet QPMBV was determined by gravimetric method.

$$water\ uptake = \frac{M_{wet} - M_{dry}}{M_{dry}} \times 100\% \qquad [2.2]$$

***Ion-exchange capacity*:** The ion-exchange capacity (IEC) of the QPMBV membrane was measured by acid-based back-titration. The dry QPMBV sample was immersed in 6M KOH solution overnight to exchange into OH- form. After washing with an adequate amount of deionized water to obtain a pH value of 7, the sample was soaked in 30mL of 0.01M standardized HCl solution for 1 day to ensure the neutralization of OH- in the membrane. The IEC value was then determined from back-titration of the excess HCl with 0.01M NaOH solution, which can be calculated by:

$$IEC = \frac{(V_{HCl} - V_{NaOH}) \times C}{m_{dry}} (mmol \cdot g^{-1}) \qquad [2.3]$$

Where V_{HCl} was the volume of HCl solution for membrane soaking; V_{NaOH} was the volume of NaOH solution used in back-titration; C was the concentration of HCl and NaOH solution. m_{dry} is the mass of the dry membrane.

2.2.3 Fuel cell polarization performance test

The electrochemical performance of the QPMBV membrane was tested using a fuel cell test station (Arbin ®) at different temperatures with RH of 60%. Hydrogen and oxygen were used as the fuel and oxidant respectively. QPMBV membrane, which was soaked in 6M KOH solution for ion exchange, was taken out and washed with de-ionized water prior to MEA assembly. The QPMBV membrane was sandwiched by two pieces of catalyst-loaded carbon cloth using a hydraulic press. Catalyst loading amount was 1.0mg/cm^2 (based on Pt), and the surface area of MEA was 5cm^2. The fuel cell was charged and discharged on an Arbin fuel cell test station between open circuit potential and 0.1V at 5 mV/s.

2. 3 Results and Discussion

2.3.1 Copolymer characterization

GPC results of the obtained PMBV with different monomer molar ratios were shown in Figure 2.4. MWs and PDIs of the copolymers were listed in Table 2.1. All three samples had MWs on the order of 10^5 g/mol and PDIs of about 3. The T_g of all obtained PMBV copolymers were around 40 ℃, as indicated in Figure 2.5.

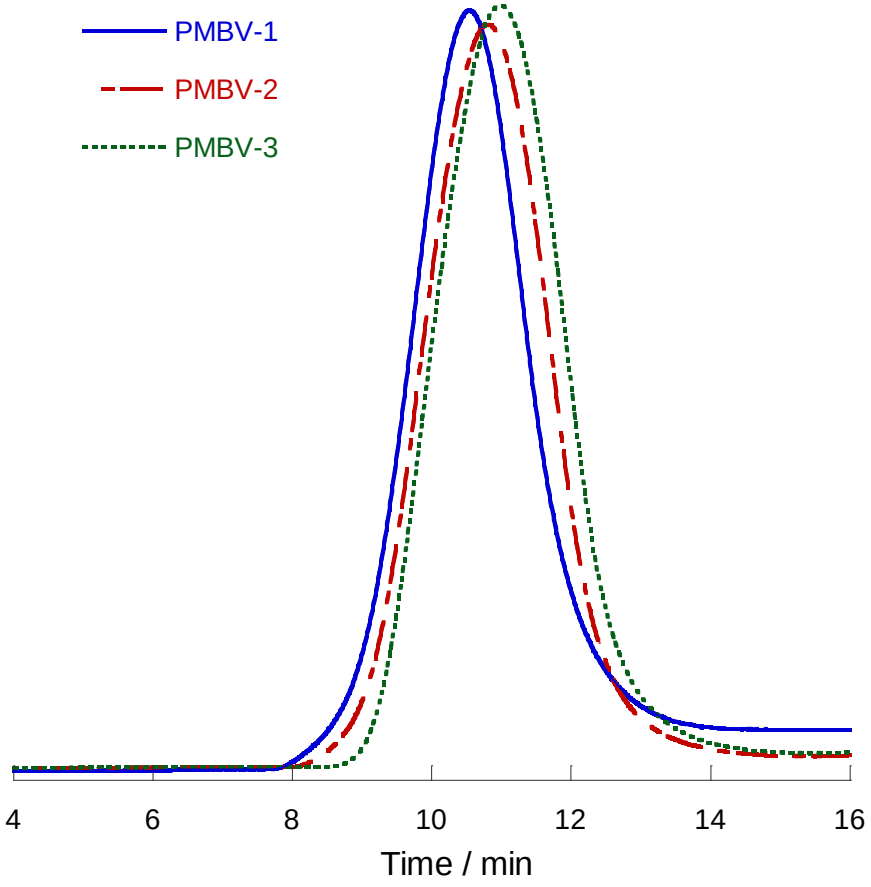

Figure 2.4 GPC characterization of PMBV with different mole ratios.

Table 2.1 Composition, MW and PDI of PMBV

	PMBV-1	PMBV-2	PMBV-3
Molar ratios (MMA: BA: VBC) % in monomers	50:40:10	53:40:7	55:40:5
Molar ratios (MMA: BA: VBC) % in copolymers	47:27:26	53:30:17	66:27:7
MW(Mn)(g/mol)	2.9×10^5	2.6×10^5	2.5×10^5
PDI	3.3	3.2	2.5

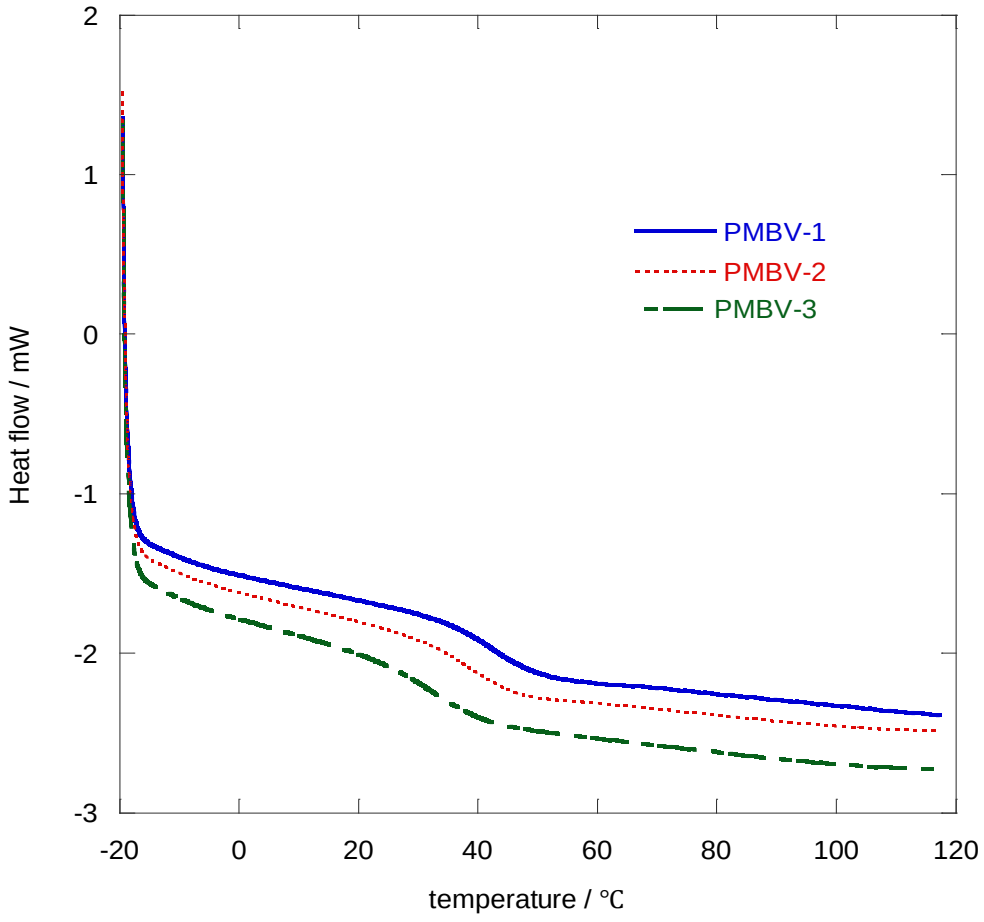

Figure 2.5 DSC characterization of PMBV.

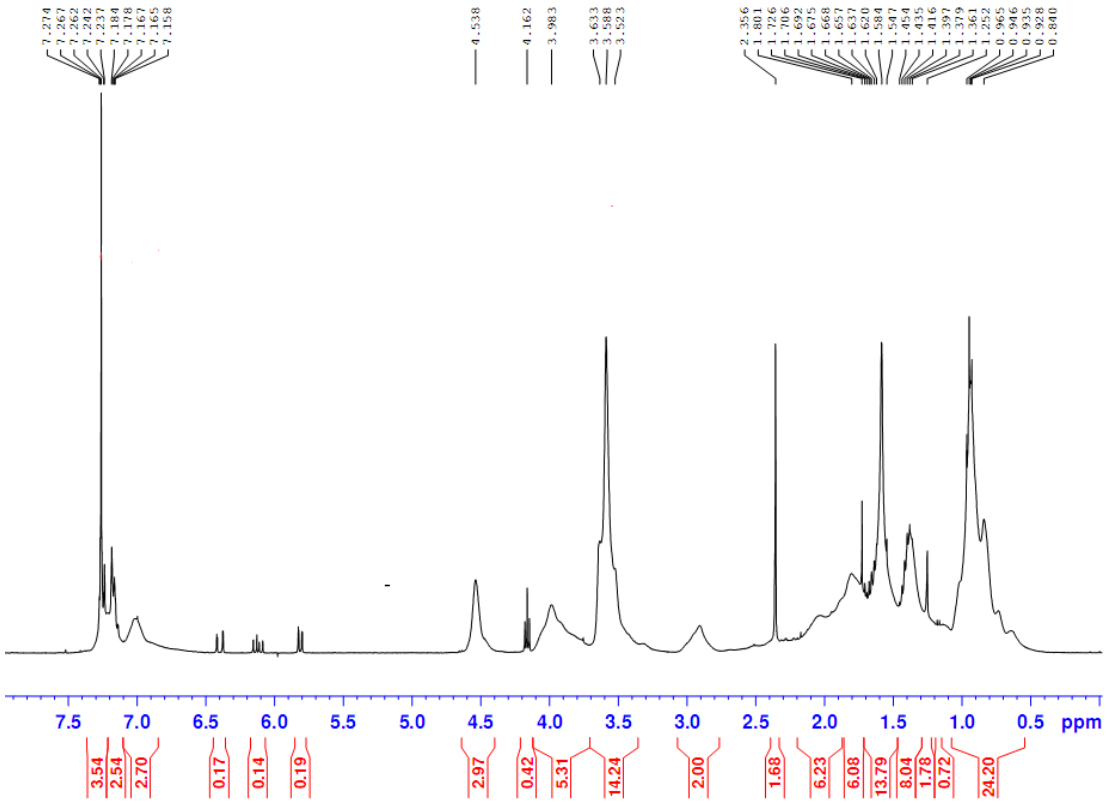

Figure 2.6 ^{1}H-NMR Characterization of PMBV.

^{1}H-NMR tests were performed to obtain the exact composition of the obtained PMBV copolymers, as shown in the representative spectra in Figure 2.6. Chemical shifts (δ ppm) of 4.538 (s, 2H, -CH_2Cl in VBC) [63], 3.983 (s, 2H, -OCH_2- in BA) [64, 65] and 3.588 (t, 3H, -OCH_3 in MMA) [64, 65] were the characteristic peaks for VBC, BA and MMA, respectively. The molar ratio of components in the copolymer can be calculated from the integrals of the corresponding characteristic peaks. The copolymer compositions calculated from ^{1}H-NMR results were listed in Table 2.1. From Table 2.1, it can be seen that BA incorporation in all three copolymers were similar, but considerably lower than their percentages in the reactants mixture. One possible explanation was that the reactivity ratio of BA was much lower than that of MMA and VBC [66, 67] in this ternary monomer mixture. Therefore the incorporation

of BA was unfavorable compared to copolymerization of MMA and VBC, which had comparable reactivity ratios [66, 67]. As the copolymerization proceeded, it became more difficult for BA monomers to access the growing polymer chains. Therefore, when the reaction was stopped, a portion of BA monomers remained unreacted. Consequently, the percentage of VBC in the copolymers was higher than the corresponding composition in the reactant mixtures. The composition of PMBV copolymers followed the trend that higher VBC monomer composition in the reactant mixture resulted in higher VBC incorporation in the obtained copolymer. Therefore, the ^{1}H-NMR results demonstrated that the composition of the PMBV copolymers can be designed by varying the monomer ratios so that the properties of the resulting QPMBV can be tailored as well.

2.3.2 Mechanical properties

Tensile tests were performed on PMBV and QPMBV (both dry and wet) membranes at room temperature to determine the Young's modulus and the tensile strength of the membranes. Figure 2.7 showed the stress-strain curves of dry PMBV membranes and Figure 2.8 illustrated the stress-strain performance of QPMBV membranes in dry and wet environment. The wet QPMBV membranes for tensile tests were prepared by immersing the membranes in de-ionized water for 20 minutes. The water uptake of wet QPMBV was listed on Table 2.2. The obtained Young's moduli and tensile strengths from Figures 7 and 8 were listed in Table 2.3.

Table 2.2 Water uptake of QPMBV membranes

QPMBV-1	QPMBV-2	QPMBV-3
238.8 %	16.5 %	2.8 %

Table 2.3 Young's modulus and strength for PMBV and QPMBV membranes

sample	Young's Modulus (GPa)			Tensile strength (MPa)		
	PMBV	QPMBV	Wet QPMBV	PMBV	QPMBV	Wet QPMBV
1	0.68	0.5	0.01	34	25	3.2
2	0.36	0.25	0.07	37	27.5	9.9
3	0.32	0.16	0.11	27	25.5	18.5

Young's modulus is the slope of the initial linear portion of the stress-strain curve and represents the stiffness of the material, while tensile strength is the ultimate stress before the membrane fractures [68]. For the dry PMBV membranes (Figure 2.7), as VBC composition increased in the copolymer, the initial slope of the stress-strain curve became steeper, suggesting an increase in Young's modulus. Therefore, PMBV-1 was the stiffest membrane and fractured at an elongation of 5%. PMBV-3 is the most ductile membrane of these three, as it had the lowest Young's modulus and tensile strength. VBC is more rigid than MMA, since the benzyl group in VBC has a large steric hindrance. Therefore, stiffness of dry copolymers increased with the increase in VBC composition. Compared to the PMBV membranes, the corresponding dry QPMBV membranes had lower Young's modulus and lower tensile strength. This observation suggested that the QPMBV copolymer slightly lost mechanical strength during quaternization process, which was consistent with the ionomer nature of QPMBV. As dry PMBV, stiffness of dry QPMBV copolymers increased with the increase in VBC composition.

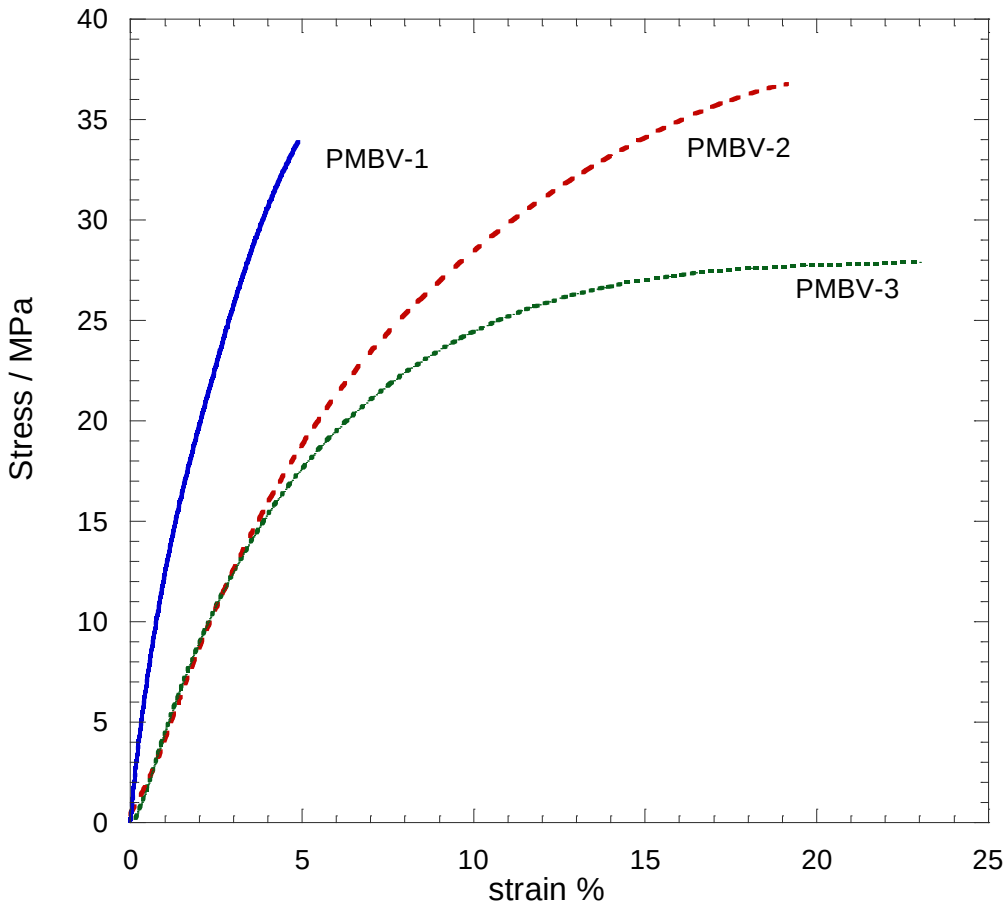

Figure 2.7 Stress-strain curves for dry PMBV copolymer membranes.

The Young's modulus of the dry QPMBV membranes were comparable to that for dry Nafion used in PEMFC (300MPa) [69]. The tensile strengths of the dry QPMBV membranes with different compositions remained close, meanwhile the elongation before fracture decreased with increasing VBC composition. Since AFC operates in wet condition, the properties of QPMBV in wet environment are more important to achieve high fuel cell performance and long durability.

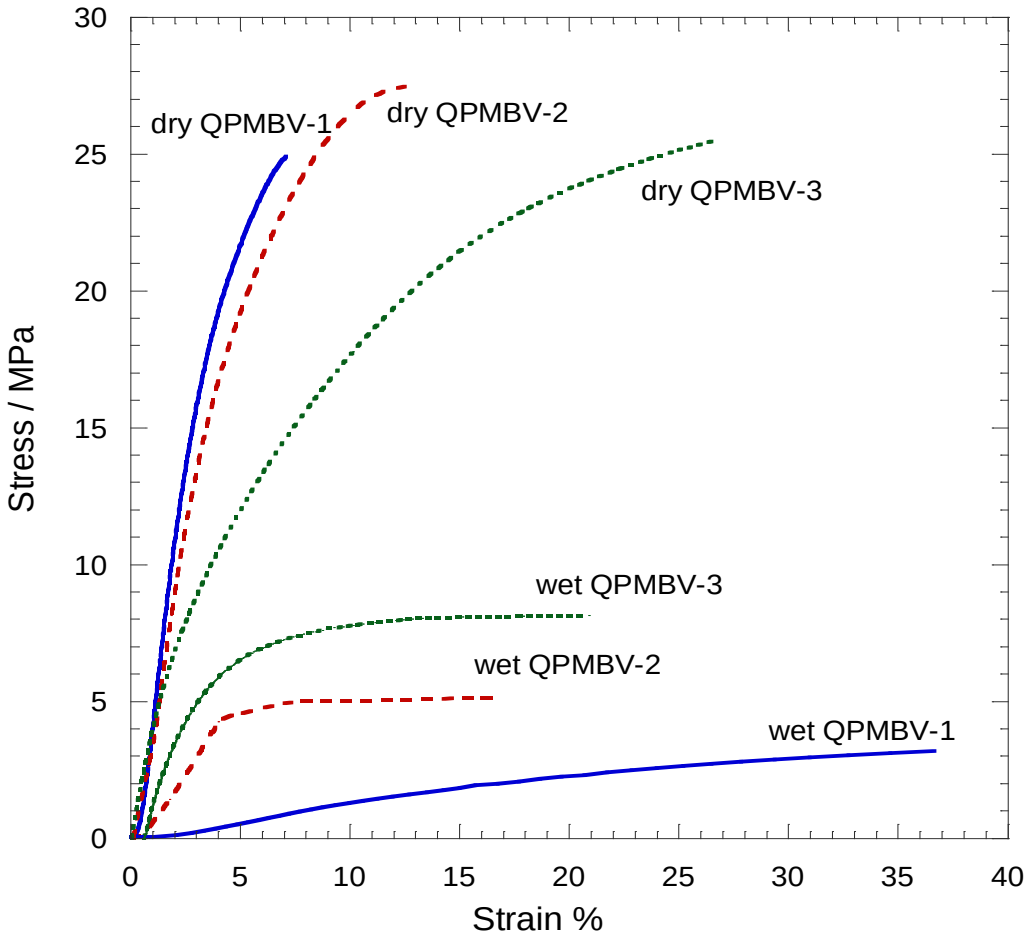

Figure 2.8 Stress-strain curves for QPMBV copolymer membranes.

Interestingly, after immersing the QPMBV membranes in de-ionized water for 20 minutes, completely opposite behaviors were observed in wet QPMBV membranes (as shown in Figure 2.8), i.e. tensile strength decreased and elongation increased with increasing VBC composition. This was because quaternized VBC was hydrophilic. The wet QPMBV with higher VBC composition absorbed more water as indicated in Table 2.2, thus becoming more ductile. On the other hand, MMA and BA portions of the copolymer still sustained reasonable mechanical properties of the membranes after wetting. The mechanical properties of wet QPMBV membranes increased with higher composition of MMA and BA, but they decreased with the increase of VBC

that was required in QPMBV to achieve high ionic conductivity. Therefore, it is possible to synthesize QPMBV membranes which have both high mechanical property and high ionic conductivity in wet condition through tuning the composition of QPMBV.

2.3.3 Conductivity measurement

Figure 2.9 showed the conductivities of OH^- exchanged QPMBV membranes at various temperatures. An increase in conductivity was observed when temperature was increased. Among three membranes, QPMBV-1 has the best conductivity due to the highest composition of quaternized VBC groups. QPMBV-1 membrane could reach a maximum conductivity of 8.2×10^{-3} S/cm at 80 ℃.

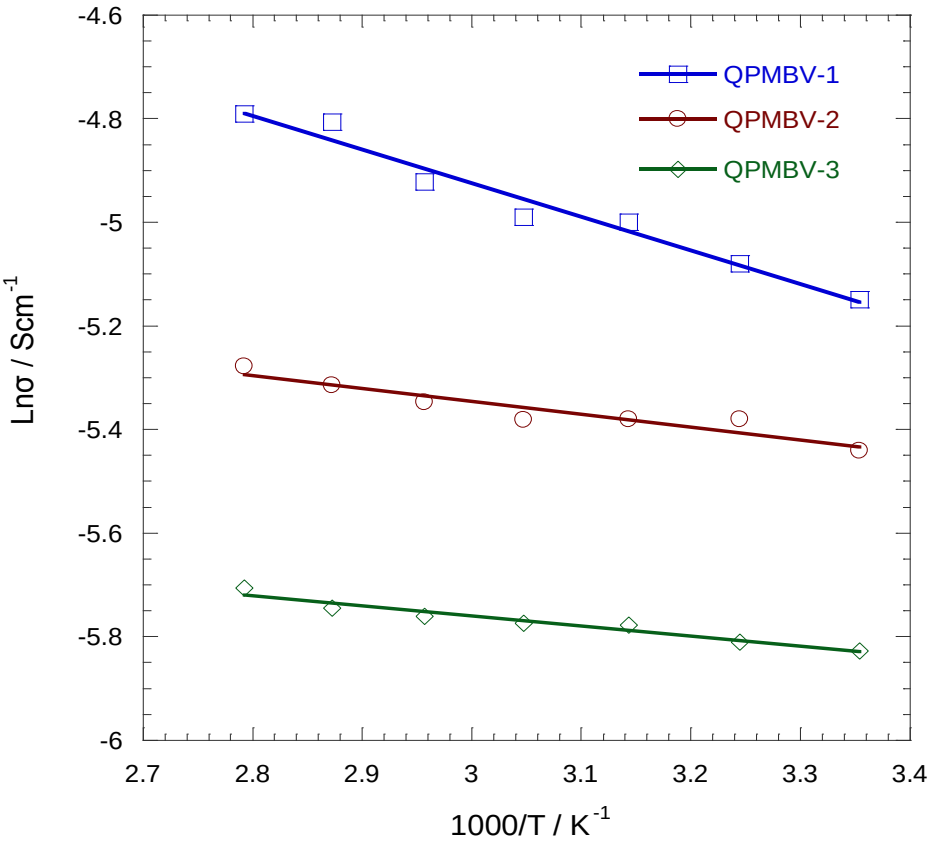

Figure 2.9 Conductivities of QPMBV membranes at relative humidity of 80%.

Combining the results of mechnical properties and conductivity, it was clear that higher VBC composition resulted in higher OH- conductivity，however, also impairing the mechnical properties of the membrane in the humidified working condition. The key was that the mechanical property functional groups in the copolymer, MMA and BA, can provide physical strength to enble the QPMBV membranes to work in the fuel cell.

2.3.4 Fuel cell performance test

The performance of three OH^- exchanged QPMBV electrolyte membranes in AFC was measured using the Arbin fuel cell test station. AFC polarization curves were obtained by potential scan at the rate of 5 mV/s from OCP (open circuit potential) (1.00V) down to 0.1V. Figure 2.10 showed the polarization curves of the three OH^- exchanged QPMBV membranes at 60 ℃ in RH of 60%. As shown in Figure 2.10, the performance of the membranes improved as the VBC composition increased in the copolymers. The peak power density of QPMBV-1 was 35mW/cm^2 when current density was 80mA/cm^2 and voltage was 0.44 V. These results were consistent with the conductivity results as described previously. QPMBV-1 membrane had the highest VBC incorporation (26 mol.%) so that it had the highest OH^- conductivity, thus resulting in the best AFC performance among these three membranes.

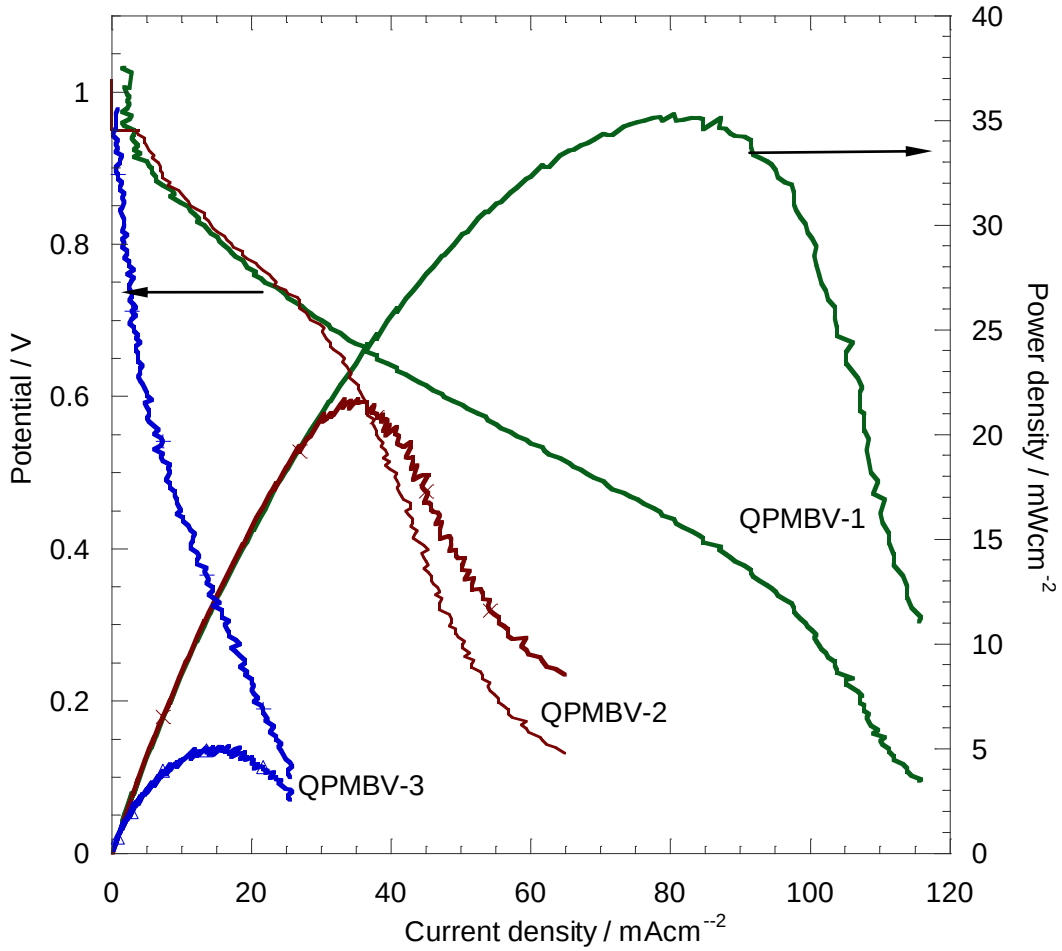

Figure 2.10 polarization & Power density curves of QPMBV membranes at 60 ℃.

The temperature dependence of OH^- exchanged QPMBV electrolyte membrane fuel cells was also determined by changing the cell temperature from 40°C to 80°C. Figure 2.11 showed the AFC performances of OH^- exchanged QPMBV-1 membrane at different temperatures with the same RH of 60%. As expected, performances improved as temperature increased. At 80 ℃, the maximum current density was 180 mA/cm^2 while peak power density reached 59 mW/cm^2.

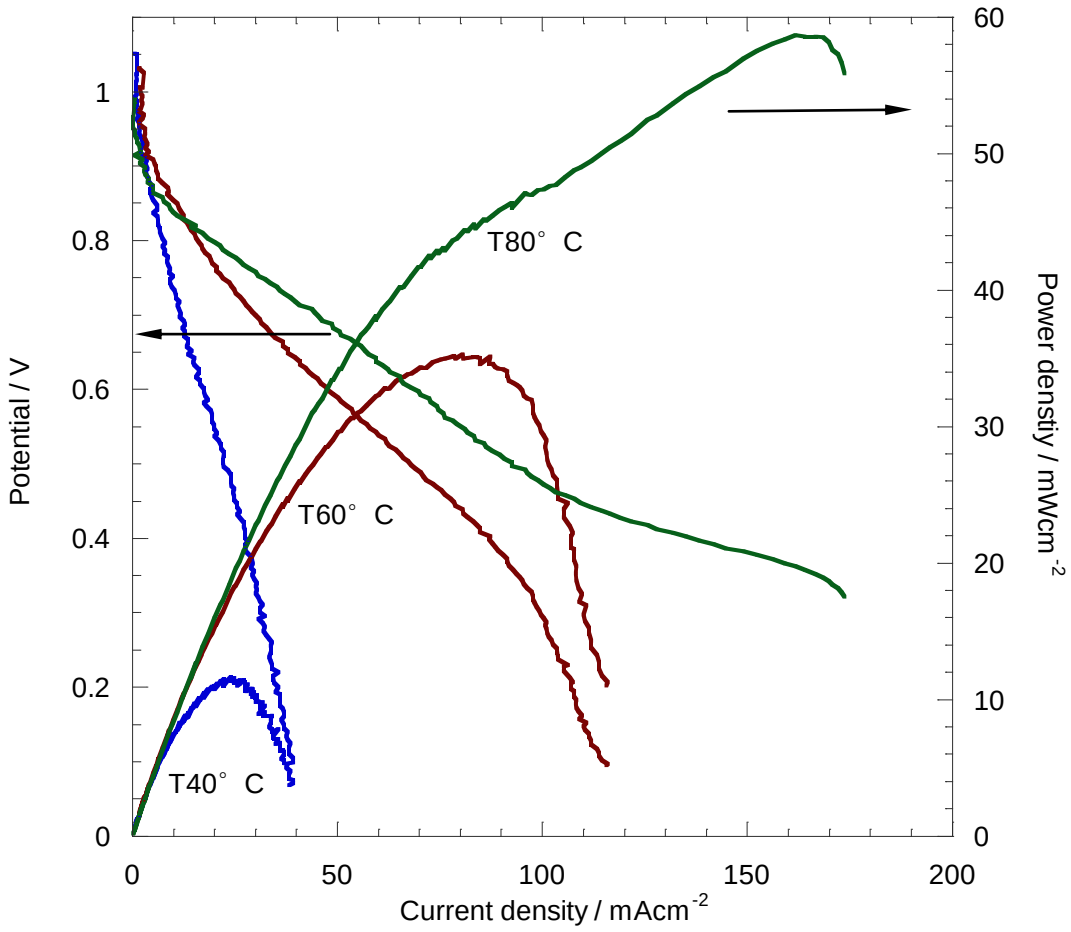

Figure 2.11 polarization curves and power density curves of QPMBV membrane at different temperatures in RH of 60%.

The anion conductive (QPMBV) membrane fuel cell reported here, although it was a prototype, represented an important advancement in the development of fuel cell membranes. It has demonstrated a feasible method for preparation APE anion conductive membranes via free radical solution polymerization of selected functional monomers for AFCs.

2. 4 Conclusion

Successful synthesis of proof-of-concept AFC polymer electrolytes based on a ternary copolymer, namely poly(methyl methacrylate-*co*-butyl acrylate-*co*-vinylbenzyl chloride), was reported. Instead of modification of pre-existing polymers, a new route of preparing APEs OH^- conductive membranes via copolymerization of selected functional monomers was reported in this study. The purpose of this study was to demonstrate the feasibility of obtaining desired AFC APEs through specific monomer selections and a designed synthesis procedure. All three monomers used in the study were selected based on their unique functionalities, and the synthesis was intentionally designed to reflect the effects of different recipes on membrane mechanical and electrochemical properties. The synthesis was free radical solution polymerization, which was followed by quaternization and membrane casting to obtain the APE. The intrinsic OH^- conductivity of the free-standing APE membranes can reach 8.2×10^{-3} S/cm at 80 ℃. The maximum current density was 180 mA/cm^2 while peak power density reached 59 mW/cm^2.

The alkaline fuel cells using copolymer APEs demonstrated the feasibility of the preparation of these membranes. The results of this study clearly demonstrated that the trend of membrane properties was well controlled by the researchers' intentions. Given the results, more sophisticated miniemulsion copolymerization was employed to make new APEs with more controllable and tunable properties.

Chapter 3

Miniemulsion Copolymerized Acrylate-Polymer-Based PMBV Alkaline Polymer Electrolyte Membrane

The results presented in this chapter have been published in the *ChemSusChem and ECS Transaction.*

Y. Luo, J. Guo, C. Wang, D. Chu, "An Acrylate-Polymer-Based Electrolyte Membrane for Alkaline Fuel Cells Applications," *ChemSusChem,* 4(11) (**2011**) 1557

Y. Luo, J. Guo, C. Wang, K. Y. Choi, D. Chu, "High Molecular Weight Copolymer Alkaline Fuel Cell Membrane via Miniemulsion Polymerization", *ECS Transaction,* 33(1) (**2010**)1893.

3.1 Introduction

3.1.1 Problems with Free Radical Solution Polymerization

In the previous study, we reported a novel APE made from poly (methyl methacrylate-co-butyl acrylate-co-vinylbenzyl chloride) (PMBV) [70]. This copolymer was synthesized using solution free radical polymerization. Xu and co-workers also reported an independent study of APE made from a copolymer with similar polymerization method [71]. Despite promising performance, our previous study encountered two problems: The three monomers, methyl methacrylate (MMA), butyl acrylate (BA), and 4-vinylbenzyl chloride (VBC), had different reactivity ratios so

that they polymerized at different reaction rates. Due to the slow diffusion of the propagating copolymer chains and the diluted monomer concentration in the solution polymerization, the monomers with lower reactivity ratios had little possibility for complete conversion. Therefore, the copolymer composition did not match the designed monomer ratio. The second concern was that the molecular weight of the copolymer in our previous study was not as high as expected, which could considerably weaken the mechanical strength. To address these problems, we demonstrate a novel bottom-up synthesis of PMBV using miniemulsion polymerization for the first time in the present study. Unlike chloromethylation of existing polymers, we synthesized our PMBV with various monomers that were intentionally selected to meet the requirements for conductivity and mechanical strength. Specifically, VBC (15 mol. %) had the chloromethyl functional group that could be quaternized and successively ion-exchanged to have OH- conductivity [72]. Polymerized MMA was a polymer with rigidity and toughness so that the MMA monomer (80 mol. %) was designated to provide mechanical strength. Addition of a small portion of BA (5 mol. %) was to alleviate the brittleness from the MMA and VBC to afford some flexibility of the resultant APE.

3.1.2 Mechanism of Miniemulsion Copolymerization

The miniemulsion polymerization is a unique emulsion polymerization technique [73, 74]. High shear force (e.g. sonication) is usually employed to disperse monomers in water phase as droplets. Figure 3.1 illustrates the mechanism of miniemulsion polymerization system. The significant difference between miniemulsion and emulsion is the much smaller and more uniform droplet size. Most of the surfactant is

adsorbed on the droplet surface due to the large surface area. [75] Therefore, the monomer droplets can be stably dispersed in water phase as individual polymerization loci. Polymerization is primarily initiated in the droplets via free radical entering from water phase. As illustrated in Figure 3.1, the monomer (mixture of MMA, BA, and VBC) droplets are stabilized in water phase by surfactants (sodium dodecyl sulfate, SDS) and co-stabilizer (hexadecane, HD) which is an extremely hydrophobic nonreactive reagent. Free radicals are generated by water phase initiator (potassium persulfate, KPS).

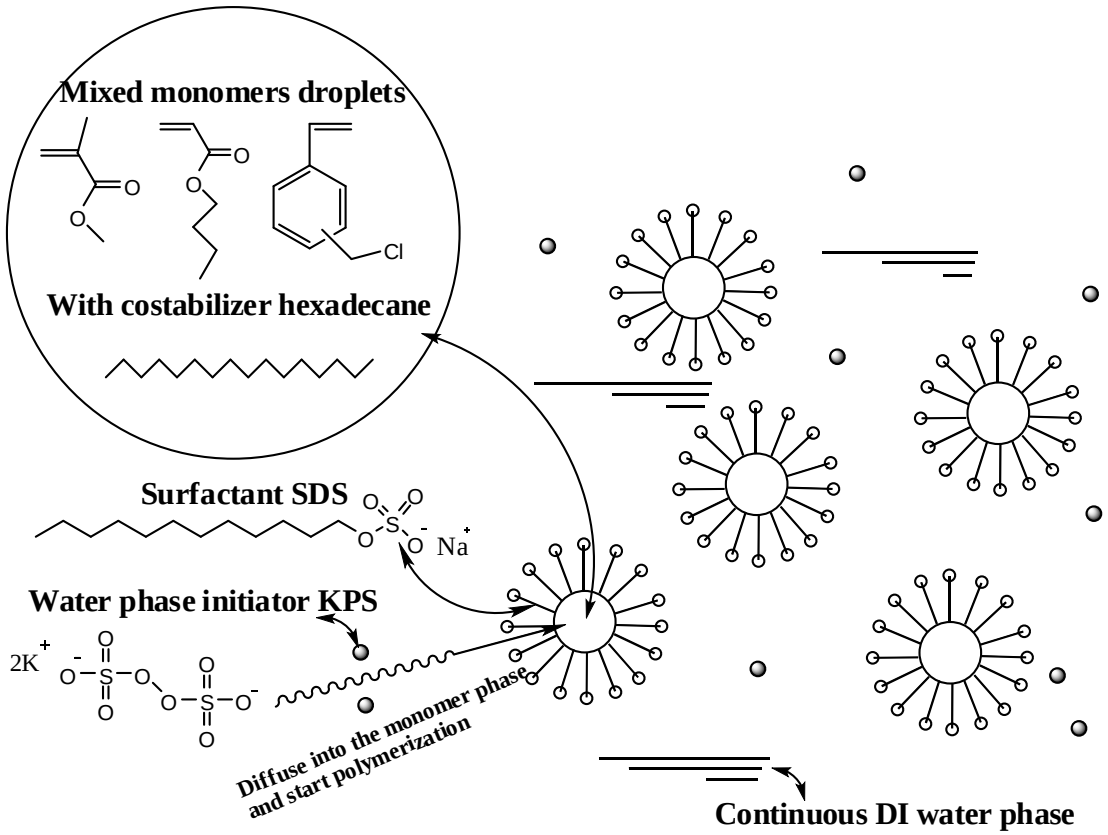

Figure 3.1 Synthesis of the QPMBV-APE: miniemulsion copolymerization.

3.1.3 Advantages of Miniemulsion Copolymerization

In miniemulsion, each monomer droplet can be considered as an individual reactor for bulk polymerization. Because of the small reactor (i.e. droplet) size, the effect of slow diffusion of the propagating chains can be alleviated, and high monomer conversion can be achieved. Therefore, the composition of obtained copolymer is in good agreement with the monomer ratio. Also, high molecular weight can be achieved via miniemulsion polymerization with mild conditions, eliminating the difficulties of mixing and heat management in bulk polymerization [76]. Moreover, water was used as the reaction medium in this miniemulsion copolymerization, which is environmentally friendly.

3.2 Experimental

3.2.1 Miniemulsion copolymerization

Miniemulsion was prepared by dispersing 30g mixture of monomers with designed molar ratio (MMA: BA: VBC = 80: 5: 15 mol %) and 0.12g hexadecane into 150 ml aqueous SDS (0.01 mol L^{-1}) solution by ultrasonic shearing to form a stable miniemulsion with a homogenizer (Omni® Sonic Ruptor 400) for 9 min at 30% power output. The polymerization was initiated by injection of initiator KPS (0.01 mol L^{-1} of the water phase) into the miniemulsion at 70 ℃ under nitrogen protection. The reaction was terminated after 4 hours by quenching in ice bath. The copolymer was filtered and dried in fume hood overnight and was further dried in vacuum oven at 60 ℃ for 24 hours.

***Conversion Test*:** Prior to the copolymerization, aluminum weight pans pre-loaded with trace amount of hydroquinone (as polymerization terminator) were weighed and recorded. During the copolymerization, small amount of miniemulsion reaction content was drawn from the reactor flask from various intervals, and put in the aluminum pan and weighted. After completely drying the drawn miniemulsion content in vacuum oven overnight, the obtained residue (with the pan) was weighed again. The monomer conversion was calculated by gravimetric method using following equation

$$Conversion = \frac{W_{dry} - W_{wet} \times (SDS + KPS + HD)wt\%}{W_{wet} \times \eta} \qquad [3.1]$$

where W_{dry} was the weight of the residue in the weighing plate; (*SDS+KPS+HD*) *wt*% is the total weight percentage of SDS (surfactant), KPS (initiator), and HD (costabilizer) in the reactant mixture; W_{wet} was the weight of the miniemulsion content drawn to the weight pan; and η is the weight percentage of monomers in the entire reactant mixture.

Glass Transition Temperature: The glass transition temperature (T_g) of PMBV copolymer could be estimated by the following expression

$$\frac{1}{Tg} = \frac{W_{PMMA}}{Tg_{PMMA}} + \frac{W_{PBA}}{Tg_{PBA}} + \frac{W_{PVBC}}{Tg_{PVBC}} \qquad [3.2]$$

Where *W* with subscript is the mass ratio of each component in the polymer, and T_g with subscript represents the glass transition temperature of the corresponding homopolymer (Data were obtained from the Polymer Hand Book) [77]. The T_g of

PMBV was calculated from Equation 3.2. DSC (Differential scanning calorimetry, TA Instruments Q100) was also used to determine the T_g of PMBV.

3.2.2 Membrane preparation

The obtained PMBV was dissolved in dimethylformamide (DMF) at 80 ℃ and quaternized with trimethylamine (Me_3N, Sigma-Aldrich) for 2 hours at 80 ℃ by bubbling Me_3N into the solution with modest stirring. The obtained QPMBV solution in DMF was then casted as a film and dried in the vacuum oven at 60 ℃ for 24 hours. The obtained membrane was soaked in 6M KOH solution overnight to exchange Cl^- to OH^-. The OH^- exchanged membrane was washed with DI water until pH of 7 was reached.

Element Analysis: The degree of quaternization was determined by elemental analysis (Atlantic Microlab® of combustion). Assuming all functional group VBC was reacted with TMA (Me_3N), the theoretical composition of N in the QPMBV copolymer can be calculated

$$W_N = \frac{M_N \times W_{VBC}}{M_{MMA} \times W_{MMA} + M_{BA} \times W_{BA} + (M_{VBC} + M_{Me_3N}) \times W_{VBC}} \times 100\% \quad [3.3]$$

where M with subscript is the molecular weight of the corresponding monomer, compound, or element; W with subscript is the composition molar ratio of the corresponding substance. Using this formula, the theoretical weight percentage of N element was 2 wt. % in the QPMBV.

Combustion test result suggested 2.26 wt. % N in the QPMBV after two hours of quaternization, and did not change afterwards. This value is within the experimental error (±0.5%). The excess amount of N is possibly due to the trace of DMF solvent left in the membrane even after vacuum drying.

The OH^- weight percentage of the exchanged cation sites can be calculated as

$$W_{OH} = IEC \times M_{OH} \times 100\% \qquad [3.5]$$

where MOH is the molecular weight of OH-. The calculation showed that the changed OH- weight percentage was 2.2%. That indicated an IEE (Equation 3.6) of 89.6% for paired cation sites that changed from Cl- to OH- form.

$$IEE = \frac{W_{OH}}{W_N \times \frac{M_{OH}}{M_N}} \qquad [3.6]$$

3. 3Results & Discussion

Figure 3.2 was the overall monomer conversion as a function of reaction time. It indicated 97% conversion of the monomers after 120 min.

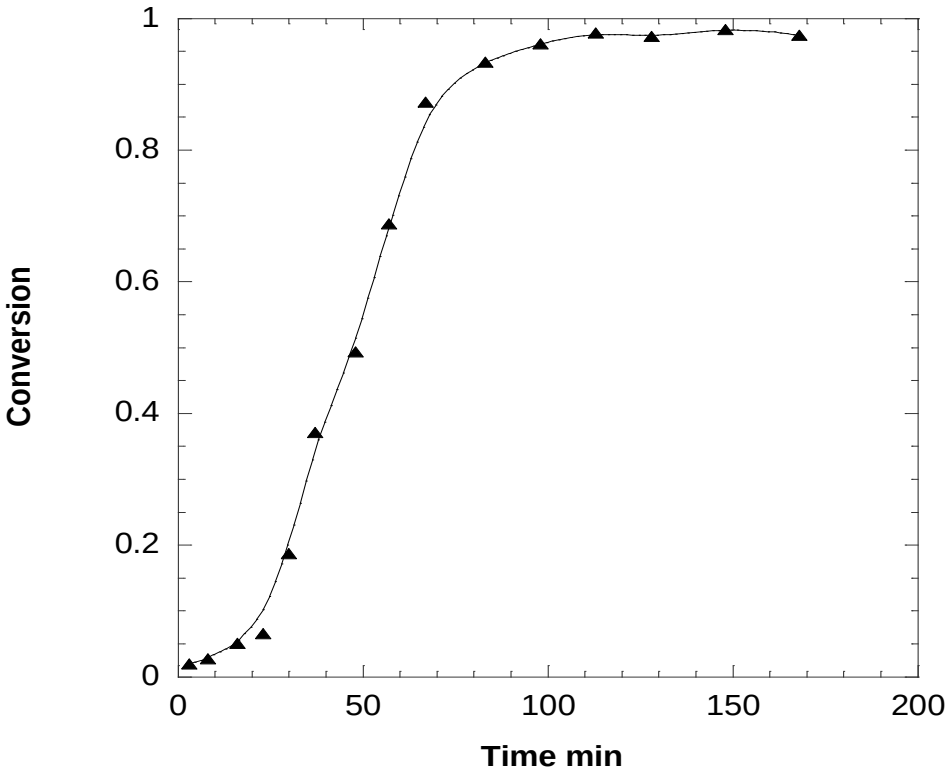

Figure 3.2. Miniemulsion copolymerization monomer conversion plot.

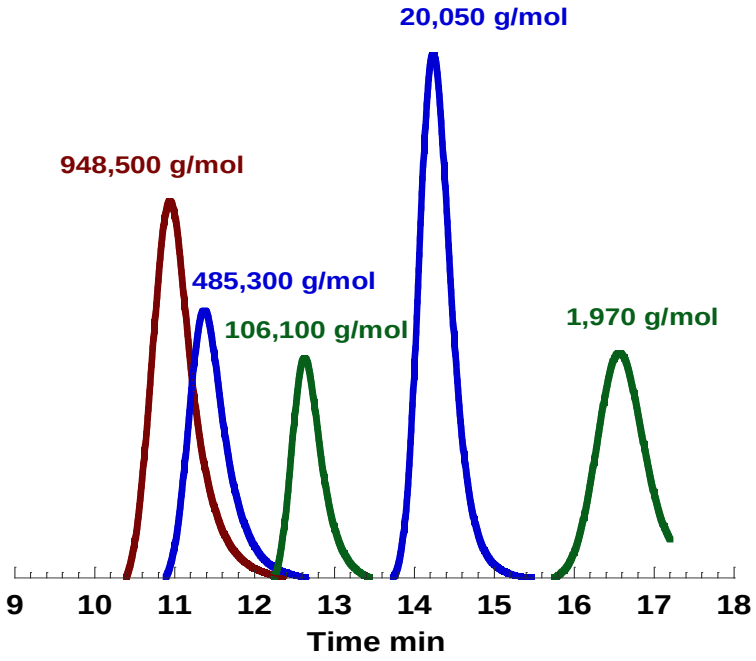

Figure 3.3 GPC spectra of standard polymer.

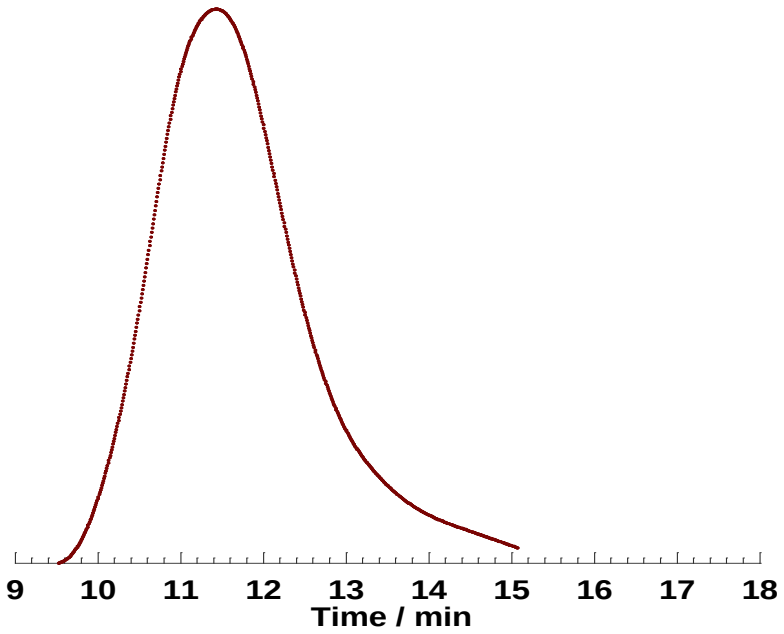

Figure 3.4 GPC spectrum of PMBV.

Table 3.1 Molecular weight of PMBV

	PMBV
Number-average MW g/mol	6.4×10^{5}
Weight-average MW g/mol	1.5×10^{6}
PDI	2.3

The molecular weight of the obtained PMBV copolymer was 1.5×106 g mol^{-1}, which was six times higher than that of the copolymer in our previous study discussed in Chapter 2 [70].

The composition of the obtained PMBV was 78.8: 4.8: 16.4 (molar % of MMA: BA: VBC) from calculation based on the ^{1}H-NMR spectrum. This composition was in

good agreement with the monomer ratio in the reactant mixture (80: 5: 15), as shown in Figure 3.3, 3.4 and Table 3.2.

Table 3.2 Composition of PMBV

	MMA	BA	VBC
Composition in PMBV mol.%	78.8	4.8	16.4
Recipe Monomer Ratio mol.%	80	5	15

The glass transition temperature (T_g) of the PMBV copolymer was 102 ℃ from the DSC (differential scanning calorimetry) test as shown in Figure 3.5, which was in agreement with the result calculated as 93 ℃ based on the composition [78], as shown in Table 3.3.

Table 3.3 Estimated *Tg* in ideal situation for PMBV

	Tg (℃)
PMMA (78.8 mol. %)	105
PBA (4.8 mol. %)	-49
PVBC (16.4 mol. %)	114
PMBV	92.9

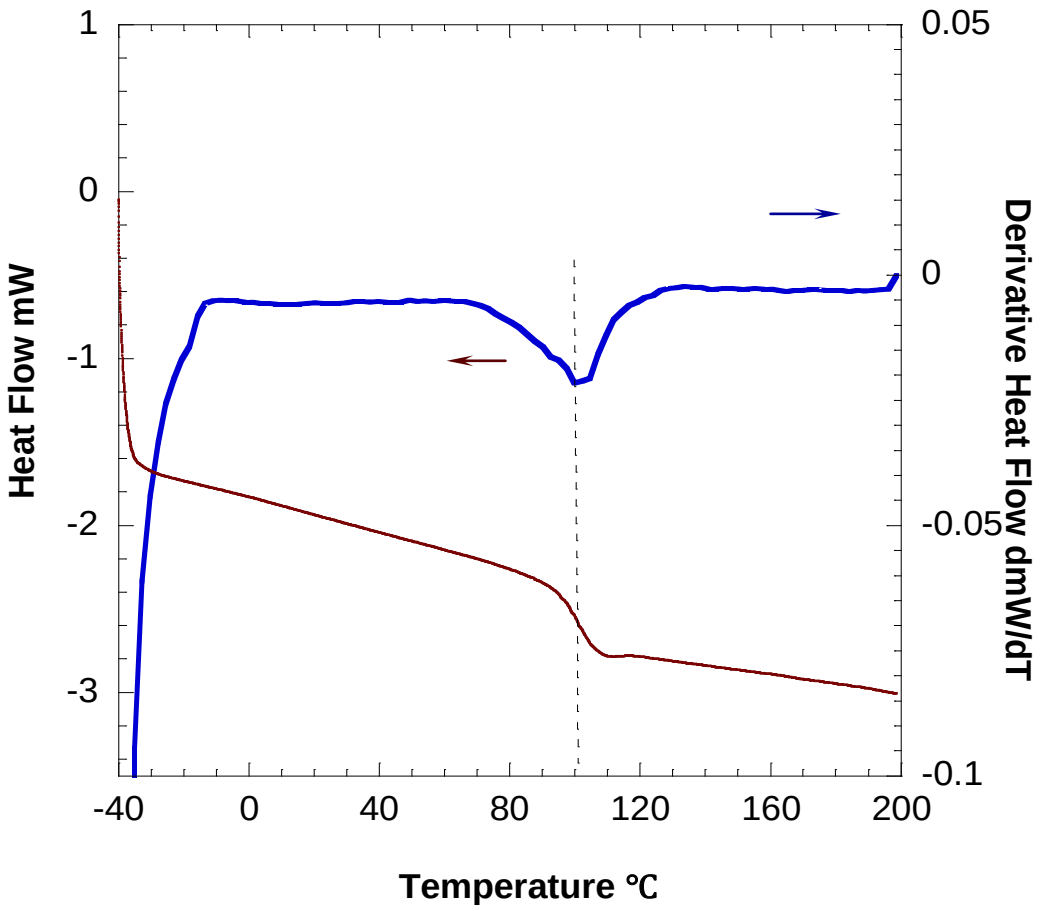

Figure 3.5 DSC thermo gram of PMBV.

The complete synthesis route of the APE was shown in Figure 3.6. Firstly, the PMBV copolymer was synthesized from miniemulsion polymerization. The PMBV was continued with quaternization by reaction with trimethylamine (Me_3N) in DMF (dimethylformamide) solution. The quaternized PMBV (QPMBV) was then cast into membrane and soaked in 6M KOH solution for 24 hours at room temperature for ion-exchange from Cl^- to OH^-.

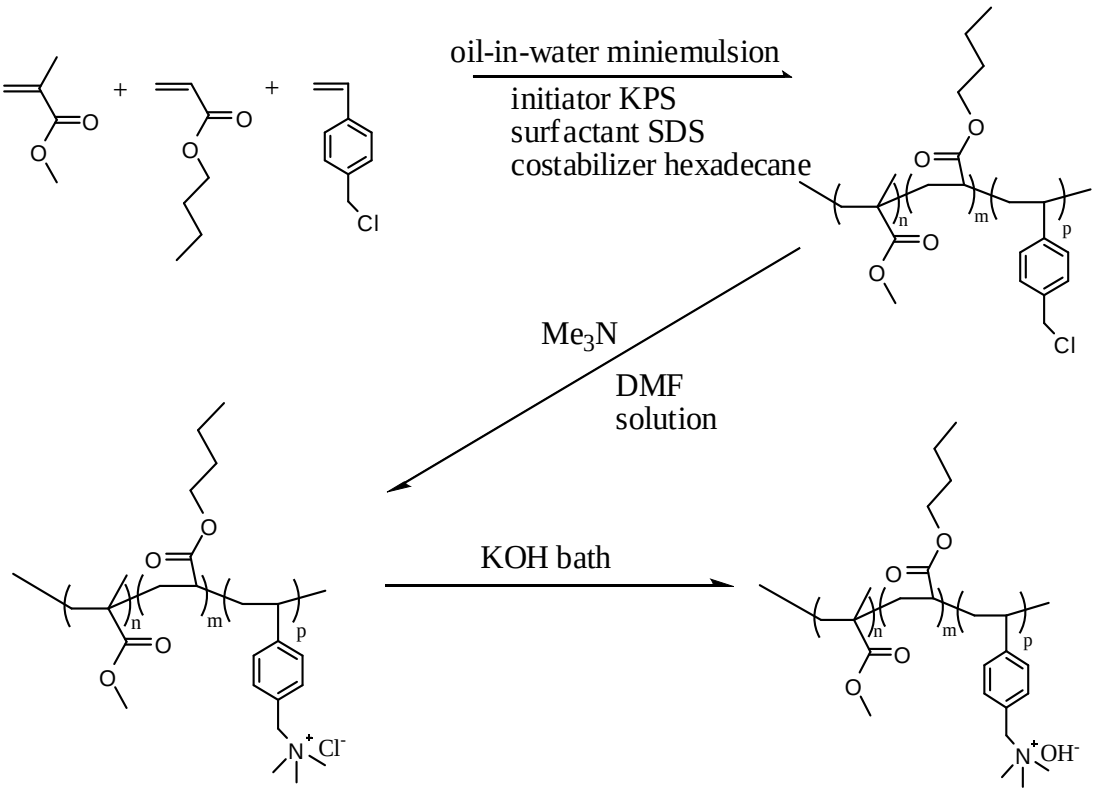

Figure 3.6 Synthesis of the QPMBV-APE: miniemulsion copolymerization, APE quaternization and ion-exchanging.

After ion-exchange, the polymer membrane was washed with abundant water until pH reached 7. The final product, QPMBV-APE, was obtained after complete drying. The elemental analysis revealed a completion of quaternization (all VBC groups were quaternized). Acid-based back-titration measurement [79] indicated ion exchange capacity (IEC) of 1.28 mmol g^{-1}, and the efficiency of ion-exchange was estimated as ~90%. It is worth mentioning that the conducting ions in the QPMBV-APE were identified by titration method. The titration results indicated that in approximately 60 min after the QPMBV-APE being washed to neutral, most of the conducting ions changed from OH^- to HCO_3^- and/or CO_3^{2-}. The conductivity stability in high-pH

environment was also tested in 6M KOH solution. As shown in Figure 3.7, the stability test indicated a slight 3.3 % IEC decrease of the QPMBV-APE being soaked in 6M KOH solution for 7 days.

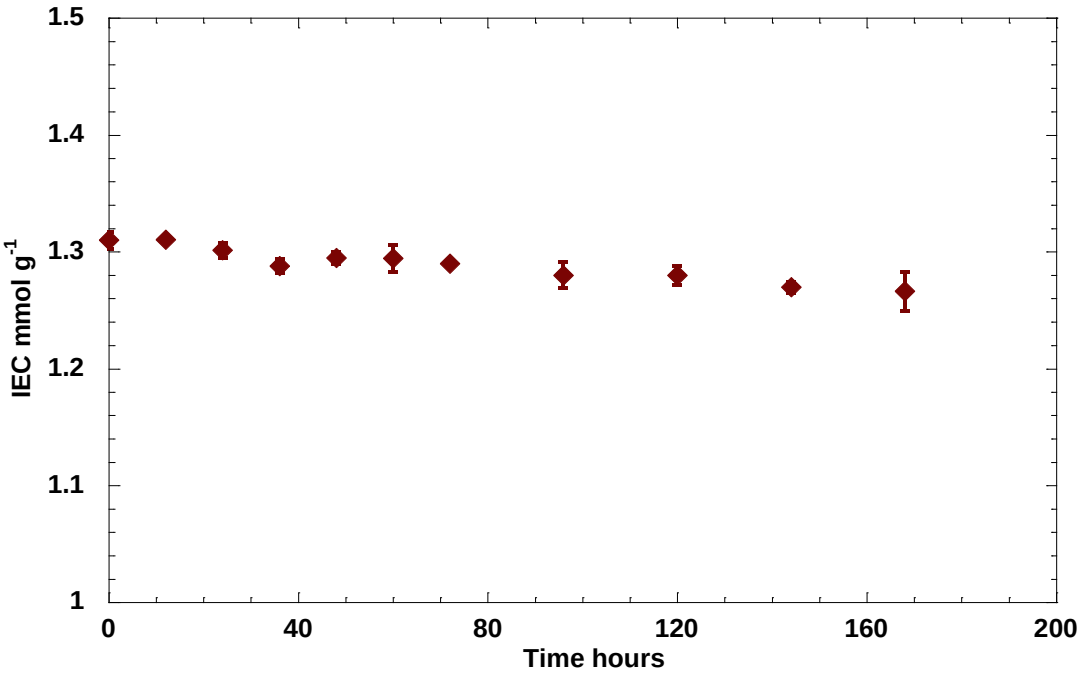

Figure 3.7 Ion exchange capacity of the QPMBV-APE as a function of time in 6M KOH solution.

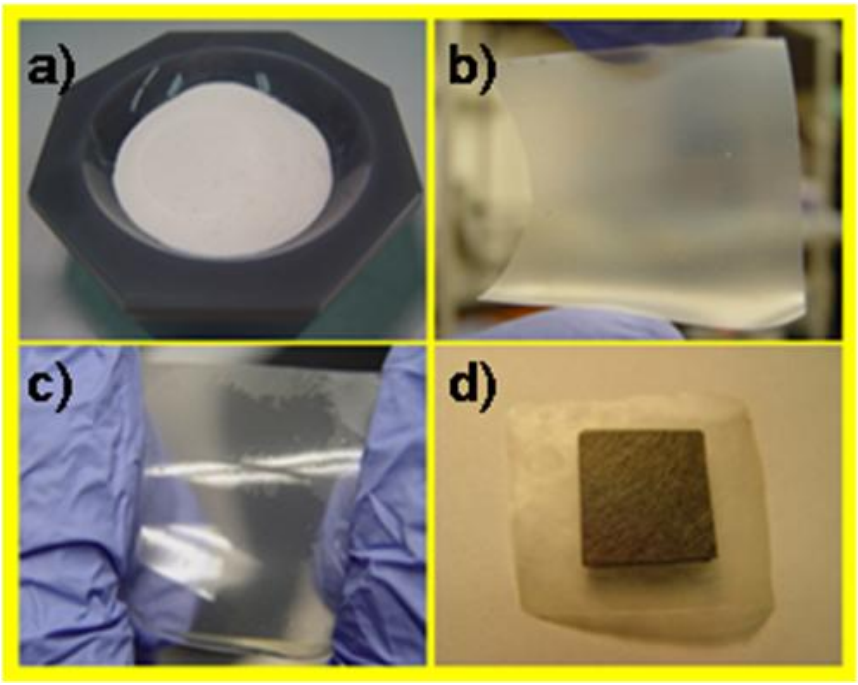

Figure 3.8 a) Synthesized PMBV copolymer powder; b) QPMBV membrane being bended; c) ion-exchanged QPMBV-APE membrane being stretched; and d) MEA with QPMBV-APE membrane.

The products in each synthesis step were shown in Figure 3.8. Figure 3.8a) was the PMBV copolymer from the miniemulsion copolymerization; b) was the QPMBV copolymer membrane before ion-exchange; c) was the final QPMBV-APE membrane after ion-exchange; and d) was the membrane electrode assembly (MEA) with the QPMBV-APE membrane.

Both the water uptake and anionic conductivity of the QPMBV electrolyte membranes were measured under fuel cell operation conditions (80% RH and 40^{o}C - 70^{o}C temperature ranges). Figure 3.9 showed the water uptake of the QPMBV-APE membrane at 80% RH as a function of temperature based on triplicate measurements.

The water uptake at 80% RH is between 20 wt. % and 30 wt.% in the temperature range from 40 to 70 ℃.

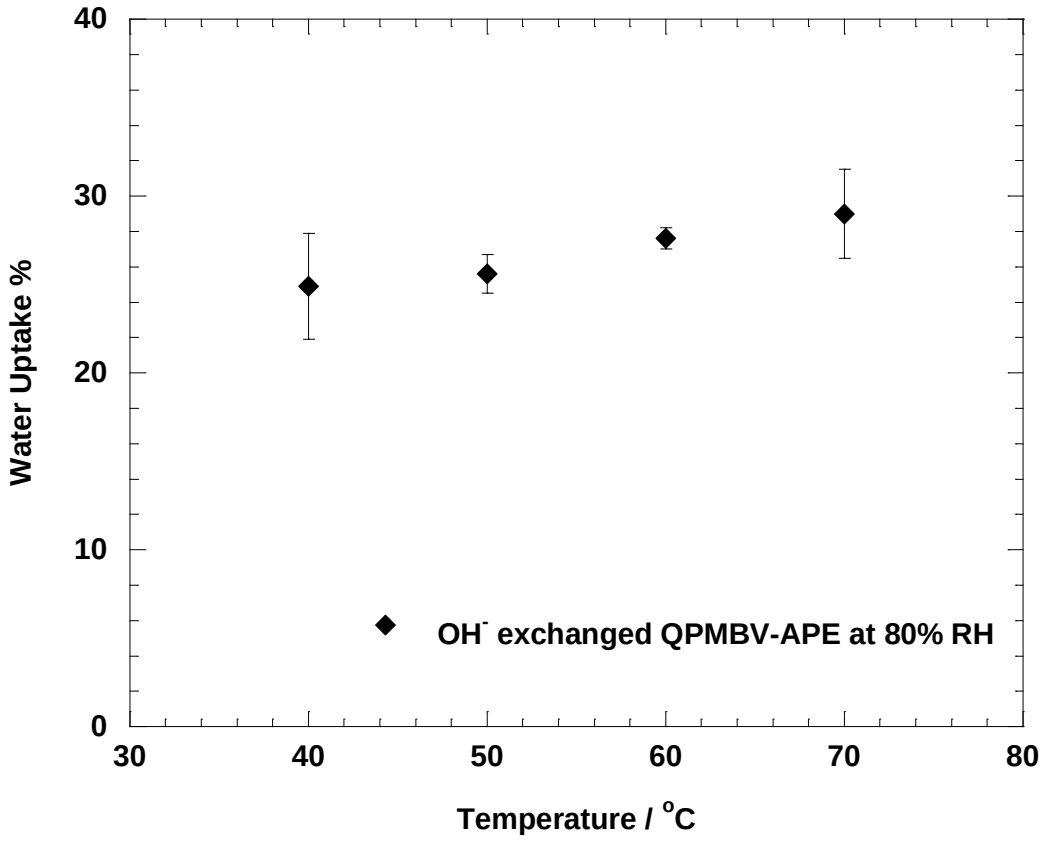

Figure 3.9 Water uptake of OH- exchanged QPMBV-APE membrane as a function of temperature at 80% RH.

QPMBV-APE tensile test was performed at the stretch rate of 1N/min at room temperature. The tensile test was performed in the worst scenario of fuel cell operation environment, i.e. the QPMBV-APE was fully saturated with DI water by soaking in DI water for one hour before the test. Water uptake at full water saturation was determined by gravimetric method. The strain vs. stress plot was shown in Figure

3.10, and the obtained mechanical properties were listed in Table 3.4. The Young's modulus and elongation indicated an elastic QPMBV-APE membrane.

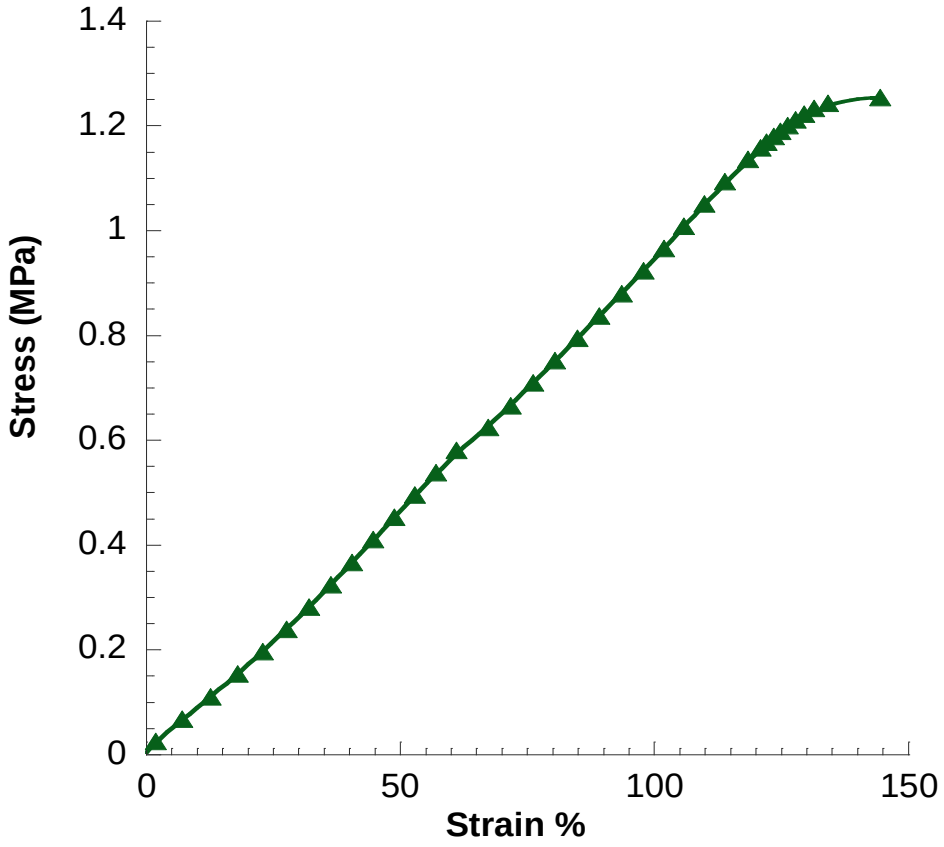

Figure 3.10 stress-strain plot for water saturated QPMBV-APE.

Table 3.4 Basic properties of QPMBV-APE

Properties at ambient temperature	QPMBV-APE
Thickness(μm)	50
Young's modulus(MPa) [a]	0.93
Yield Stress(MPa) [a]	1.25
Elongation at yield [a]	130%
Water uptake [a]	325 ±32 %

The anionic conductivity of the QPMBV-APE was measured in a four-probe testing cell (BekkTech, BT-112) using EIS. The original data was in Figure 3.11. Figure 3.12 showed the conductivities from 50 to 80 ℃ at 80% RH, giving activation energy of 52.2 $KJmol^{-1}$. The anionic conductivity of QPMBV can reach 0.043 Scm^{-1}. The high conductivities of QPMBV-APE could be attributed to the 15 mol. % anions attached to the VBC group in the copolymer.

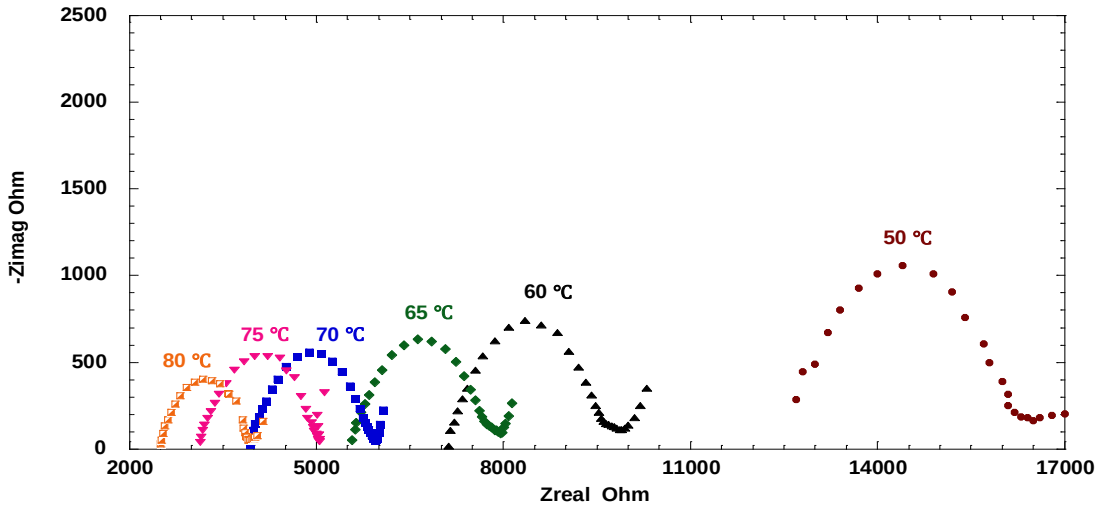

Figure 3.11. Nyquist plot of APE from 50 ℃ to 80℃

Table 3.7 Conductivities of QPMBV-APE at different temperatures at 80% RH

T (℃)	50	60	65	70	75	80
Conductivity(S/cm)	0.84×10^{-2}	1.5×10^{-2}	1.9×10^{-2}	2.7×10^{-2}	3.4×10^{-2}	4.3×10^{-2}

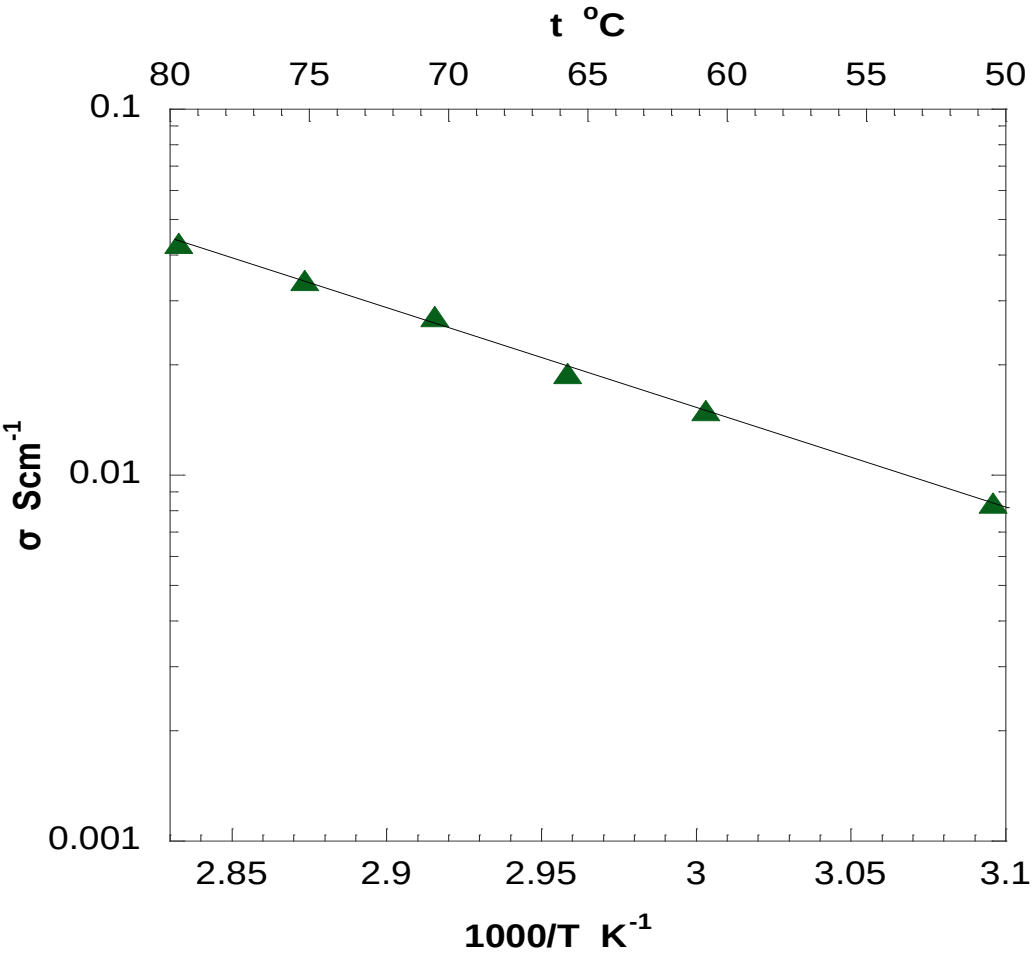

Figure 3.12 Conductivity of QPMBV-APE membrane as a function of temperature.

Prior to APEFC performance test, the MEA was fabricated following a standard procedure [80] detailed in experimental using a 50um QPMBV-APE membrane as electrolyte and QPMBV in ethanol/water solution as ionomer. Pt was used as the catalyst with a loading of 0.4 mg cm^{-2}. Hydrogen and oxygen were used as the fuel and oxidant respectively at 100 ± 2 sccm (standard cm^3 min^{-1}).

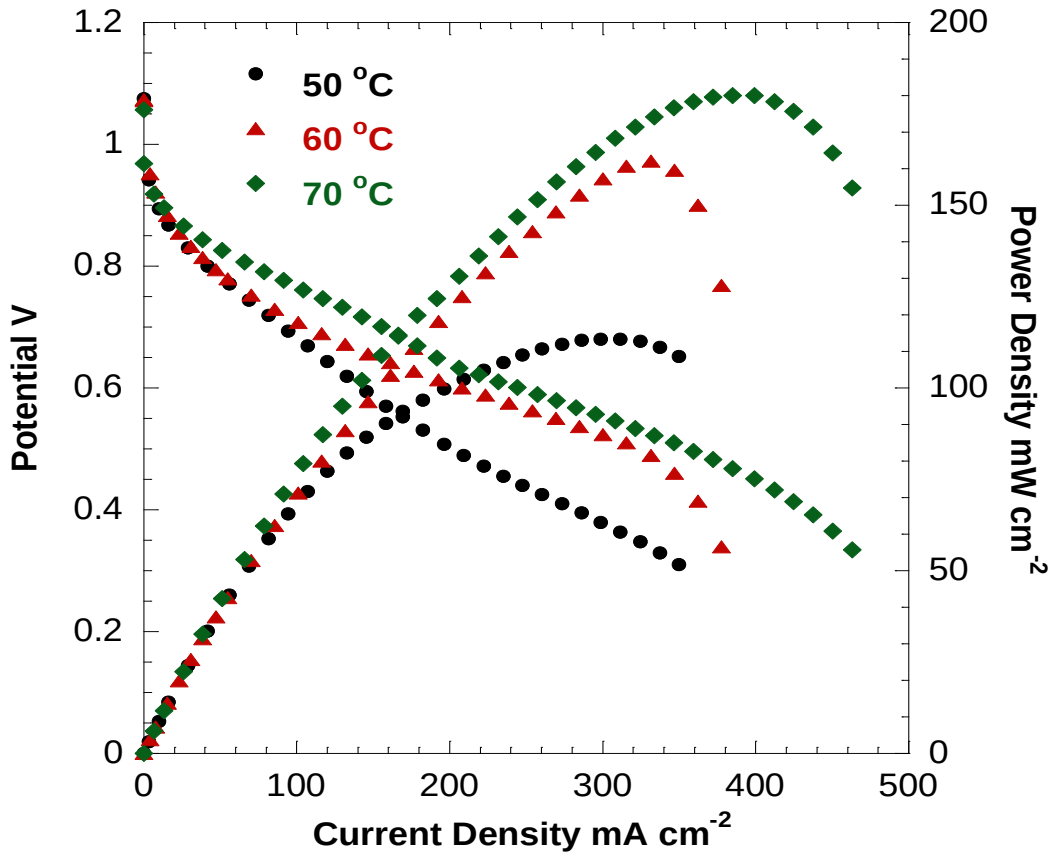

Figure 3.13 Polarization curves of QPMBV-APEFC at 80 % RH.

The performance of QPMBV-APE fuel cells was tested at 80% relative humidity (RH) at various temperatures using a current scan at the rate of 3 mA s^{-1} with 1 atm back pressure. The use of a low current scan rate was to ensure that the fuel cell performance reached steady state. As shown in Figure 3.13, the initial voltage drop (~100 mV) was due to the activation loss mainly from interfacial electrochemical charge transfer reaction in the catalyst layer of the MEA [81]. After the activation loss, the fuel cell voltage deceased gradually with the increase of current density. The fuel cell performance enhanced when the temperature increased from 50°C to 70°C. At 70°C, the current density could reach 500 mA cm^{-2}, and the fuel cell could deliver a

peak power density of 180 mW cm^{-2}. Even at lower temperatures of 60 ℃ and 50 ℃, the fuel cell performance using the QPMBV-APE demonstrated maximum powers of 160 and 115 $mWcm^{-2}$, respectively. This was among the best performances reported for APE membranes [82, 83-86]. The energy output was about 4 time higher than our previous study [70], which can be attributed to the 5 times higher anionic conductivity and twice thinner membrane we used. In spite of less Pt catalyst loading, these advancements warranted the better performance.

3.4 Conclusion

In conclusion, a novel APE was synthesized via miniemulsion copolymerization. Our results indicated that the intentionally incorporated VBC functional groups were almost completely quaternized and ion-exchanged by miniemulsion copolymerization. The exceptional APEFC performance (a peak power density of 180 mW cm^{-2}) showed great potential for this QPMBV-APE.

Not only a promising APE was synthesized, but this study also demonstrated a novel concept: alkaline polymer electrolytes can be designed bottom-up through miniemulsion polymerization with precise selection of functional monomers. Furthermore, miniemulsion copolymerization process is capable to synthesize high molecular weight APE with superior mechanical properties. Controlling the polymerization process and making APE tunable through the polymerization monomer adjustment is the next focus for our approach to obtain the ideal APE.

Chapter 4

Tunable composition and High Molecular Weight QPMBV-APEs for Alkaline Fuel Cells

The results presented in this chapter have been published in the *Macromol. Chem. Phys*:

Y. Luo, J. Guo, C. Wang, D. Chu, "Tunable High Molecular Weight Anion Exchange Membranes for Alkaline Fuel Cells", *Macromol. Chem. Phys*., 212 (2011) 2094.

Featured on Cover

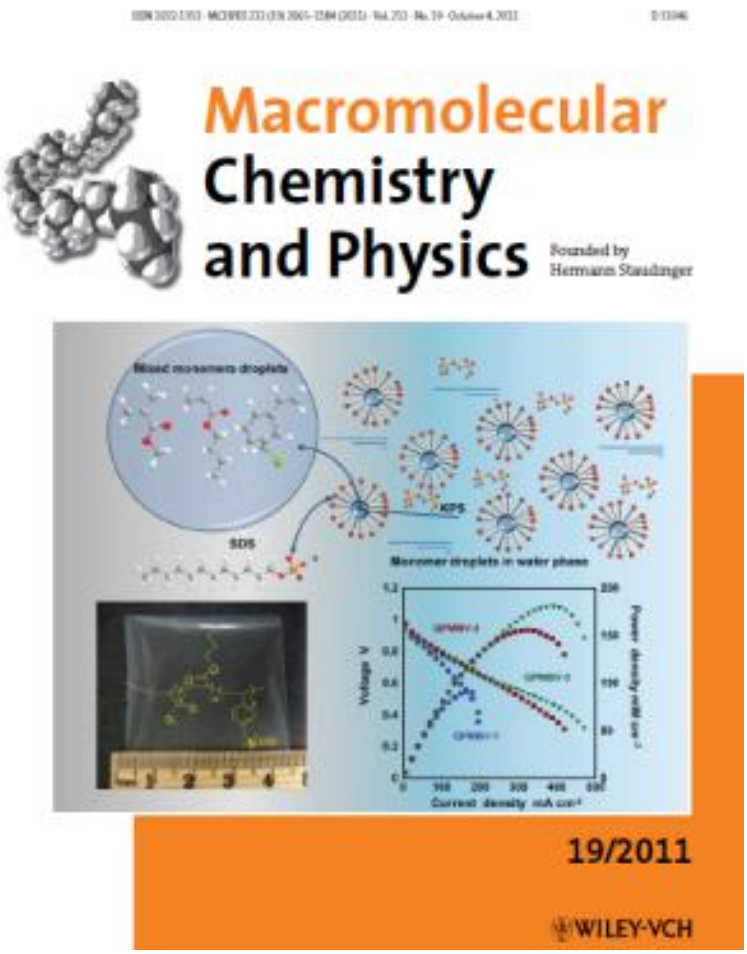

4.1 Introduction

The aforementioned QPMBV in Chapter 3 has shown greatly enhanced molecular weight as well as improved conversion of each monomer in polymerization through miniemulsion copolymerization. This unique polymerization technique therefore is expected to be able to precisely tune the composition by monomer ratio adjustment, which could balance the mechanical properties and conductivity of the resulting APEs. Moreover, it can be used to synthesize high molecular weight QPMBVs to enhance the mechanical properties.

The effects of the QPMBV-APEs composition tuning on the membrane properties and their fuel cell performance would be focused on the following aspects: (1) effects of higher molecular weight on mechanical strength and water uptake (2) The role of VBC incorporation in both conductivity and mechanical strength of the resulting APEs; (3) The influence of Glass transition temperature T_g through composition adjustment in corresponding APEFC durability tests at elevated temperatures; and (4) the water hydrophilicity factor of the non-conductive portion (mechanical support from MMA and BA) of the membrane in mechanical strength of APE membranes.

Only by learning how those factors work on the APE properties, we can further modify and optimize our QPMBV-APE membranes to achieve better performance on APEFCs. Therefore, the objective of Chapter 4 is to synthesize a series of PMBV copolymers with different and adjusted composition, i.e. the ratio of MMA: BA: VBC, to study their effects on resulting APEs, considering those factors above. The correlation between PMBV composition, OH^- conductivity and mechanical strength would be qualitatively investigated.

4. 2 Experimental

4.2.1 Miniemulsion copolymerization of a series designed PMBVs

Three PMBV copolymers with different compositions, denoted as PMBV-1, PMBV-2, and PMBV-3, were synthesized. Miniemulsion was prepared by dispersing mixture of monomers (30 g) with designed ratio (MMA: BA: VBC mol %) and hexadecane (0.12 g) into aqueous SDS solution (0.01 mol L^{-1}, 150 ml) by vigorous agitation while sonication was applied at the same time with a homogenizer (Omni® Sonic Ruptor 400) for 9 min. The copolymerization process was the same as stated in Chapter 3.

4.2.2 Thermogravimetric analysis for PMBV and QPMBVs

Thermogravimetric analysis (TGA, TA Instruments Q500) was used to characterize the thermal stability of the obtained QPMBV-APEs. The heating rate was 10 ℃ min^{-1} under nitrogen protection from room temperature to 600 ℃.

4. 3 Results & Discussion

4.3.1 Miniemulsion Copolymerization of a series of PMBVs

Three PMBV copolymers with different compositions, denoted as PMBV-1, PMBV-2, and PMBV-3, were synthesized. The composition, molecular weight, and glass transition temperature of the obtained PMBVs were listed in Table 4.1.

Table 4.1 Properties of PMBV copolymers via miniemulsion polymerization

	PMBV-1	PMBV-2	PMBV-3
Molar ratios % in monomers [MMA: BA:VBC mol%]	80:10:10	75:10:15	80:5:15
Composition in copolymers [MMA: BA: VBC mol%]	75:12:13	71:11:18	78:5:17
MW [g mol^{-1}]	2.3×10^6	1.8×10^6	1.5×10^6
T_g [^oC][a)]	82	87	101
T_g[^oC][b)]	78.1	80.0	94.3

[a)] Measured experimentally; [b)] Calculated by Equation 3.3.

Composition of the PMBV copolymers was still determined from ^{1}H-NMR spectra. Chemical shifts (δ ppm) of 4.538 (s, 2H, -CH2Cl), 3.983 (s, 2H, -OCH2-) and 3.588 (t, 3H, -OCH3) were the characteristic peaks for VBC, BA and MMA, respectively. Since the characteristic peaks indicated the components in the copolymer, the integrated peak area can be used to calculate the composition of the PMBVs**.** Due to the high yield of the monomers in miniemulsion copolymerization, the synthesized PMBVs had very consistent composition with the monomer ratios as shown in Table 4.1. The molecular weight (MW) of all three PMBV copolymers, as shown in Table 4.1, were all above 10^6 g mol^{-1}, which was almost one order of magnitude higher than those in our previous work by solution polymerization [**70**]. The improvement in MW was attributed to the robust miniemulsion copolymerization process. MW is also vital to improve the APE durability for fuel cell operation as discussed later in detail. The results in Table 4.1 clearly indicated that this miniemulsion copolymerization technique enabled synthesis of high MW copolymer and precise control of the copolymer composition.

4.3.2. Glass transition temperature of PMBVs

APEFCs are typically operated in temperatures under 80 ℃, it is obviously essential to have an APE in glassy state (below T_g) during operation to achieve high durability. The glass transition temperature (T_g) of polymer refers to a temperature below which the polymer chains will have low mobility resulting in higher mechanical strength [87]. In a temperature higher than T_g, polymers will transfer to rubbery state in which polymer chains are in segmental motion, thus leading to unstable mechanical properties. T_g of the obtained PMBV copolymers were measured by DSC as shown in Figure 4.1, and were listed in Table 4.1. The measured T_g results were consistent with the predicted values from the copolymer compositions equation.

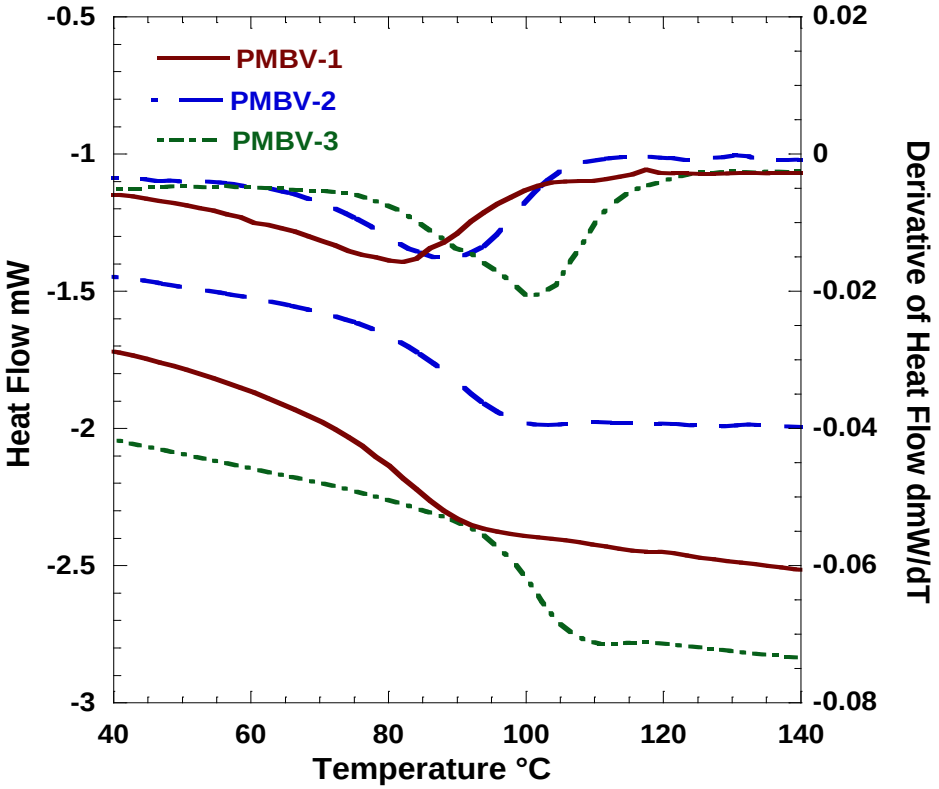

Figure 4.1 DSC spectra of PMBVs.

Homopolymers of MMA and VBC are both glassy polymers with similar T_g above 100 ℃, and homopolymers of BA has a significantly lower T_g at about -49 ℃. PMBV-1 and PMBV-2 copolymers had very similar percentage of BA content, 12 mol% and 11 mol% respectively, which resulted in similar T_g (82 ^{o}C and 87 ^{o}C) of these two copolymers. On the contrary, copolymer PMBV-3 had distinct lower BA content (5 mol%), resulting in much higher T_g of 101 ℃.

4.3.3 Properties characterization of QPMBV-APEs

QPMBV-APEs membranes were obtained by successive steps including quaternization of PMBV copolymers, film casting, ion-exchanging, and washing-drying process. The thickness of all membranes was controlled at 50 μm using an adjustable casting blade. The quaternization degree of VBC in QPMBV-APEs was evaluated using combustion elemental analysis [88]. The combustion elemental analysis demonstrated a completion of quaternization (all VBC groups were quaternized) after 2 hr of quaternization. The obtained QPMBV-APEs were transparent colorless membranes with little swelling in KOH solution (6 mol L^{-1}). The properties of QPMBV-APEs were listed in Table 4.2.

The IEC results in Table 4.2 showed that QPMBV-2 and QPMBV-3 had similar concentrations of OH^- in the membrane. Also, the OH^- concentrations in QPMBV-2 and QPMBV-3 were considerably higher than that in QPMBV-1. The IEC results were consistent with the membrane compositions, as QPMBV-2 and QPMBV-3 had similar (17 mol% and 18 mol% respectively) quaternized VBC groups. Meanwhile QPMBV-1 had 5 mol% less VBC than QPMBV-2 and QPMBV-3.

Table 4.2 Properties of QPMBV-APEs

		QPMBV-1	QPMBV-2	QPMBV-3
Thickness [μm]		50	50	50
IEC [mmol g^{-1}]		1.12	1.32	1.28
Young's Modulus [MPa]		1330	1770	1630
Water uptake [wt. %]*		44.6	197.5	325
Dimensional swelling ratio*	Length [%]	7.8	38.5	31.6
	Width [%]	17.3	52.1	29.0
	Thickness [%]	85.7	116.7	91.7

* The water uptake and dimensional change of the QPMBV membranes were measured at room temperature and fully water saturated condition.

The large difference of water uptakes of these three QPMBV-APEs in Table 4.2 was attributed to their difference in IEC, molecular weight, and composition. For instance, the large difference of water uptakes between QPMBV-1 (44.6 wt.%) and QPMBV-2 (197.5 wt.%) was not solely attributed to the modest difference of IECs of QPMBV-1 (1.12 mmol g^{-1}) and QPMBV-2 (1.32 mmol g^{-1}). The higher molecular weight of QPMBV-1 (2.3×10^6 g mol^{-1} for QPMBV-1 and 1.8×10^6 g mol^{-1} for QPMBV-2) also contributed to the difference in water uptake. Higher molecular weight resulted in less water uptake of the QPMBV-AAEM membrane. Comparing QPMBV-2 with QPMBV-3, in this case the difference of their IECs was even smaller, 1.32 mmol g^{-1} and 1.28 mmol g^{-1}, respectively. Therefore, the much higher water uptake of QPMBV-3 membrane was induced by a combination of its lower molecular weight, and its higher MMA content (78 mol%) and lower BA content (5 mol%) than QPMBV-2 (71 mol% and 11 mol% of MMA and BA, respectively). As monomers, the solubility of MMA in water is 15 g L^{-1} [89], which is ten times higher than the

water solubility of BA that is 1.4 g L-1 [89]. Therefore, higher water uptake of QPMBV-3 membrane was induced by more MMA and less BA composition, and lower molecular weight. The high water uptake of QPMBV-2 and QPMBV-3 could be drastically reduced by crosslinking process using divinylbenzene as the crosslinking agent, without scarifying the anionic conductivity.

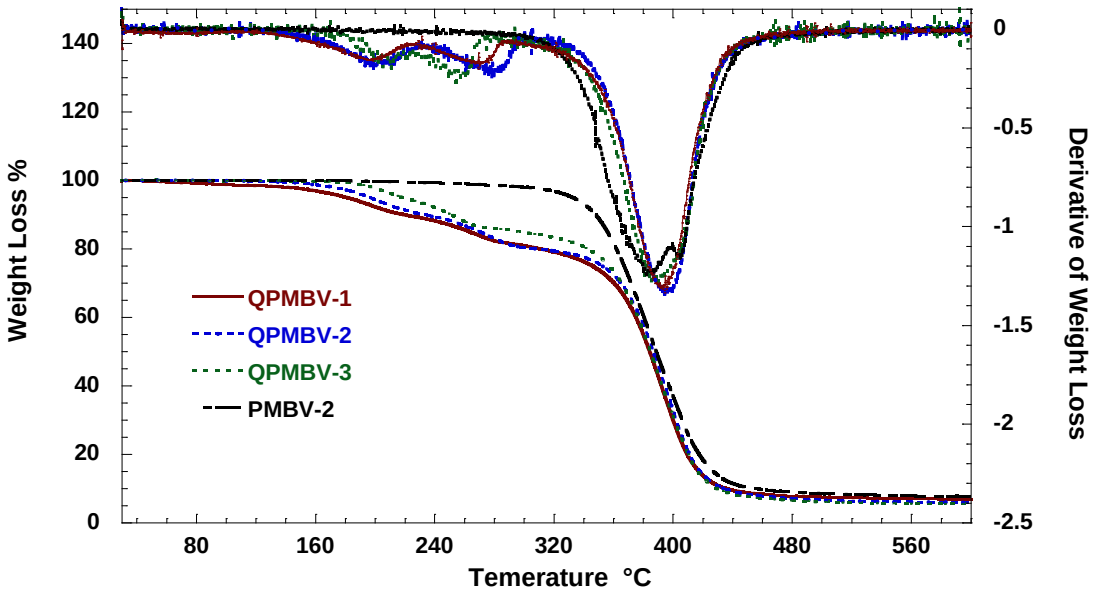

Figure 4.2 TGA curves of PMBV and QPMBV copolymers.

The thermal stability of the QPMBV-APEs was characterized by the TGA as shown in Figure 4.2. The weight loss vs. temperature curve for a precursor polymer, PMBV-2, was also shown in Figure 4.2 as comparison. The only weight loss for PMBV-2 took place at 390 ℃, which was due to the degradation of polymer chains. For the QPMBV-AAEMs, they all followed a similar weight loss transition pattern. The first transitions all began from 160 to 240 ℃, which was probably corresponded to the removal of -CH_3 on the quaternary ammonium groups [90]. The successive weight loss transition was from 240 to 310 ℃, which was due to the removal of quaternary

ammonium groups from polymer chains [91]. The last visible weight loss transition was around 390 ℃, indicating the decomposition of QPMBV polymer chains. The TGA analysis indicated that the QPMBV-APEs were thermally stable under 160 ℃ without degradation of the functional groups. The thermal stability of our QPMBV-APEs was similar to APEs synthesized from chloromethylation of phenyl structured polymers including poly (arylene ether sulfone) (QAPSF) [92] and chloroacetylated poly (2,6-dimethyl-1,4-phenylene oxide) with bromomethylated poly(2,6-dimethyl-1,4-phenylene oxide) [93]. The mechanical strength of QPMBV-APEs was also measured by tensile test using DMA. The high Young's modulus (>1 GPa) of our QPMBV-APEs was comparable to those synthesized from chloromethylation of polysulphone (QAPS) [94].

The conductivities of QPMBV-APEs were shown in Figure 4.3. The temperature and humidity were controlled using Arbin® fuel cell test station, as well as the fuel cell performance testing. The conductivity increased as the temperature went up from 50 to 80 ℃. QPMBV-2 and QPMBV-3 could reach the highest conductivity around 4×10^{-2} S cm^{-1} at 80 ℃ with 80% relative humidity (RH), while the highest conductivity of QPMBV-1 was 1.9×10^{-2} S cm^{-1} at the same conditions. The two-fold lower conductivity of QPMBV-1 was due to its lower IEC and lower water uptake. The high conductivity of our QPMBV-APEs, especially QPMBV-2 and QPMBV-3, was better than that of the AAEMs synthesized by chloromethylation of poly(2, 6-dimethyl-1,4-phenylene oxide) (0.035 S cm^{-1} at 90 ℃) [95], poly (tetrafluoroethene-co-hexafluropropylene) (0.03 S cm^{-1} fully hydrated at 30 ℃) [96], and polysulfone-methylene quaternary phosphonium hydroxide (TPQPOH, 0.027 S cm^{-1} fully

hydrated at 30 ℃) [97]. The activation energy of our QPMBV-APEs was around 50 KJ mol^{-1}, which was similar to the QAPSF APEs (43.8KJ mol^{-1}) [98]. Both mechanical properties and conductivities indicated our tuned QPMBV-APE as a great candidate for APEFC application.

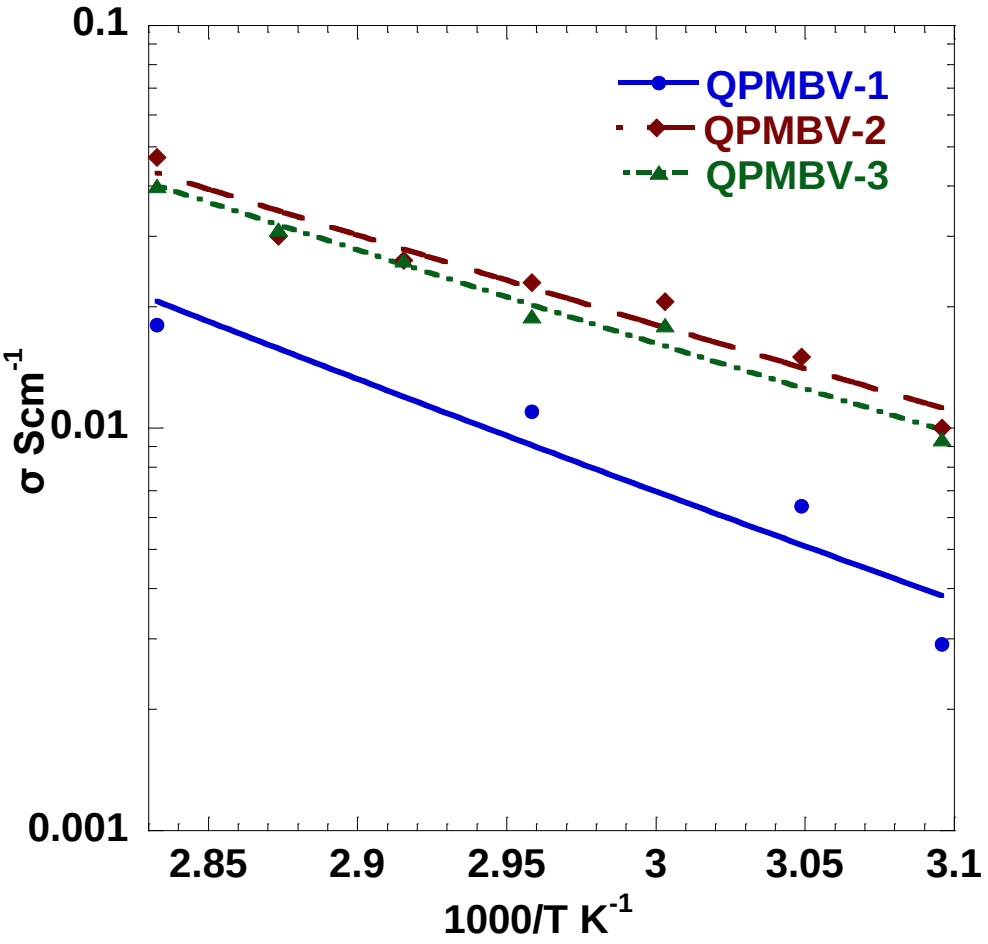

Figure 4.3 Conductivities for QPMBVs at 80% RH.

4.3.4 Fuel cell performances

With the demonstrated high mechanical strength and anionic conductivity, exceptional fuel cell performance can be expected from the QPMBV-APE fuel cells. Figures 4.4 and 4.5 were the polarization performances of APEFCs using QPMBV-APEs.

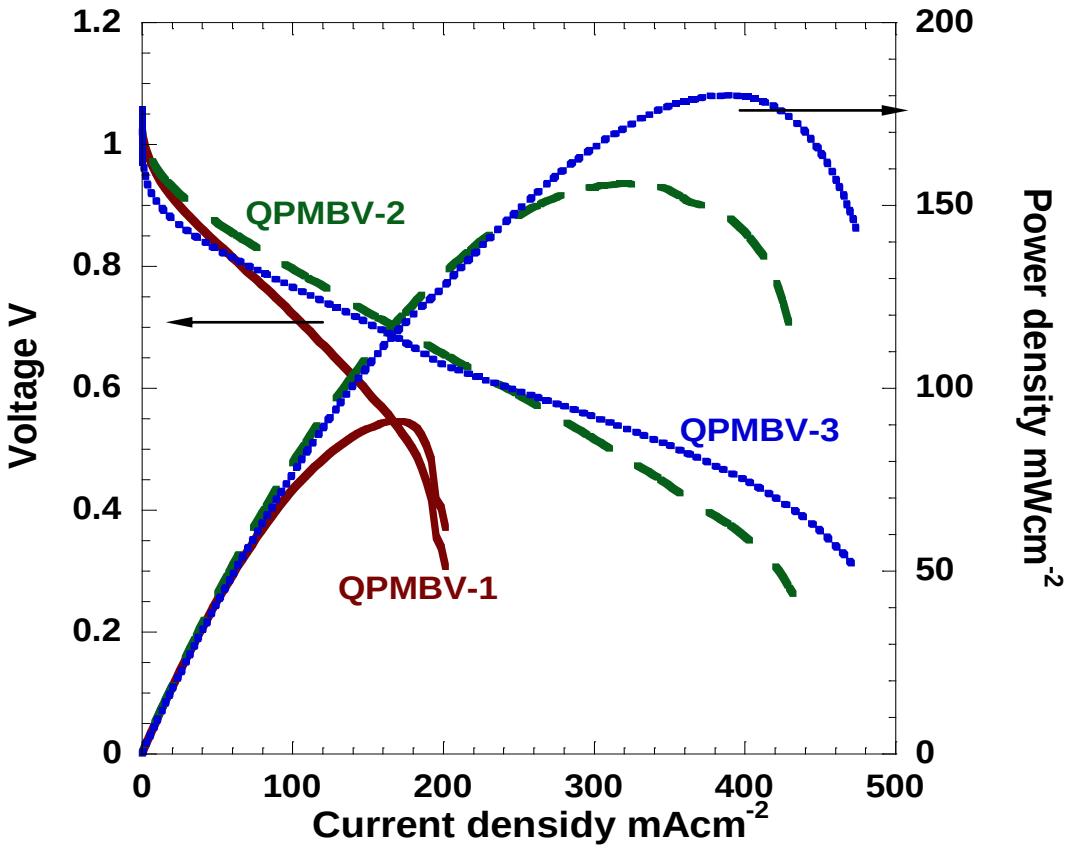

Figure 4.4 Polarization curves for QPMBVs at 70 ℃ and 80% RH.

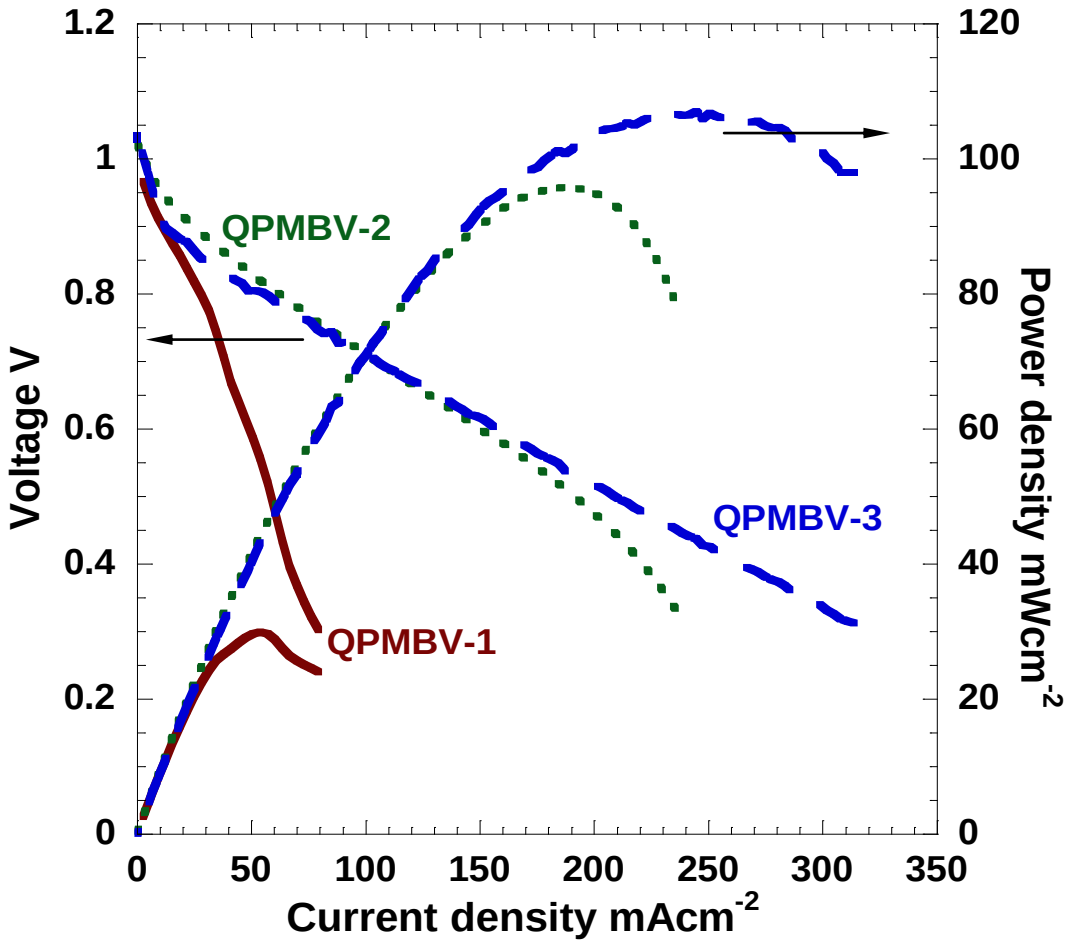

Figure 4.5 Polarization curves for QPMBVs at 60 ℃ and 80% RH.

The performance of QPMBV fuel cell was increased with increasing temperature. The QPMBV-3 membrane delivered peak power density of 180 mW cm^{-2} at 0.45 V and maximum current density of 500mA cm^{-2} at 70 ℃. The deliverable power density of the QPMBV-APEs was 80 mW cm^{-2} higher than that of QAPS membranes [99], and was also comparable to that of TPQPOH membranes (250 mW cm^{-2}) [92]; however, which was achieved with a much higher back pressure (3 atm). The relatively lower power output of QPMBV-1 was due to its lower anionic conductivity as described previously. The polarization performance of QPMBV-3 was also better than QPMBV-2 due to its lower BA content and higher MMA content. As previously

mentioned, more relatively hydrophilic composition of QPMBV-3 membrane could attract more water thus facilitating polarization performance. As shown in Figure 4.4, QPMBV-2, with 6 mol% more BA and 7 mol% less MMA compared with QPMBV-3, showed a slightly higher ohmic loss and a clearly earlier concentration loss. Same behavior was also observed in Figure 4.5 at a lower temperature of 60 ℃.

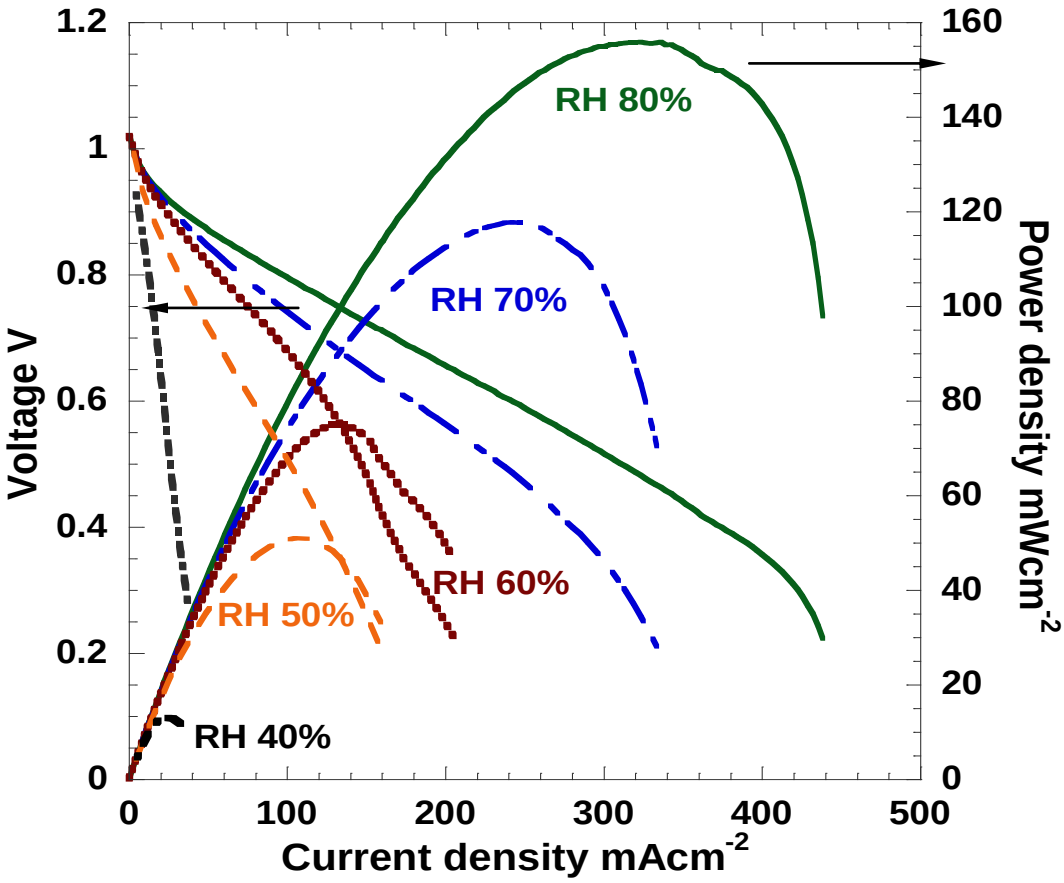

Figure 4.6 Polarization curves of QPMBV-2 at 70 ℃ and different RH.

Besides the temperature effect, RH effects on the polarization behavior of APEFCs were also investigated. It was shown in Figure 4.6 that lower RH resulted in decreased performance of APEFCs, as both ohmic loss and concentration loss exacerbated. This distinct dependency on RH illustrated that water retention was

important for OH^- transport in APE membranes. To ensure an energy density higher than 50 mW cm^{-2} in our APEFC system, minimum 50% RH was required.

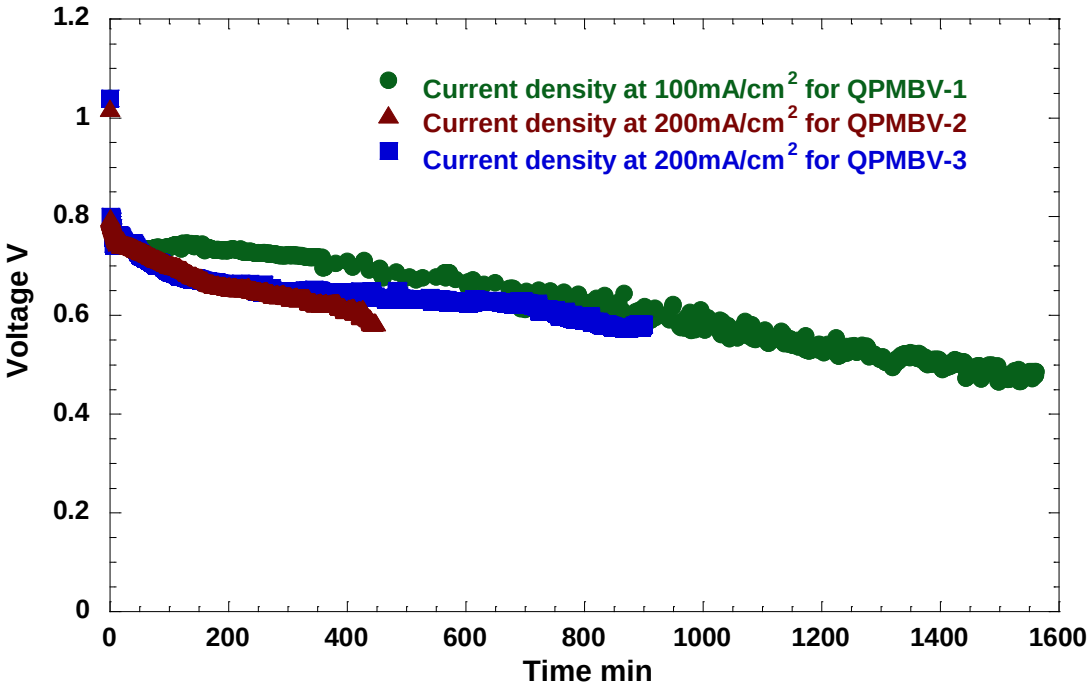

Figure 4.7 Durability test for QPMBVs at 70 ℃ and 80% RH.

To date, little investigation on membrane durability has been conducted on APEFCs. However, this test is of great importance for the long term prospect of APEFCs. In this study, the effect of different compositions on durability of QPMBV-APEs was tested. Specifically, QPMBV-2 and QPMBV-3 were tested at the current density of 200 mA cm^{-2}, and QPMBV-1 was tested at the current density of 100 mA cm^{-2} due to its lower current at the peak power density. From Figure 4.7, the corresponding stable voltage was around 0.7 V, which was consistent with the data shown in the polarization curves in Figure 4.4. The durability performance showed that QPMBV-3 could deliver stable current for 15 hours while QPMBV-2 could deliver 8 hours under the same operating conditions and very similar conductivities. The better durability of

QPMBV-3 compared to QPMBV-2 was attributed to its higher glass transition temperature, i.e. a more rigid APE in the working environment could help improve the durability. The QPMBV-1 membrane delivered the best durability performance despite the lower current density. It was shown in Figure 4.7 that 26 hours of stable current delivering was achieved by QPMBV-1. This was obviously due to its lower VBC content, i.e. water uptake, as well as the highest molecular weight among these three membranes.

4.4 Conclusion

A series of QPMBV-AAEMs were synthesized with designed composition using miniemulsion copolymerization. Our QPMBV-APEs demonstrated one of the best overall performance including high deliverable power density and durability. Moreover, the simple and robust synthesis technique and low cost materials provide a promising alternative to current APE technologies.

The effects of the QPMBV-APE composition on the membrane properties and their fuel cell performances can be summarized as follows: (1) Higher molecular weight can improve the mechanical strength of the membrane, as well as reduce the water uptake; (2) Higher concentration of the anionic conductive sites (i.e. VBC in our membranes) can improve the conductivity but at same time impair the mechanical properties; (3) increasing the glass transition temperature of the copolymer by lowering the low T_g content can improve the membrane durability working at elevated temperatures; and (4) the water hydrophilicity of the non-conductive portion (mechanical support) of the membrane is also of great importance to the water uptake, i.e. mechanical strength of the APE membranes.

Therefore, due to these complex composition effects, one particular APE membrane should be precisely designed and synthesized to optimize its performance. For instance, MMA can be replaced by another monomer with similar or higher polymer glass transition temperature and less hydrophilicity. Meanwhile, the feasibility of achieving high molecular weight and the processibility of the copolymer has to be considered. For this particular QPMBV-APE system, to further enhance both mechanical strength and conductivity, an interpolymer network (IPN) will be applied

to make the crosslinked QPMBV-APE membranes. The crosslinking agent will be used to improve the mechanical support by holding QPMBV in the network. More VBC could be incorporated into the QPMBV matrix to enhance the conductivity without sacrificing the mechanical strength.

Chapter 5

Kinetics Factors in Copolymerization of APEs for Alkaline Fuel Cell Application

The results presented in this chapter have been published in the *J. Membr. Sci*:

Y. Luo, J. Guo, Y. Liu, Q. Shao, C. Wang, and D. Chu, "Copolymerization of Methyl Methacrylate and Vinylbenzyl Chloride towards Alkaline Anion Exchange Membrane for Fuel Cell Applications", *J. Membr. Sci.*, 423-424(2012)209.

5.1 Introduction

Our previously investigated quaternized poly (methyl methacrylate-co-butyl acrylate-co-vinylbenzyl chloride) (QPMBV) APE showed exceptional fuel cell performance. Different monomer ratios have been tried to adjust the components in copolymers thus tailoring the properties of the QPMBV-APEs. However, in-depth investigation of miniemulsion copolymerization for this particular ternary system is still not developed. Most conditions in previous experiments, including surfactant and initiator for the polymerization was just referenced from a MMA-BA miniemulsion copolymerization system [75] and thus has not been optimized for the proposed copolymer.

Therefore, the focus of this study is to investigate in detail a number of fundamental polymerization factors to learn the correlation between the functional copolymer

components and the corresponding properties in APEs. In the present Chapter, we also increased the T_g of copolymer precursors by eliminating butyl acrylate from monomers, which was a low T_g component. Molecular weight was further optimized through investigating binary copolymerization kinetics after removal of butyl acrylate. The newly obtained binary copolymer is named poly (methyl methacrylate-co-vinylbenzyl chloride) (PMV). We specifically focus on the role of monomer composition drift adjustment in electrochemical conductivity and the effect of molecular weight enhancement on mechanical strength in this newly developed PMV-APE system.

5.2 Experimental

5.2.1 Miniemulsion copolymerization of PMV

Miniemulsion polymerization was prepared by dispersing 30g methyl methacrylate (MMA) and vinylbenzyl chloride (VBC) mixture and 0.12g hexadecane (HD) into 150 ml aqueous sodium dodecyl sulphate (SDS) solution by ultra-sonication. The polymerization was initiated by injection of potassium persulfate (KPS) into the miniemulsion at 70℃ under nitrogen protection. The reaction was terminated after 4 hrs by quenching in an ice bath. The copolymer was filtered and dried in vacuum overnight.

5.2.2 Morphology characterization

AFM (AppNano ACT-SS-10) was used to characterize the morphologies of the pure polymer membrane, quaternized membrane, and crosslinked quaternized membrane.

Static mode of the cantilever with an n-type silicon tip was forced on the spin-coated membrane on a silicon wafer to collect the image from a laser deflection.

5.3. Results & Discussion

5.3.1 Composition drift effect

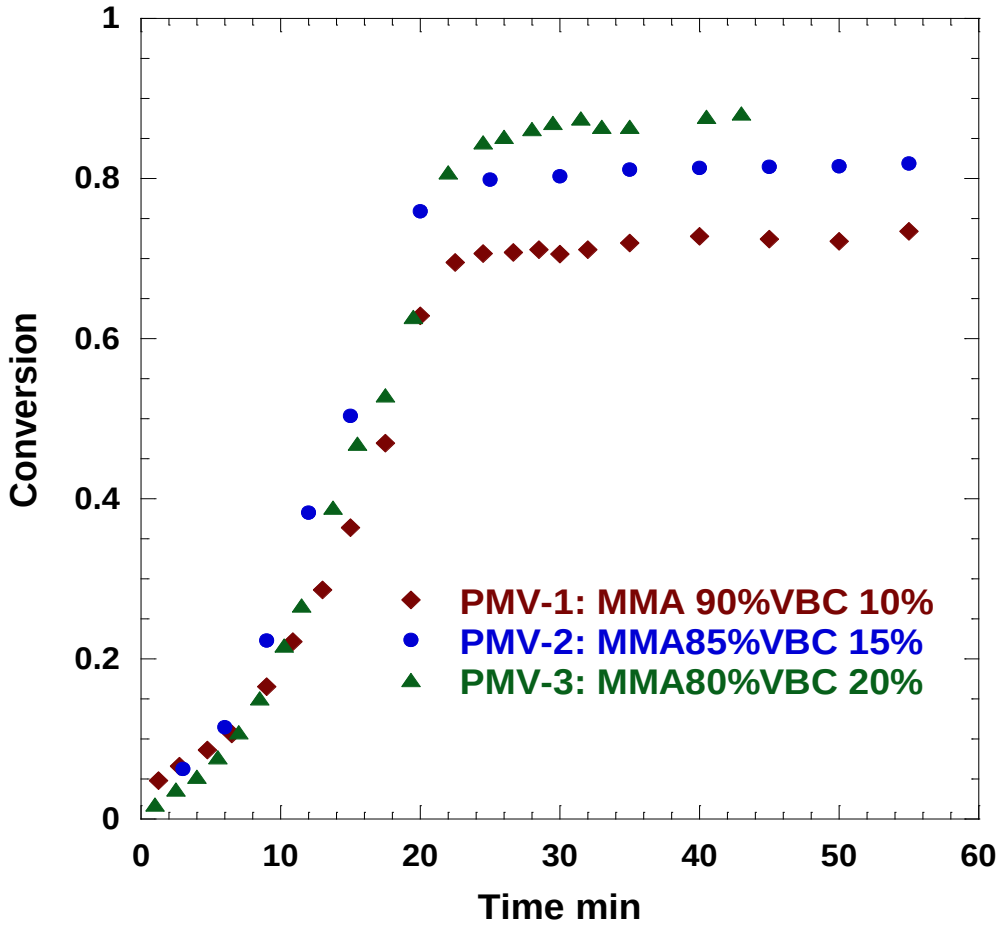

Figure 5.1 Overall monomer conversion with various compositions in copolymerization.

Three PMV copolymers with various compositions were synthesized by miniemulsion copolymerization. Figure 5.1 showed the overall conversion of monomer as a function of reaction time. It was obvious that the conversion for all

three samples increased rapidly in the initial polymerization time, and then leveled off after approximately 25 minutes. The difference in final conversion with various compositions could be attributed to the Trommsdrorff effect [100], which was common in MMA included polymerization for its self-acceleration phenomenon. As shown in Figure 5.1, decreasing in MMA component resulted in higher overall conversion of monomers.

The correlation between reactivity ratio of monomers and monomer concentration fraction could be expressed as Equation 5.1 [101], when the conversion of monomers was lower than 5% (in the first 5 minutes of reactions). In the low conversion range, the fraction of unreacted monomer in the system at an instant moment can be assumed to be the same as the initial monomer fraction. The monomer fraction in polymer can be simply obtained from integration of copolymer composition that was measured from ^{1}H-NMR spectra.

$$r_2 = f_1^0\{\frac{1}{F_1}(1+ f_1^0 r_1) - 1\} \qquad [5.1]$$

Where r_2 is the reactivity ratio of VBC and r_1 is the reactivity ratio of MMA; f_1^0 is the initial monomer fraction of MMA in mixture of MMA and VBC; F_1 is the MMA composition in the copolymer calculated from ^{1}H-NMR spectra.

The Mayo-Lewis plot [26] was plotted in Figure 5.2 based on Equation 5.1 with 3 different initial monomer fractions (QPMV-1, 2, and 3 as in Table 5.1). The intersection point gave the value of reactivity ratios of MMA and VBC. The reactivity ratio indicated the relative preference of radical monomers reacting to its own kind

over the other monomer. It was shown in Figure 5.2 that the reactivity ratios of both MMA and VBC were lower than 1 (approximately 0.3 and 0.7, respectively), indicating the tendency for a random copolymer. Moreover, r_1 was two times lower than r_2, indicating that VBC was more likely to be polymerized in the initial stage of the copolymerization, while MMA was likely to be self-polymerized later in the system.

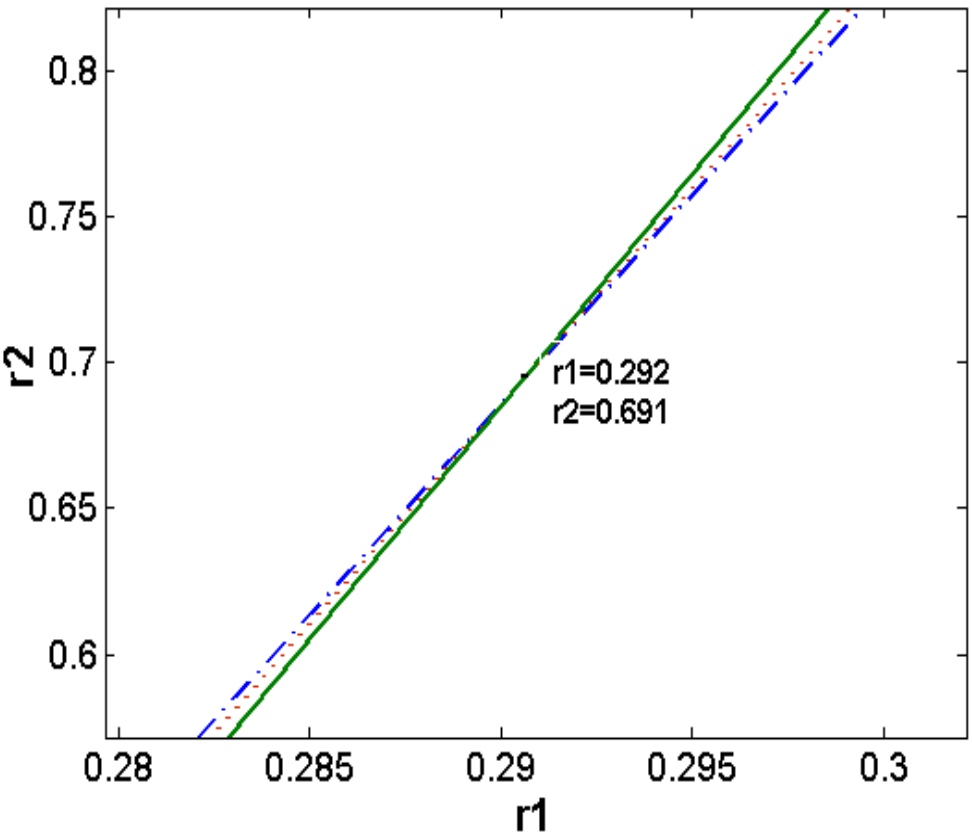

Figure 5.2 Reactivity ratios for MMA and VBC (r_1: MMA; r_2: VBC).

Once reactivity ratios were obtained, copolymer composition drift from the unreacted monomers fraction could be established by Equations 5.2 and 5.3. f_1 is the instantaneous unreacted MMA monomer fraction in the system, which could be related to conversion through the mass balance between the monomers and the

obtained copolymer, as rearranged in Equation 5.2. F_1 is the MMA fraction in the copolymer as expressed in Equation 5.3.

$$C = 1 - [\frac{f_1}{f_1^0}]^{\frac{r_2}{1-r_2}} [\frac{1-f_1}{f_2^0}]^{\frac{r_1}{1-r_1}} [\frac{f_1^0 - \frac{1-r_2}{2-r_1-r_2}}{f_1 - \frac{1-r_2}{2-r_1-r_2}}]^{\frac{1-r_1 r_2}{(1-r_1)(1-r_2)}} \quad [5.2]$$

Where f_1^0 and f_2^0 are the initial monomer fraction of MMA and VBC, respectively.

$$F_1 = \frac{f_1^0 - (1-C) f_1}{C} \quad [5.3]$$

From Equations 5.2 and 5.3, f_1 and F_1 can be plotted as functions of C, as shown in Figure 3. The calculated F_1 vs. C was consistent with the ^{1}H-NMR measurements from the conversion test samples. From Figure 3, the important information was that the resulting copolymer composition after polymerization was determined when f_1 approached to 1 and conversion reached its limit. Moreover, the MMA composition in the copolymer was all around 5% less than the initial MMA fraction in the monomer mixture, as denoted in Figure 3.

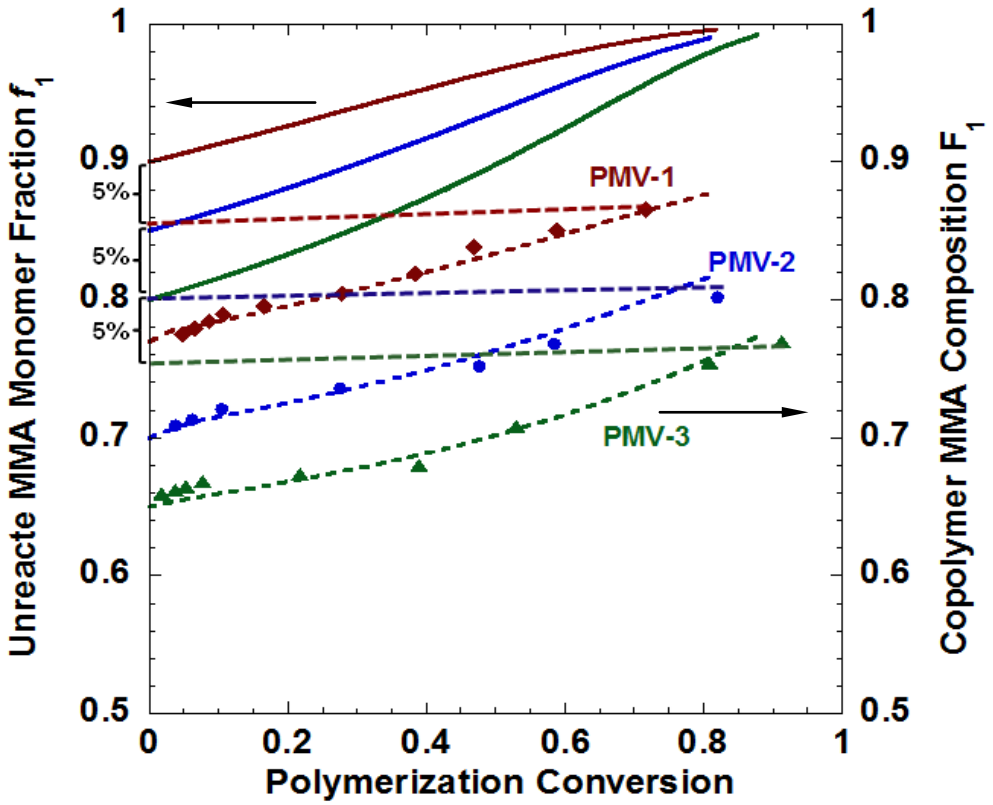

Figure 5.3 Correlation of unreacted monomer fraction f_1 (solid line) and the composition in the resulted copolymer F_1 (dotted line) as a function of conversion C.

Therefore, the simple correlation between copolymer composition and the initial monomer fraction was disclosed in Figure 5.3. At the very beginning of the polymerization, copolymer composition was around 15% lower than the initial monomer fraction, as the conversion was close to zero. As the polymerization approached to the end of conversion, the composition of the copolymer became all around 5% lower than the initial monomer fraction. This investigation established the simple relation between composition in copolymer and the monomer fraction, which guided us to design the composition in copolymer as needed by initial adjustment of monomer fraction, not only qualitatively but also quantitatively.

The properties of the obtained membranes including conductivity and water uptake at room temperature were listed in Table 5.1. The ionic conductivity of QPMV membranes as function of temperature was shown in Figure 5.4. The conductivity in Figure 5.4 demonstrated that increasing in VBC component enhanced the conductivity. The highest conductivity could reach 0.1 S cm^{-1} for the sample with 20% VBC at 80℃. However, the water uptake results indicated that all three membranes have high swelling ratios that increased with increasing VBC content, which made them unrealistic for fuel cell operation. To address this problem, we enhanced the molecular weight and crosslinked the polymer to improve the mechanical properties, which will be detailed in Chapter 6. Initial monomer mixture with 10 mol. % VBC and 90 mol. % MMA was chosen to be carried out in the study, as it had the lowest water-uptake before improvement.

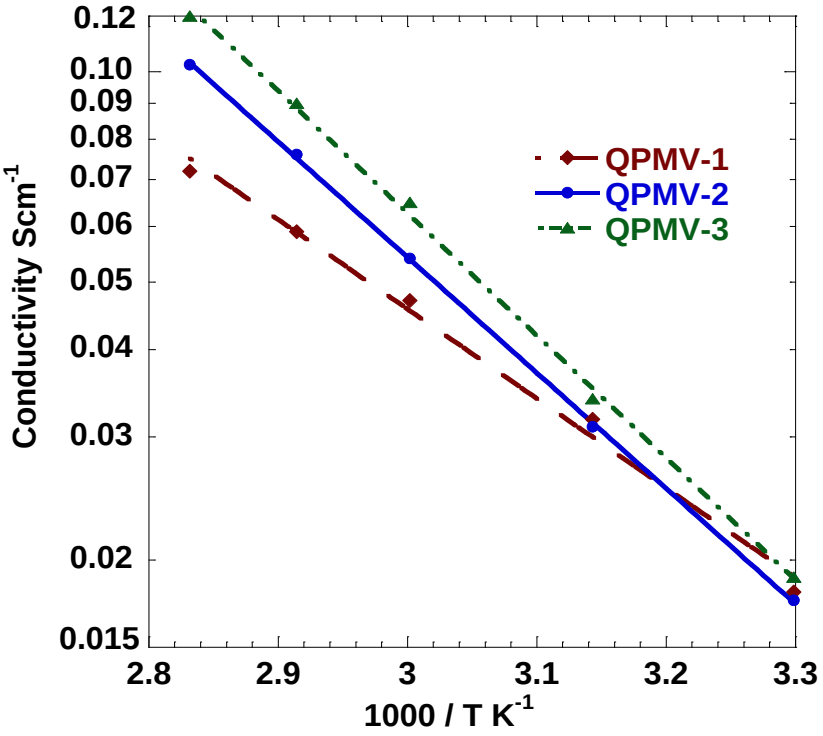

Figure 5.4 Conductivities for various compositions of PMVs.

Table 5.1 Properties of QPMVs.

Copolymer PMV and quaternized QPMV	Initial Composition (MMA:VBC mol%)	Molecular weight (10^6g/mol)	Conductivity in saturated water at RT 10^{-2} S/cm	Water-uptake (%)	Young's modulus (GPa)
1	90:10	2.5	1.72	197.0	2.3
2	85:15	2.4	1.80	362.3	2.2
3	80:20	2.4	1.89	646.3	2.4
4	90:10	4.1	1.69	186.1	2.7
5	90:10	6.6	1.73	190.8	3.3

5.3.2 Molecular Weight Optimization

Increasing molecular weight can effectively improve the mechanical strength of the QPMV membranes [70,102]. In this study, the effects of the concentration of initiator and surfactant used in copolymerization on the molecular weight were investigated.

As illustrated in Figure 5.5, decreasing in KPS concentration, i.e. lower free radical concentration, certainly led to higher molecular weight. Less KPS initiators would have less primary free radicals available in the copolymerization system, while monomers concentration remained the same. Therefore, each polymer chain was enlarged by attaching more monomers, resulting in an increased molecular weight. It was shown in Figure 5.5 that KPS concentration at 0.025 mol L^{-1} could result in a

molecular weight of 4×10^6 g mol^{-1}. When KPS concentration was fixed at 0.025 mol L^{-1}, the concentration of surfactant, SDS, also demonstrated influence on molecular weight as shown in Figure 5.6. Increase in SDS concentration would increase the molecular weight. More SDS in the system would decrease miniemulsion monomer droplet size, confirmed by DLS test as shown in Figure 5.6. With a decrease in droplet size, the number of droplets increased. Therefore, the number of free radical relative to one droplet decreased, which also resulted in less polymer chains with higher molecular weight.

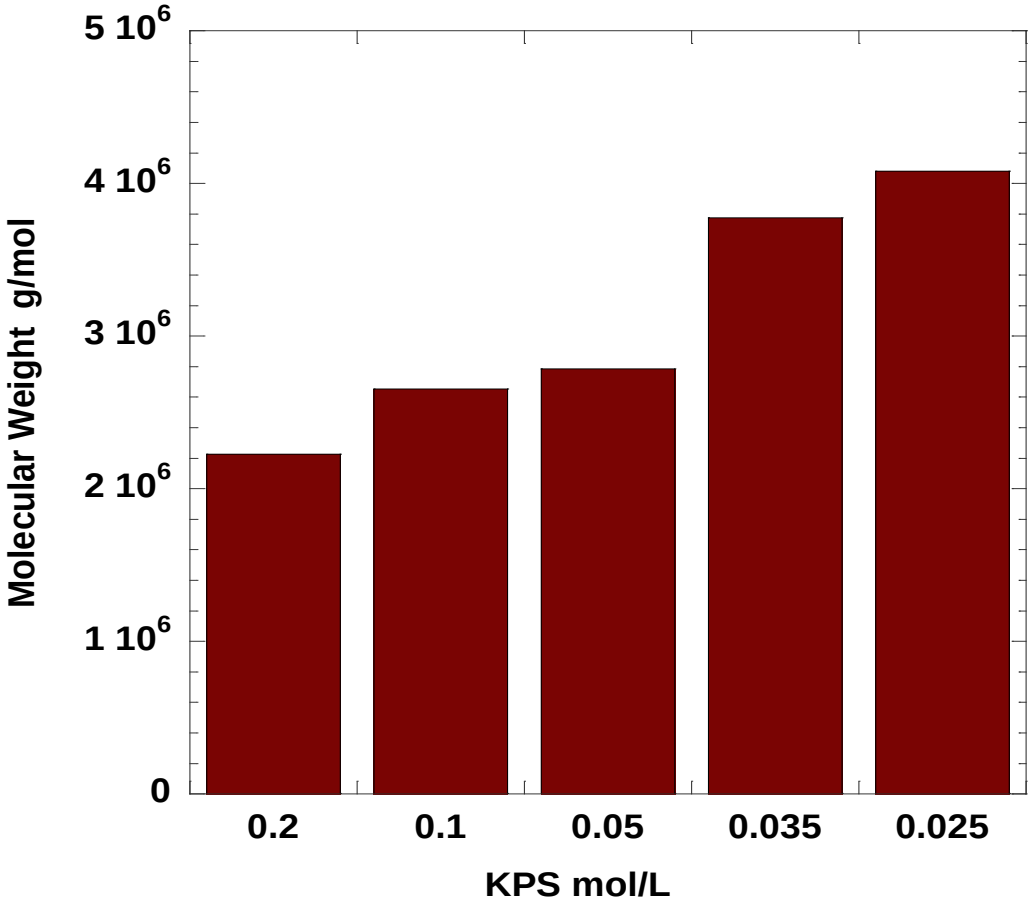

Figure 5.5 KPS impact on molecular weight.

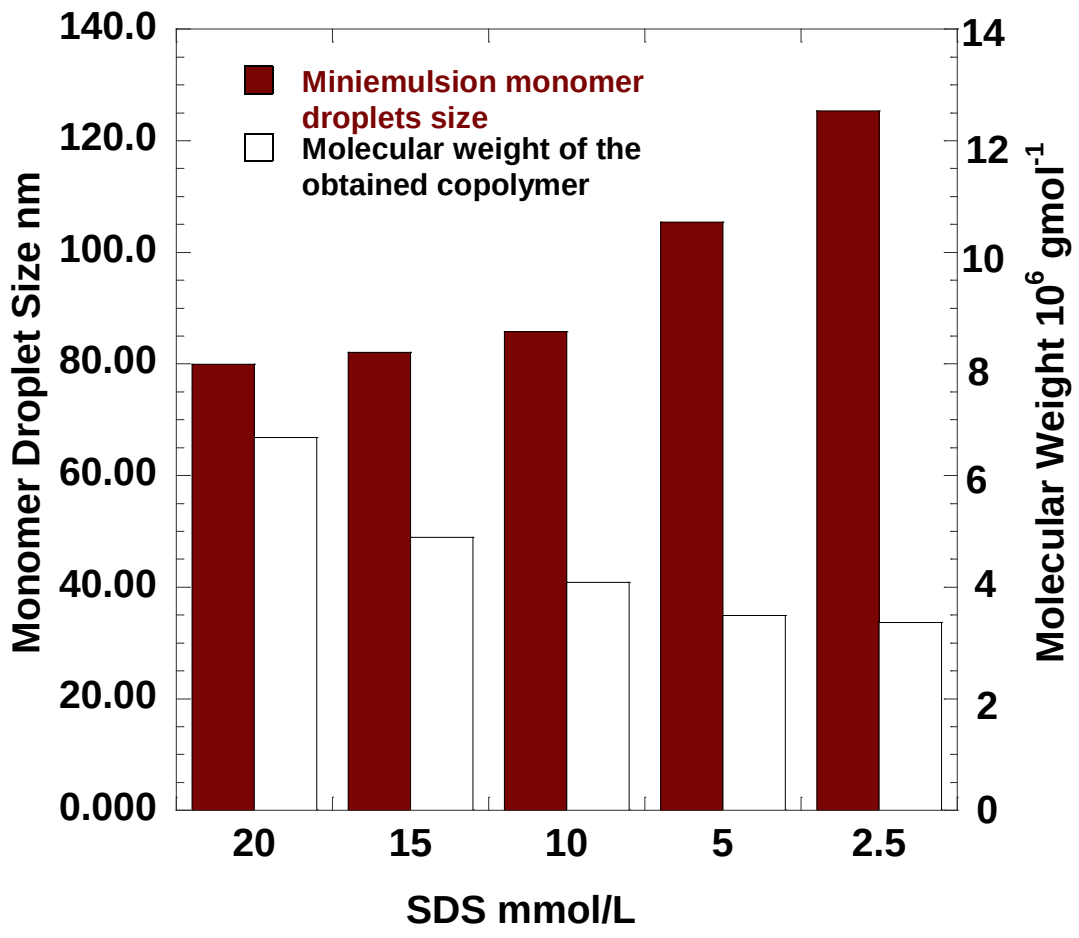

Figure 5.6 SDS impact on molecular weight at a fixed KPS of 0.025 mol/L.

After the optimization, the molecular weight could reach 6.6×10^6 g mol^{-1}. The morphology of this polymer was further characterized by AFM after spin coating as a thin film. Figure 5.7 (a) and (c) were the topography and phase images of optimized PMV respectively. Figure 5.7 (b) and (d) were the 3D topography and phase images respectively. It was shown from Figure 5.7 that the copolymer could form a homogeneously smooth and dense PMV membrane with little ionic channels, as compared to the membranes after processing and crosslinking, which will be discussed in detail in Chapter 6.

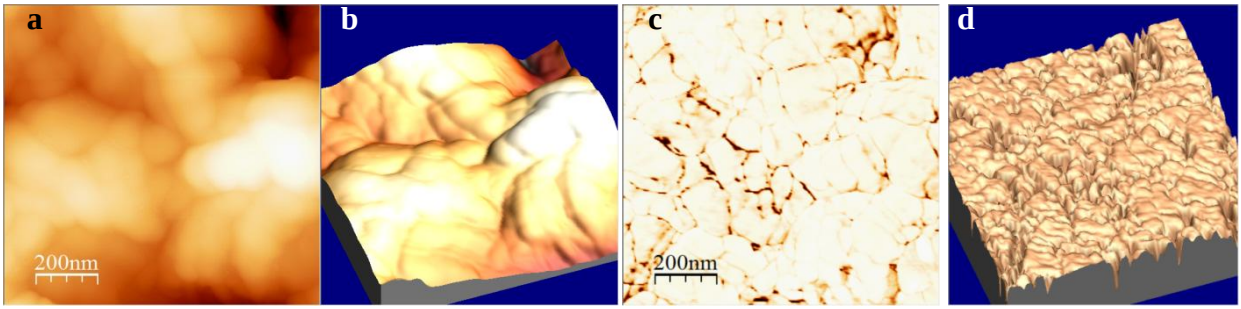

Figure 5.7 AFM images for optimized PMV. (a) the topography, (b) the 3-D topography, (c) phase images, and (d) 3D phase images of optimized PMV.

The conductivity and mechanical strength of the QPMV membranes with the same composition but different molecular weight were tested and shown in Figures 5.8 and 5.9, respectively. The electrochemical conductivities shown in Figure 5.8 indicated that molecular weight of QPMV polymer did not change the ionic conductivities.

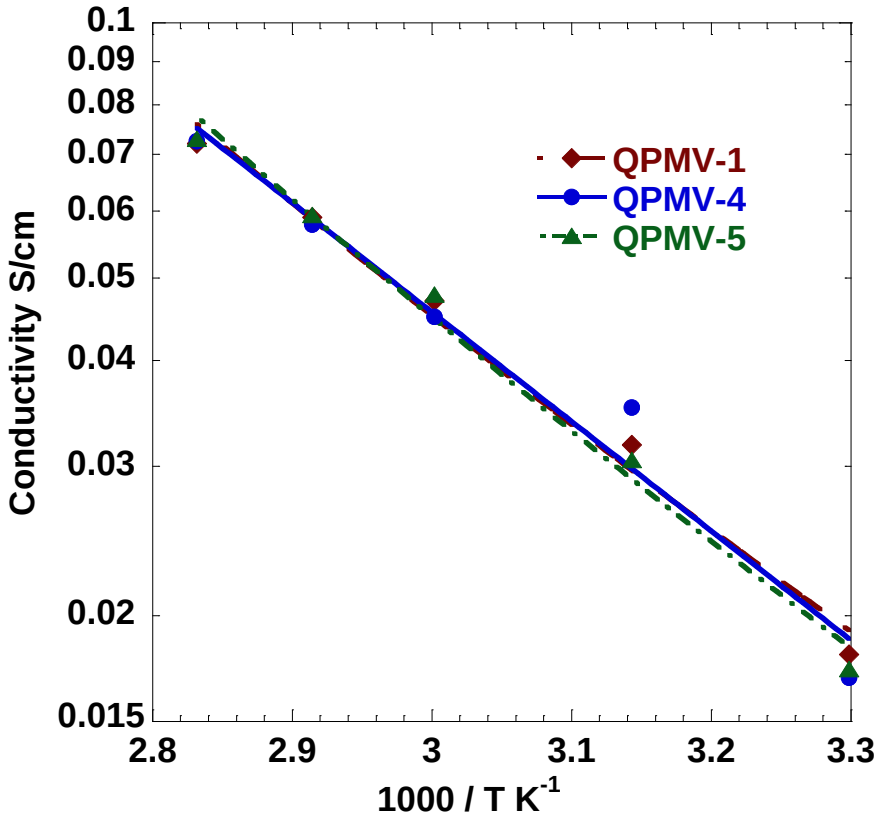

Figure 5.8 Conductivities for QPMVs with various molecular weights

However, both Young's modulus and tensile strength of the membranes were increased as the molecular weight increased as seen in Figure 5.9. The optimized QPMV-5 had the highest Young's modulus of 3.3 GPa and the highest tensile strength of 29.5 MPa, which implied a strong and tough membrane material. The water uptakes were also listed in Table 5.1. It was shown that molecular weight did not influence much on water-uptake, which indicated that water-uptake was mostly dependent on the hydrophobic and hydrophilic composition. To further lower the water uptake, which was critical in fuel cell application, the crosslinking method would be employed.

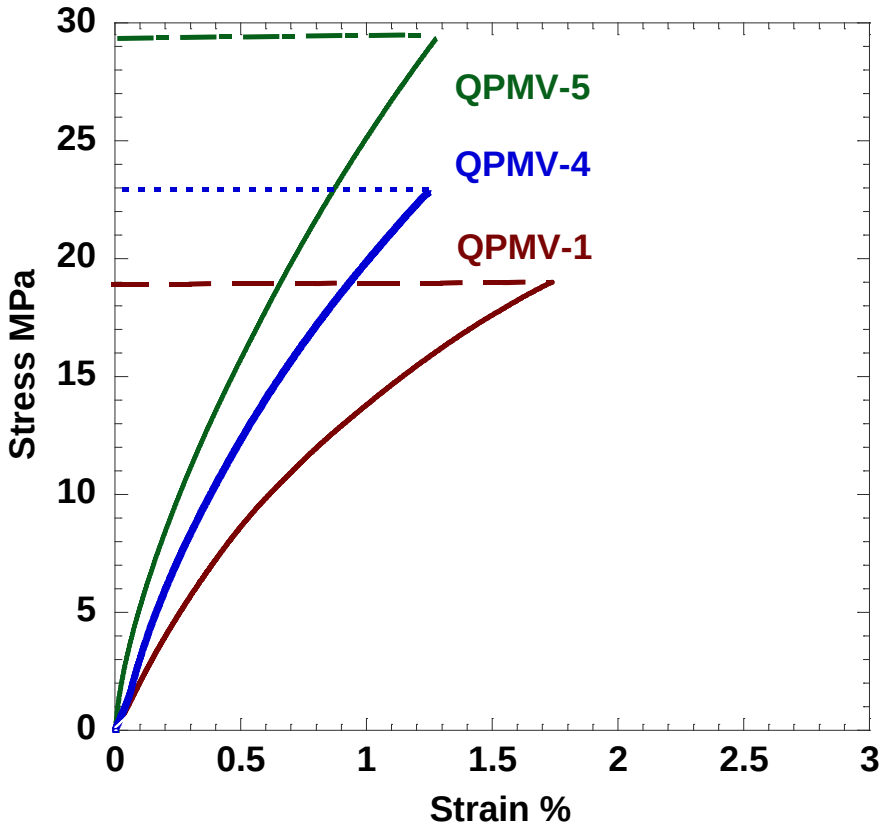

Figure 5.9 Tensile tests for PMVs with various molecular weights

To demonstrate the feasibility of the APE for practical APEFC applications, the optimized APE, QPMV-5 was tested in a fuel cell assembly for its polarization performance and power density. Prior to fuel cell tests, the dry metal-ion free APE was sandwiched by two 5 cm^2 catalyst loaded (Pt loading of 0.4 ± 0.05 mg cm^{-2}) carbon papers by hot-press. Hydrogen and pure oxygen was used as the fuel and oxidant in the test, respectively. The obtained polarization curve was plotted in Figure 5.10, which demonstrated the maximum current density of 300 mA cm^{-2} at 70 ℃ with a peak power density of 80 mW cm^{-2}.

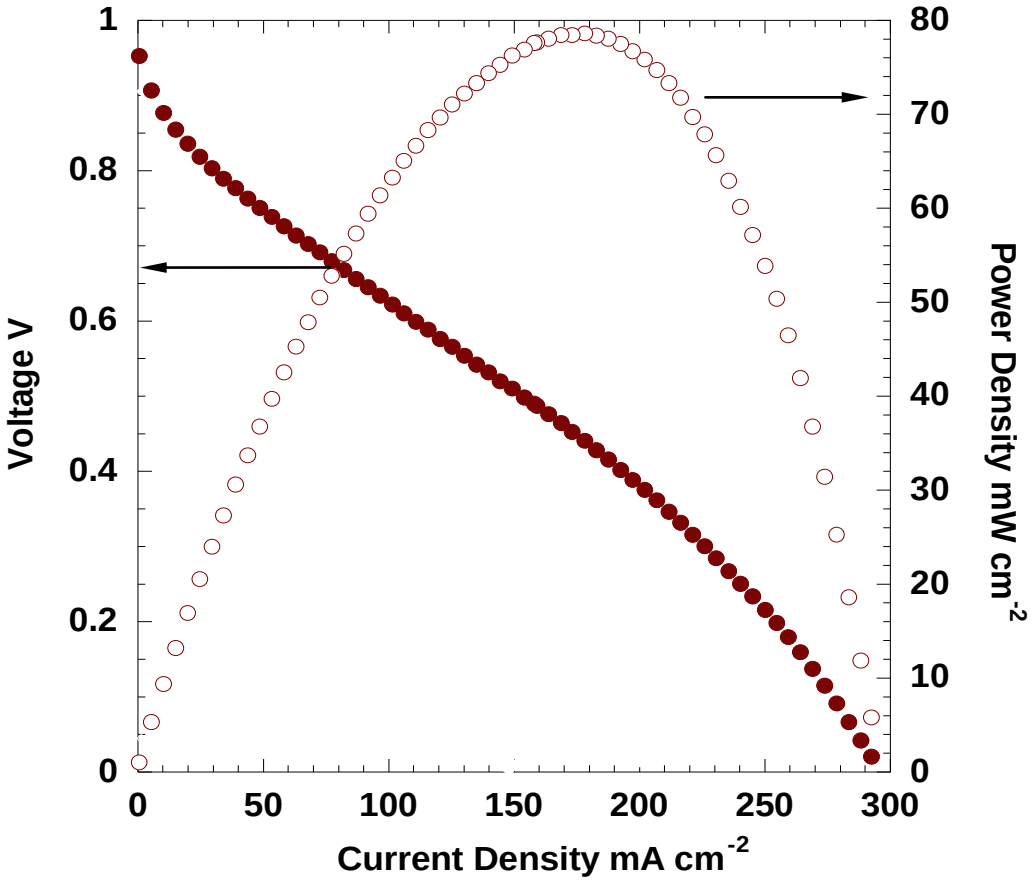

Figure 5.10 polarization curve of 10% crosslinked AAEM at 70°C

5.4 Conclusion

In this study, the copolymerization reaction kinetics were systematically investigated to fundamentally understand the polymerization mechanism and to precisely control the electrolyte properties including conductivity, mechanical strength, and water mass-uptake. This investigation demonstrated a controllable polymerization procedure of PMV membrane with tunable and balanced properties, which is promising for the alkaline fuel cell technology.

Based on the detailed study on the effects of BA removal, copolymer composition drift, and molecular weight, the properties of QPMV-based APE were optimized. Quantitative correlation between the initial monomer ratio and the resulting copolymer composition has been established to predict the ratio of hydrophobic/hydrophilic portions in the obtained membranes. The effect of initiator and surfactant concentrations on molecular weight was also investigated. Decreasing initiator KPS and increasing surfactant SDS could effectively increase the molecular weight, leading to improved mechanical properties including Young's modulus and tensile strength.

Chapter 6:

Fuel Cell Durability Enhancement by Crosslinking APE from PMV Copolymers

The results presented in this chapter have been published in the *Electrochem. Commun:*

Y. Luo, J. Guo, C. Wang, D. Chu, "Fuel Cell Durability Enhancement by Crosslinking Alkaline Anion Exchange Membrane Electrolyte," *Electrochem. Commun*., 16 (**2012**) 65.

6.1 Introduction

From the previous studies, several insights can be drawn. Firstly, APEFCs electrolyte could be synthesized from a bottom-up polymerization with designed hydrophobic and hydrophilic portions in polymer chains to serve mechanical support and conducting function, respectively. Also, the composition, the molecular weight (MW), and the glass transition temperature (T_g) of the copolymer could be adjusted to enhance the mechanical properties, i.e. the durability performance of APEFCs.

In this last study, we focus on enhancing the durability of QPMV by crosslinking of the copolymer. The newly obtained poly (methyl methacrylate-co-vinylbenzyl chloride) (PMV) was crosslinked as a semi-interpenetrating network (s-IPN) to reduce water uptake. In an s-IPN, one polymer is locked into another crosslinked

polymer matrix. The crosslinked polymer matrix gives mechanical support to the whole structure, while the locked in polymer provides functionality. Several s-IPNs including chitosan [44-46], poly (vinyl alcohol) [48-50], poly (arylene ether sulfone) [53], and poly (epichlorhydrin) [54] based APEs were widely investigated. Those s-IPNs demonstrated low water uptake and relatively high conductivity, yet no durability data on the fuel cell were reported.

In our study, PMV copolymer was crosslinked into an s-IPN system, using DVB (divinylbenzene) as the crosslinker. DVB can be polymerized as a crosslinked rigid network due to its phenyl ring structure and the two vinyl groups on one ring. Therefore, poly (divinylbenzene) (PDVB) can hold the QPMV providing more mechanical support. A schematic structure of QPMV-PDVB s-IPN is shown in Figure 6.1.

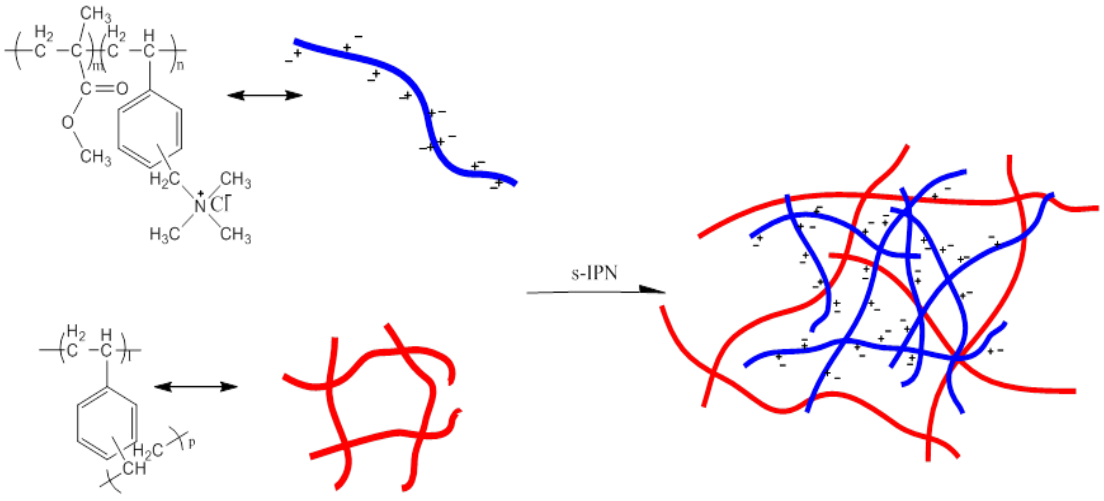

Figure 6.1 Schematics of QPMV-PDVB APE

6.2 Experimental

6.2.1 Crosslinking process and membrane preparation

The obtained PMV was dissolved in dimethylformamide (DMF) to form a 5 wt. % solution and quaternized with trimethylamine (Me_3N) for 2 hrs at 60 ℃ by bubbling Me_3N into the solution while stirring. The obtained QPMV solution in DMF was then moved into a reflux condenser connected flask under nitrogen protection. A certain amount of DVB (0 to 10 wt. % of the QPMV) was added into the system. The crosslinking process was started by the initiator AIBN (1.5 mmol/L of the DMF solution). The reaction was carried out at 60 ℃ for 24 hrs when the solution became visually more viscous.

6.2.2 Membrane preparation

The QPMV was directly cast into a film on an aluminium plate inside a chamber under nitrogen environment at 60 ℃ for overnight. The obtained membrane was further dried in vacuum oven at 60 ℃ for 24 hrs, followed by soaking in 6M KOH solution for overnight to exchange Cl^- to OH^-. The OH^- exchanged membrane was washed with DI water until pH of 7 was reached.

6.3 Results and Discussion

6.3.1 Characterization of Crosslinked QPMV-PDVB

The crosslinked QPMV-PDVB structure was confirmed by FTIR (Fourier transform infrared spectroscopy) as shown in Figure 6.2. After quaternization and crosslinking, a broad peak from 3200 to 3700 cm^{-1} (intermolecular O-H stretching) [103] appeared in

the crosslinked sample indicating that the membrane changed from hydrophobic to hydrophilic. The three peaks in PMV at 3100 (=C-H in aromatic ring of the VBC) [104], 2943(C-CH_3 in MMA) [105], and 2800 (O-CH_3 in MMA) [106] cm^{-1} were merged in crosslinked QPMV-PDVB, which was attributed to two reasons. Firstly, the =C-H structure was also in the aromatic ring of DVB, which enhanced the original intensity at 3100 cm^{-1}. Second, the quaternized QPMV-DVB would have the stretching vibrations of N-CH_3 at 2805 cm^{-1} [107]. Another noticeable enhanced peak intensity at 1600 cm^{-1} [108] was due to the conjugated C=C stretching vibrations of the aromatic ring in DVB, which confirmed that the QPMV was crosslinked into the PDVB matrix. The presented FTIR results are qualitative so that different DVB contents would not necessarily show difference in intensity. Therefore, QPMV-PDVB 5% and 10% showed similar spectra pattern.

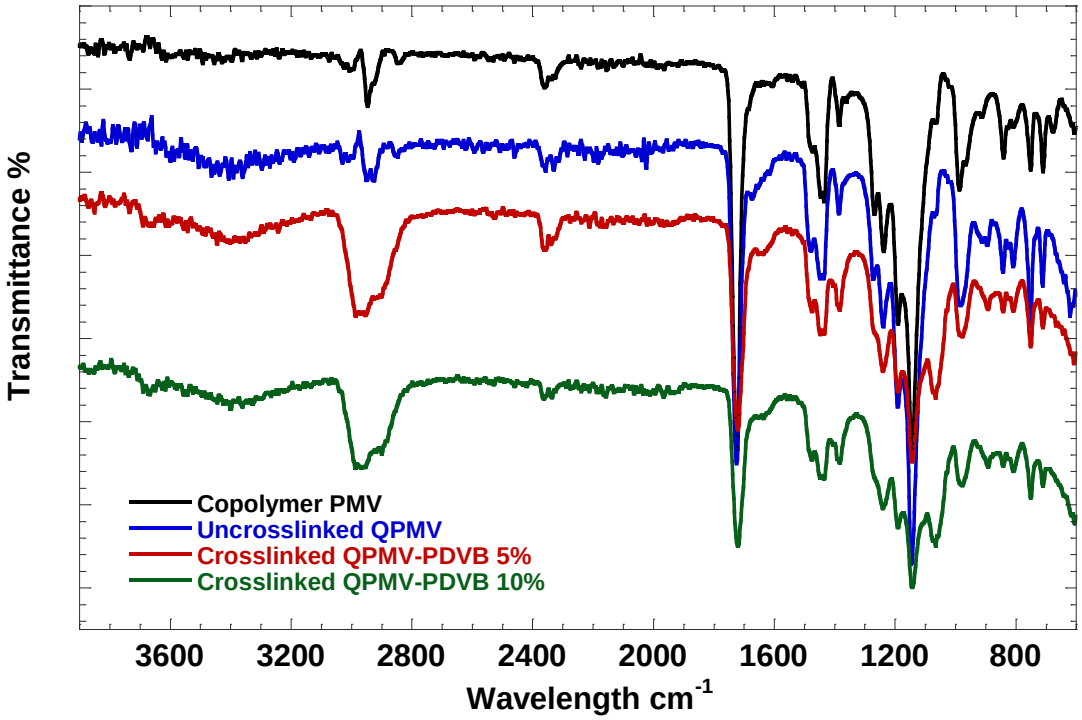

Figure 2. FTIR spectra of PMV and crosslinked QPMV-PDVB membranes.

6.3.2 Membrane Properties of QPMV-PDVB APEs

After preparation of QPMV-PDVB APEs, the ion exchange capacity (IEC), Young's modulus, water uptake, and swelling ratio were measured and shown in Table 6.1. Crosslinking decreased the IEC of the membranes by around 0.1 mmol g^{-1} for 5% crosslinking and 0.15 mmol g^{-1} for 10% crosslinking, respectively. The Young's modulus of the obtained membranes was all above 2 GPa indicating strong mechanical strength [109]. This was attributed to removing the butyl acrylate component and crosslinking. Water uptake and swelling ratio of QPMV-PDVBs were measured after soaking the membranes in de-ionized water for 3 hrs at room temperature. Both water uptake and swelling ratio of the crosslinked membrane were reduced with the increase of the crosslinker concentration. This test demonstrated that s-IPN crosslinking was an effective strategy to control the water content in the membrane.

Table 1 Properties of QPMV-PDVB APEs

DVB crosslinker percentage		**0%**	**5%**	**10%**
IEC (mmol g^{-1})		1.35	1.23	1.19
Young's Modulus [a] (GPa)		2.3	2.2	2.3
Swelling Ratio [b]	volume %	175.4	98.4	58.0
Water Uptake [b]	weight %	197.0	110.3	63.1

[a] Membranes at room temperature and ambient environment.

[b] Water saturated at room temperature.

6.3.3 Mechanism of Crosslinking QPMVs

Crosslinking was proven to be an effective method to reduce water uptake and to enhance the mechanical properties of the APEs. AFM characterization was performed for both uncrosslinked and crosslinked QPMV membranes to learn the nano-scale morphologies of the membranes. Figures 6.3a and 6.3b are the 2D and 3D topography of the uncrosslinked QPMV membrane, respectively. Figure 6.3c is the phase image of the uncrosslinked QPMV showing typical phase separation domains. The bright

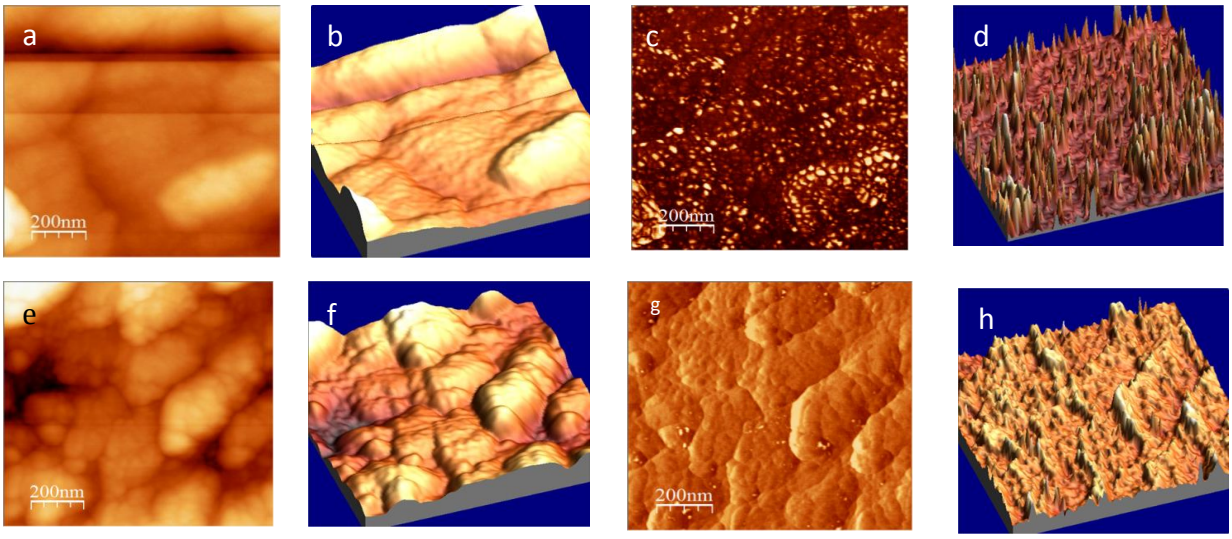

Figure 6.3 AFM images for both uncrosslinked and crosslinked QPMVs. (a) the topography of the uncrosslinked QPMV membrane; (b) the 3D topography of (a); (c) the phase image of the uncrosslinked QPMV; (d) the 3D phase image of uncrosslinked QPMV; (e) the topography of the crosslinked QPMV membrane; (f) the 3D topography of (e); (g) the phase image of the crosslinked QPMV; (h) the 3D phase image of crosslinked QPMV.

spots represented the hydrophobic part while the dark part corresponded to hydrophilic ionic conducting domains. The 3D phase image in Figure 6.3d showed a distinct view of the distribution of the ionic conducting domains. The second group of AFM images was from the crosslinked QPMV membrane. It was found that the crosslinked membrane, as shown in Figure 6.3f, had a rougher surface compared with uncrosslinked one (Figure 6.3b). In Figure 6.3g, the hydrophobic/hydrophilic portion was not as distinct as that shown in the uncrosslinked membrane (Figure 6.3c). However, the 3D phase image can still differentiate hydrophilic domains from the hydrophobic, as the conducting domains were still dispersed on the surface. The difference between Figures 6.3d and 6.3h was that the contrast between the hydrophobic portion (peaks) and the hydrophilic ionic channels (valleys) became less distinct in Figure 6.3h. This observation can certainly be attributed to crosslinking the polymer: a more rigid polymer network in the crosslinked membrane, which was helpful to resist water-uptake.

6.3.4 Conductivity of QPMV-PDVB APEs

Conductivity test was performed on the fuel cell test station under N_2 protection at 80% relative humidity (RH) using four-probe method. As shown in Figure 6.4, although the conductivity of the two crosslinked APEs was lower than the un-crosslinked one, nevertheless the conductivity of both crosslinked membranes could reach 10^{-2} S cm^{-1} above 50 ℃. The highest conductivity of the 5% crosslinked membrane could reach 2.5×10^{-2} S cm^{-1} at 80 ℃.

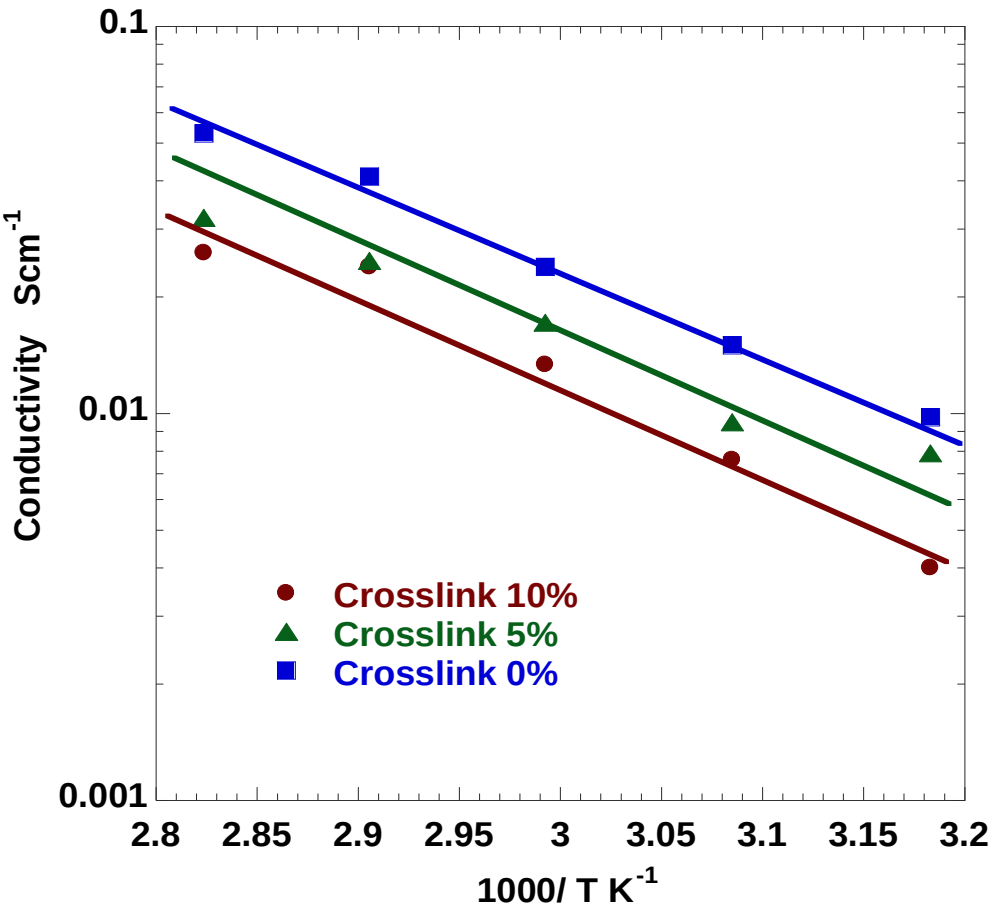

Figure 6.4. Conductivities of QPMV-PDVB APEs

6.3.5 QPMV-PDVB APEs Performance on Fuel Cell

The QPMV-PDVB APEs were tested on APEFC for both polarization and durability performance. Figure 6.5 showed the polarization performance of the 10% crosslinked APE at different temperatures. It was shown that the delivered power density was improved with increased temperature. The best performance of the 10% crosslinked APE was at 70 ℃ with a maximum power density of 80 mW cm^{-2}. This polarization performance was lower than the ones in our previous work. It could be attributed to the much lower water-uptake of the crosslinked membranes.

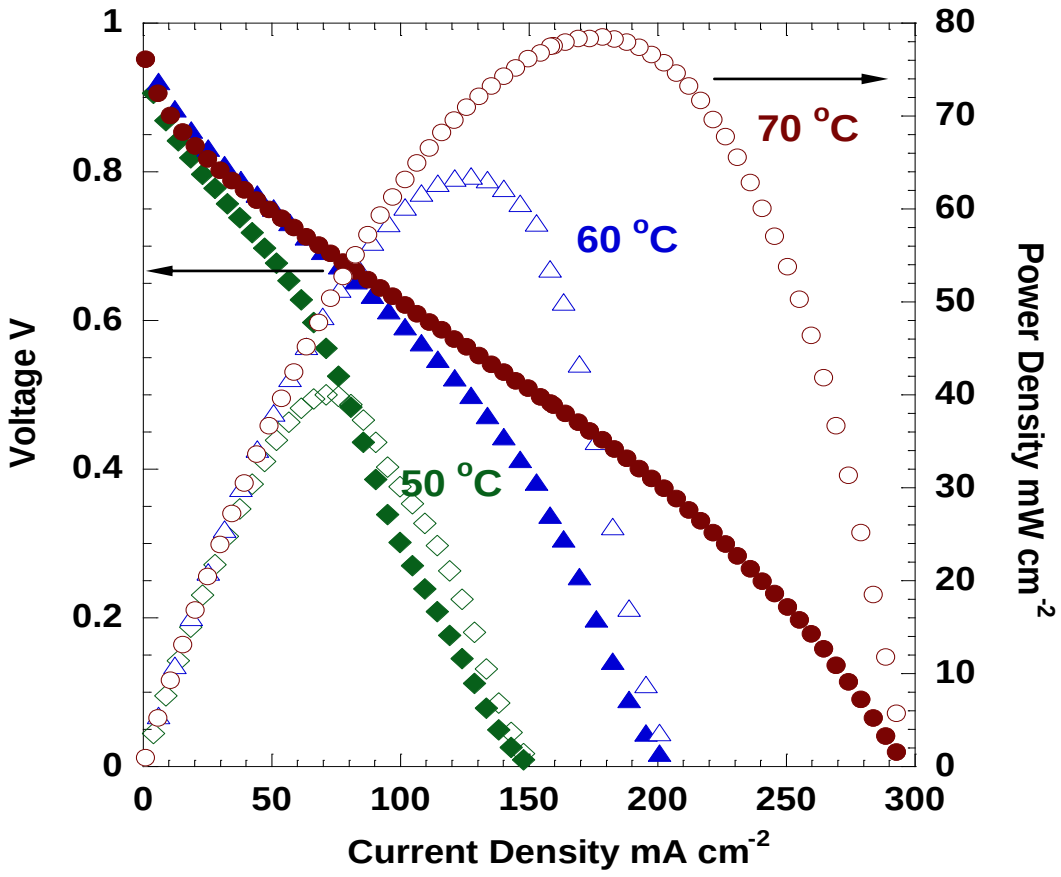

Figure 6.5 Polarization of 10% crosslinked QPMV-PDVB at different temperatures

Figure 6.6 showed the polarization performance of crosslinked APEs with different crosslinker percentage at 50 ℃. It illustrated that 10% crosslinked APE had the lowest power density, but it still could reach 46 mW cm^{-2} as its peak power density.

Due to its lowest water uptake, the 10% crosslinked QPMV-PDVB was used for the durability test. To compare the performances with our previous work, we conducted durability tests for both crosslinked 10% QPMV-PDVB and uncrosslinked QPMV membranes at 70 ^{o}C and 100 mA cm^{-2}. The results in Figure 6.7 showed that the uncrosslinked QPMV membrane could last 62 hrs on the fuel cell while the crosslinked QPMV-PDVB could run for 146 hrs. The 10% crosslinked QPMV-PDVB

could last approximately three times longer than the membrane reported in our previous work under the same conditions. This largely improved durability can be mainly attributed to the improved mechanical strength due to crosslinking and removal of butyl acrylate.

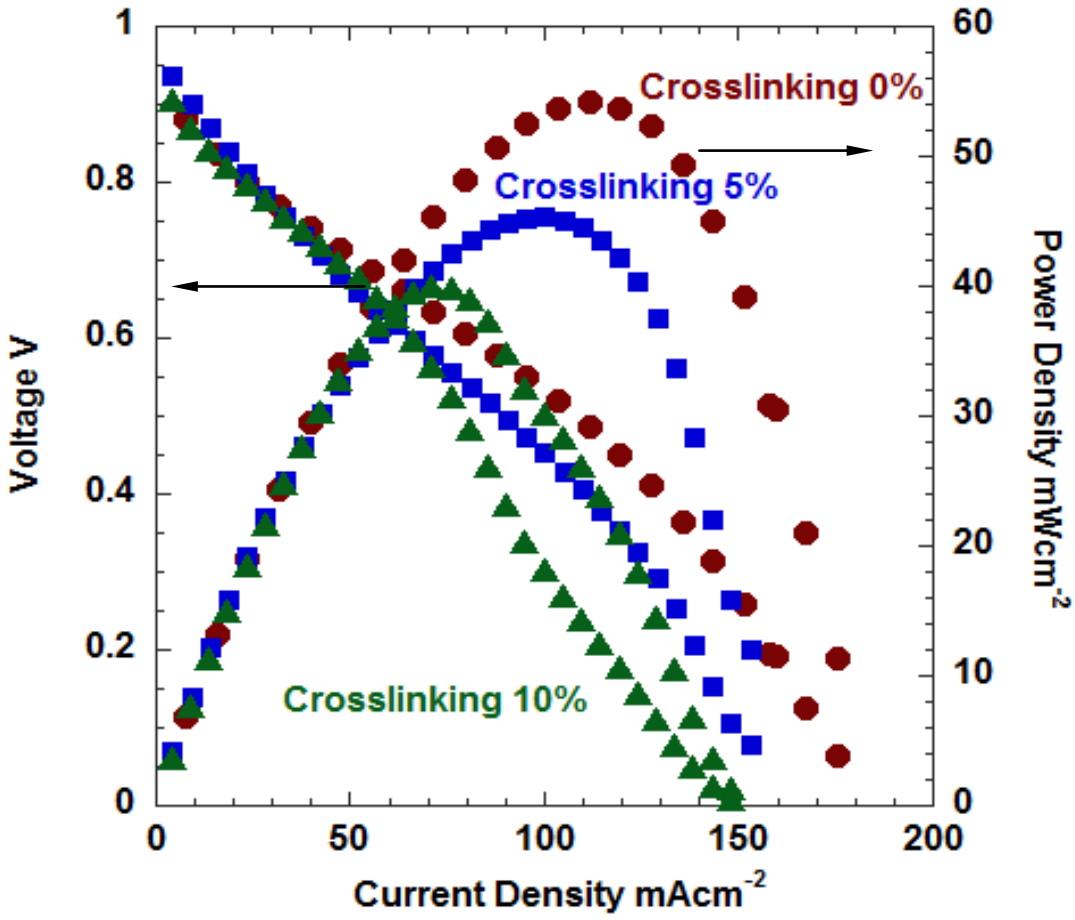

Figure 6.6 Polarization of various crosslinked AAEMs at 50 ℃

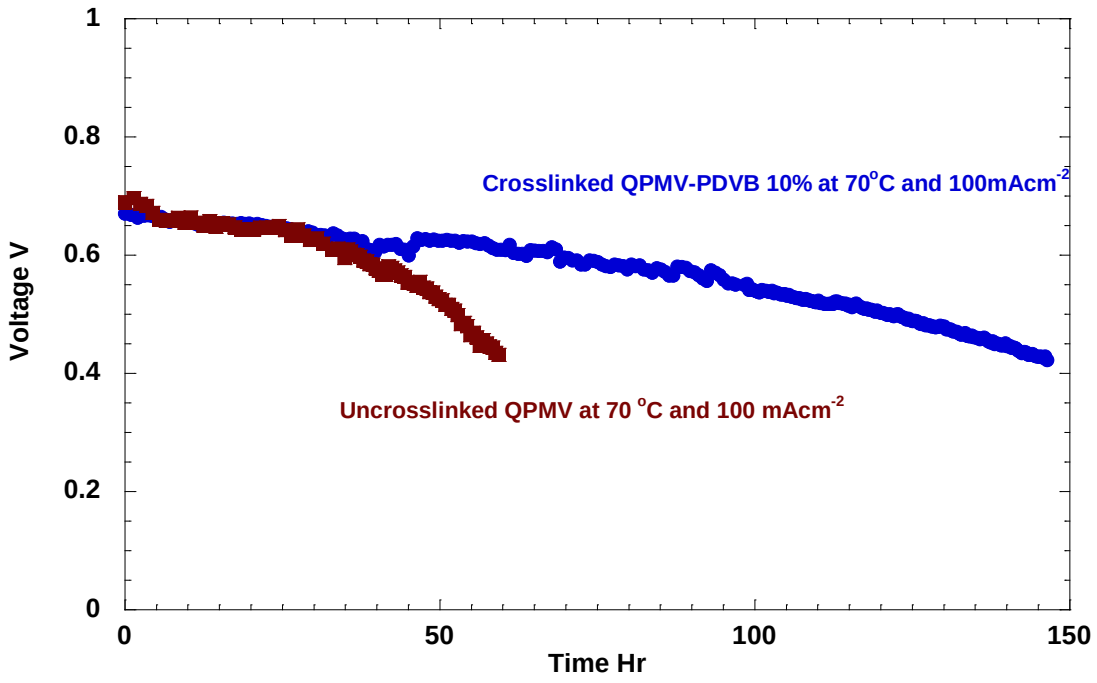

Figure 6.7 Durability tests of uncrosslinked QPMV and 10% crosslinked QPMV-PDVB AAEMs at 70 °C

Moreover, the durability of the 10% crosslinked QPMV-PDVB membrane at 50 °C and 75 $mAcm^{-2}$ (slightly lower than the peak power density) could be further improved to 420 hrs (17.5 days) as shown in Figure 6.8. Hoffman effect could be a possible reason for the gradually decreased performance. Also, it is possible that the platinum catalyst might catalyze water-shift reaction to generate H_2 and CO_2 from reaction of carbon and water, which would consume the OH^- in the AAEM during the durability test [109].

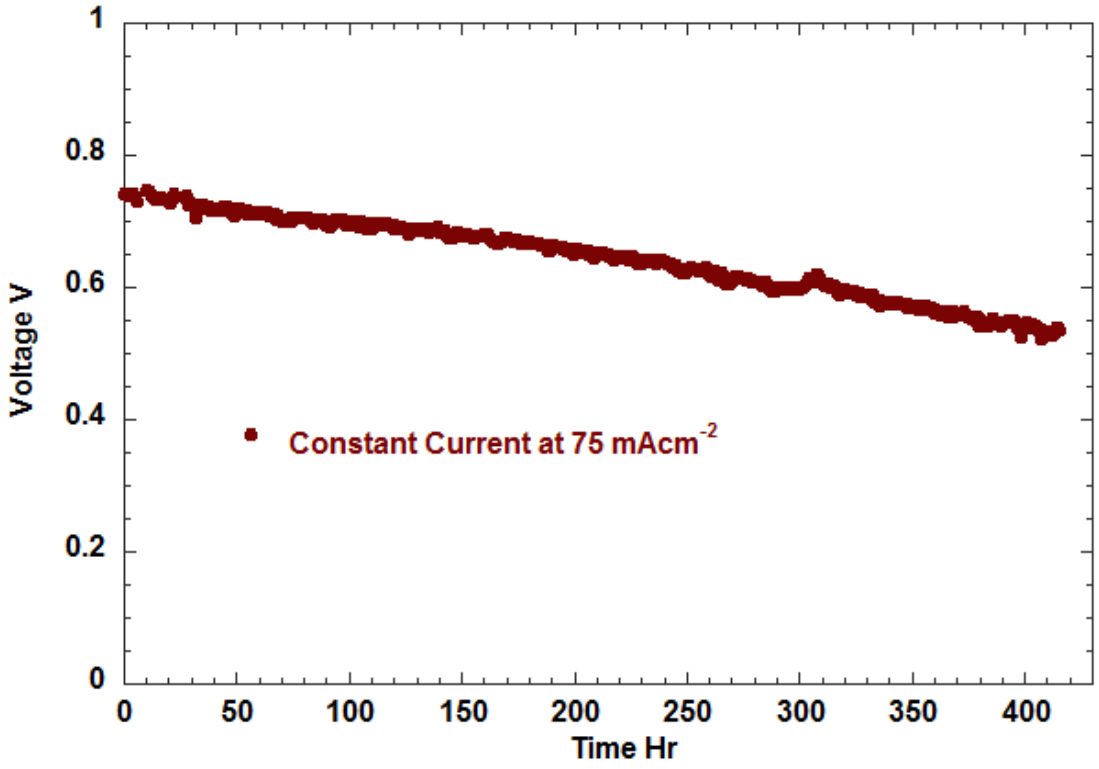

Figure 6.8 Durability test of 10% crosslinked AAEM at 50 ^{o}C

Also, the impedance tests before and after the durability test for 10% QPMV-PDVB at 70 ^{o}C were shown in Figure 6.9. It indicated that not only the ohmic resistance was increased but the resistances at both anode and cathode were also increased, which were all accounted for by the loss of voltage at the stable current density.

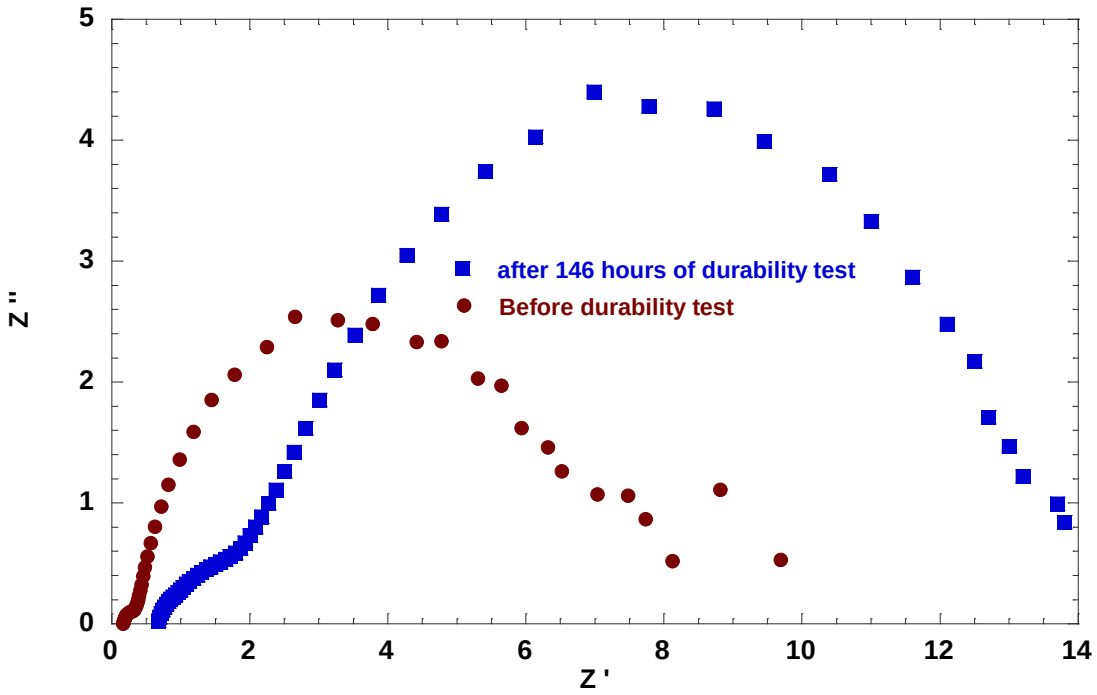

Figure 6.9 Impedance test for crosslinked QPMV-PDVB 10% APE at 70 ^{o}C before and after the durability test.

6.4 Conclusion

Two effective strategies were used in this study to improve the durability of QPMBV membranes. The first strategy was to increase glass transition temperature and molecular weight by eliminating butyl acrylate from the monomers. The second method is to reduce the water uptake and swelling ratio by crosslinking to lock the functionalized QPMV into a PDVB polymer network. Crosslinking significantly enhanced the durability performance with minor sacrifice of power density. The fuel cell with crosslinked QPMV-PDVB AAEM could continuously work for 420 hrs at 50 ^{o}C and 146 hrs at 70 ^{o}C, which was eight and three times longer than that in our previous study, respectively.

Chapter 7: Conclusion & Recommendation

7.1 Conclusion

Over the last decade, a growing demand for alternative energies has urged the development of a low cost energy conversion system alkaline fuel cell (AFC). The research detailed in this dissertation was aimed to push forward the AFC development and enlighten its potential as a next generation power source by synthesis of the key component alkaline polymeric electrolyte (APE). In this research, we have successfully synthesized a ternary copolymer, namely poly (methyl methacrylate-co-butyl acrylate-co-vinylbenzyl chloride) (PMBV) from bottom-up polymerization. The obtained precursor PMBVs were processed into membrane APEs, and both polarization and durability performance of the fuel cell was tested. Miniemulsion copolymerization has been employed in the PMBV synthesis. The advantages of miniemulsion polymerization were to give high conversion of monomers, obtain high molecular weight and eliminate the difficulties of mixing and heat management in bulk polymerization. Several polymerization kinetics factors were also investigated. Polymer composition drift effect and molecular weight optimization were used to precisely tailor the electrolyte properties including conductivity, mechanical strength, and water mass-uptake. The optimized APE can provide a maximum power output of 180 mW/cm^2 for our QPMBV membranes on AFCs, which was a remarkable improvement in this research. To further enhance the mechanical strength, two strategies were used. We removed butyl acrylate in monomer selection to increase the glass transition temperature. Moreover, crosslinking was employed to further enhance the mechanical properties of the APEs. After crosslinking, our membranes

demonstrated one of the best overall performance including high deliverable power density and durability (420 hours on fuel cell within 25% voltage decrease).

7.2 Recommendation

7.2.1 Fluorinated Polymer Backbones in APEs

Recent years have seen extensive research on the preparation and properties of alkaline polymer electrolyte. For the year 2012, there are already over 60 new references discussing different approaches to obtain APEs and their feasibilities in AFC applications. Ten publications are in Journal of Power Sources [111-120], eight are in Journal of Membrane sciences [121-128], eleven are in International Journal of Hydrogen Energy [129-139] and four are in Journal materials chemistry [140-143]. Also some high impact factor journals like Energy & Environmental Science [144, 145], RSC advances [146], JACS [147, 148], Macromolecules [149, 150] and Polymer [151] have all published the most sophisticated methods to fabricate APEs. Among them, some of the advances are still based on the conventional engineering polymer used as the backbones and continued with chloromethylation to be functionalized [152]. But it is also noticeable that more and more researchers found that fluorinated polymers are the better candidates as the backbone polymers. The original fluorinated polymers are regarded as high value-added materials due to their outstanding properties [153, 154]. Strong C-F bonds and low polarizability result from small size and high electronegativity of the fluorine atom in the polymers. Those fluorinated polymers can also exhibit high thermal stability and chemical inertness, good hydrophobicity, low relative permittivity, and low surface energy, which could profoundly enhance

the mechanical properties of the corresponding APEs. However, most research still focuses on the radiation-grafted method to attach the functional groups to the fluorinated polymers, which cost a lot from both the fluorinated engineering polymers and the radiation-grafting process. Therefore, we propose and think that it's worth a try to use fluorinated monomers to replace the conventional hydrocarbon monomers and bottom-up copolymerize the APEs. The APEs made from selected fluorinated monomers are expected to have enhanced mechanical properties, as well as much lower water uptake, because of the high hydrophobicity. It also will have the advantages of lower cost compared to ETFE, PVDF [155-157] or other fluorinated polymer based APEs. It is interesting to note that Y. Zhang et. al, has used hexafluorobutyl methacrylate (HFMA) to copolymerize with butyl methacrylate (BMA) and VBC by solution radical copolymerization to obtain the APEs [158]. All the APEs made in that paper had a water uptake as low as 15% and the polarization performance showed a power density of 55 mW/cm^2. To us, this is probably a good starting point to reselect our monomers and make our APEs again. HFMA could be used again since this is the counterpart to BA, which could provide the flexibility to the polymer chains. At the same time, the fluorinated HFMA also enhanced the hydrophobicity from BA (one of the reasons we removed BA in Chapter 5). To give a more chemically and thermally stable polymer backbone, the original MMA could also be replaced by trifluoroethyl methacrylate (TFEMA) [111]. And we still keep the VBC as the functional group to be quaternized with trimethylamine. Miniemulsion copolymerization could still be employed to improve the conversion and avoid the regional overheating in solution copolymerization.

7.2.2 Benchmark APEs Improvement

Unlike commercially available Nafion ®, as used in PEMFC, the APEs investigation is still in its infancy. However, there are still some commercial benchmark APE membranes available on the market. Most of the commercial APEs are designed originally for electrodialysis use. Some of them still require pre-soaking in KOH without DI-water resin before APEFC electrochemical testing, like ADP from Solvay and AHA from Tokuyama [159, 160]. Table 7.1 lists the most commonly cited commercial APEs in researchers' publications for properties comparison of their obtained APEs [161].

Table 7.1 Properties of Commercial APEs.

Manufacturer	Structure	IEC(mmol/g)	Thickness(um)	Conductivity (mS/cm)
Tokuyama Co. A201	Hydro-carbon	1.7	28	42
Tokuyama Co. AHA	PS/DVB	1.15-1.25	180-240	10
RAI Research Corp., R-1030	IPN-Fluorinated	1.0	100	14
Solvay S. A. Morgane ADP	Crosslinked Fluorinated	1.3-1.7	130-170	7

It is shown from Table 7.1 that Tokuyama A201 holds the most promise, since the membrane is as thin as 28 um (another type A901 is even 10um), and also has a very high conductivity 42 mS/cm at room temperature. Moreover, the swelling ratio of A201 and A901 is both under 10% in length and width. The water-uptake is 25% for A201 and 15% for A901, which is also comparable to Nafion®. The structure of A201 or A901 is still not disclosed, but is claimed to have hydrocarbon polymer

backbones attached with quaternary ammonium groups. In 2011, during the alkaline membrane fuel cell workshop, Tokuyama Co. presented the best results of their A201 and A901 membranes on AFCs. The maximum power density of A901 AFC could reach a peak power density of 325 mW/cm^2 using clean air as the cathode and H_2 as the anode, both in 95% RH at 50 ^oC, which is so far the best performance of an alkaline polymer electrolyte fuel cell to our best knowledge [162].

Also, some of the researchers mentioned in their presentations that A201 and A901 are possibly made from polychloroprene (PC) crosslinked by divinylbenze (DVB) and then continued with quaternary ammonium groups' functionalization. In this sense, elastomers that are compatible with the DVB system to make the IPN is also a direction which could improve mechanical strength as well as obtain high conductivity.

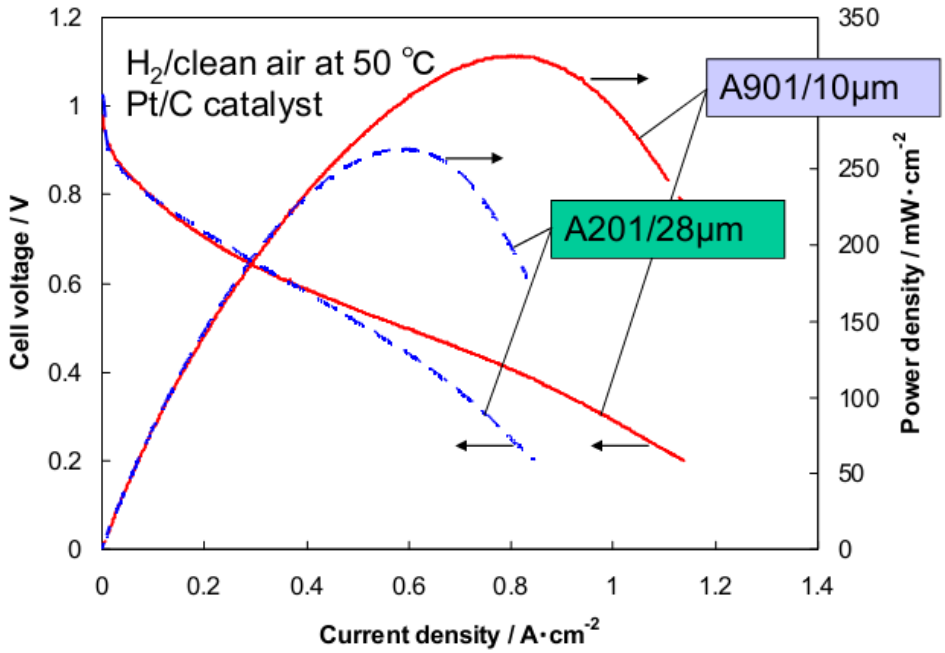

Figure 7.1 The Performance of Tokuyama A201 and A901 APEs on APEFCs [162].

7.2.3 Replace VBC with Functional Groups of Enhanced Chemical and Thermal Stability

Another direction is to use different OH- carriers. In J. Varcoe's paper this year (2012) in Energy & Environmental Science [144], they compared the stabilities of the functional groups between benzyltriemthylammonium chloride (BTMA) and 1-benzyl-3-methylimidazolium chloride (BMI). They claimed that BTMA by far is still the most stable one in alkaline solution. However, several other functional groups like bulky phosphazenium [163], alkyloxy-quaternary-ammonium [164, 165] and singly quaternized DABCO [166] are worthy of further investigation to enhance the chemical and thermal stability of the APEs in alkaline environment.

7.2.4 in-situ AFM Investigation of Conductivity and Mechanical Strength

For my particular acrylate-polymeric based APEs, another important study is to learn the mechanism of conductivity channels inside the membranes. Unlike commercial Nafion ®, as used in PEMFC, the APE investigation is still in its infancy. Many chemists employed quite different approaches to polymerize APEs with different backbones and functional groups to mimic the structure of Nafion, through which ions could move freely from one side to another inside of the membrane. However, there was still no detailed mechanism revealed of active OH^- ion channels through the particular APEs. As we know, the size of the OH^- ion is much larger and the mobility was 3 times lower, compared with H^+. Therefore, it is essential to look into the APE conducting channels at the nanoscale to guide the synthesis of novel APE polymeric materials with desired conductivity. Furthermore, the mechanical strength of APE

under compression conditions in membrane electrode assembly (MEA) with humidified environment is at stake in fuel cell operation, which is another issue associated with conductivity. The current technology to evaluate the mechanical strength is to simply employ the tensile test to measure Young's modulus. However, this test is a bulk analysis that separates the mechanical strength from ion conducting and can only reflect its intrinsic property at dry state, which is not the real case in the fuel cell. From the aforementioned two points, in-situ nanoscaled measurement for both conductivity and mechanical strength is needed to correlate with each other and thus balance the conductive and mechanical supportive parts when designing the polymer materials in bulk.

Atomic force microscopy (AFM) has recently been recognized as a visualization technique to probe the nanoscale properties of Nafion ® or relevant polymer electrolytes used in PEMFCs, which can reveal the distribution of hydrophilic and hydrophobic surface domains directly that is electrochemically active and mechanically supportive, respectively[167-170] through phase imaging of AC(alternating current) mode current-mapping. This technique could also be applied to learn about the nanoscale OH^- ion conductive channels mapping for APEFCs. Moreover, both conductivity and mechanical strength properties of the APE at a nanoscaled surface could be *in situ* quantitatively measured at the same time through AFM connected with an electrochemical impedance spectroscopy (EIS) apparatus, which is of great significance to standardize the properties testing for APE. Therefore, we also propose the details of testing procedures using this advanced AFM-EIS technology.

Conductivity

The following Figure 7.2 sketched the test equipment. The cantilever is platinum coated to make it conductive. The APE sample is placed on the gold-plated conductive stage with its corresponding ionomer as the adhesives. An EIS apparatus (Gamry Imstruments 3000, Potentiostat/ Galvanostat/ ZRA) is attached to the AFM with two wires connected to the cantilever and gold substrate.

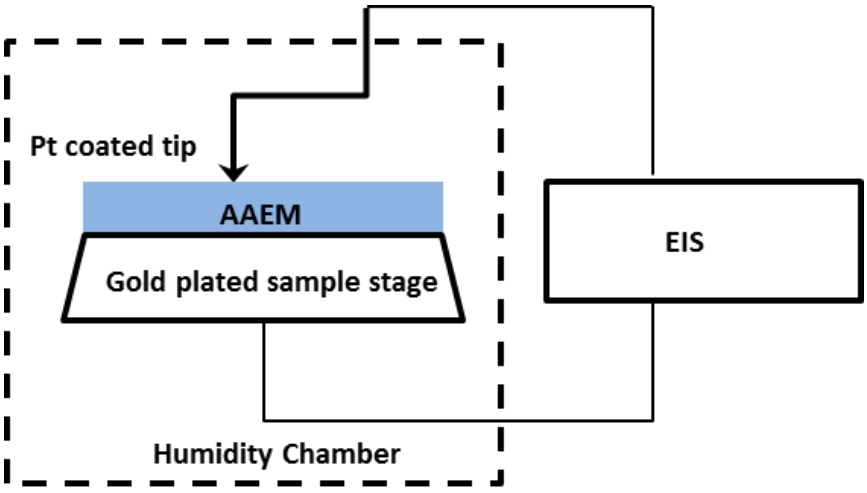

Figure 7.2 sketch of AFM-EIS equipment

With a given frequency for APE resistance (usually the frequency is the same as that in bulk analysis from the impedance), the sinusoidal voltage coming from the EIS could be added between the platinum tip and gold stage. The current response from the membrane at one nanoscaled surface point will be collected by EIS again.

By this method, not only the OH^- channels could be visualized, but the conductivity distribution could also be calculated. More importantly, the AFM cantilever and sample stage could be put into a humidity chamber. Therefore, conductivity could be

tested at various temperatures and humidities to represent the real working environment of a fuel cell. This humidity chamber also facilitates the *in situ* mechanical strength testing.

Mechanical Strength

As aforementioned, the powerful AFM technology could also *in situ* measure the mechanical strength inside a humidity chamber. The indentation of an AFM tip fixed to a cantilever into a soft APE can be modeled by Hertzian contact mechanics [170]. This theory provides a very simple but direct approach to the elasticity for a sample by the following equation:

$$F = \varepsilon d^m \frac{E}{1-\nu^2} \qquad [7.1]$$

Where F is the pressure force added by AFM tip; ε is a constant dependent on the tip geometry; d is the indentation of the tip; m characterizes the indentation behavior, which also depends on the geometry of the tip; E is the Young's modulus of the APE and ν is the Poisson's ratio of the APE sample that could be read from AFM imaging.

Therefore, the local surface mechanical strength of Young's modulus at various temperature and humidity of the AAEM could be correlated and calculated with the AFM tip force and its indentation [171].This AFM tip force could repeat to APE at different points to see the consistency of the Young's modulus response.

Conductivity and Mechanical Strength Correlation

Several control experiments could be further conducted to investigate the correlation between conductivity and mechanical strength for a dynamic evolution. Conductivity variation can be depicted at various pressures enforced by the AFM tip, which can in turn relate to the transient mechanical strength. Moreover, vibration of the force scan in different directions from the AFM cantilever will also have an effect on both conductivity and mechanical strength. A more direct correlation is to stretch the membrane with certain external strain ranges on the stage and test the conductivity and Young's modulus with the mentioned methods at the same time.

Bibliography

1. M. Ishizawa, et al., *J. Power Sources* 86 (2000) 294.

2. P. Eichenberger, *J. Power Sources* 71 (1998) 95.

3. A. Dicks, et al., *J. Power Sources* 86 (2000) 501.

4. G. Acres, *J. Power Sources* 100 (2001) 60.

5. W. Turner, M. Parten, et al., *Vehicular Technology Conference, IEEE 49th*, 2 (1999) 1385.

6. J. Yi, T. Nguyen, *J. Electrochem. Soc.* 145 (1998) 1149.

7. S. Kamarudin, F. Achmad et al., *Int J. Hydrogen Energ*, 34 (2009) 6902.

8. (1) G. McLean, T. Niet, *Int J. Hydrogen Energ* 27 (2002) 507. (2) E. Gulzow, *J Power Sources*, 61 (1996) 99. (3) K. Tomantschger, F. McClusky, et al., *J. Power Sources*, 18 (1986) 317.

9. (1)http://www.fuelfromthewater.com/stationary.htm; (2) http://ceramics.org/ ceramictechtoday/2012/05/22/cleveland-rta-nasa-renew-push-for-fuel-cell-bus-project/. (3) http://www.seao2.com/fuelcells/; (4) http://www. horizonfuelcell. com/ store/minipak.htm.

10. G. Sasikumar, J. Ihm, *Electrochim Acta*, 50 (2004) 601.

11. K. Schmidt-Rohr, Q. Chen, *Nat Mater*, 7 (2008) 75.

12. S. Hamrock, M. Yandrasites, *J. Macromal, Sci. Part C: Polym. Rev.* 46 (2006) 219.

13. J. Basechuk, X. Li, *Int. J. of Energy Res*., 25 (2001) 695.

14. http://www.eere.energy.gov/hydrogenandfuelcells/fuelcells/fc_types.html.

15. http://en.wikipedia.org/wiki/Alkaline_fuel_cell.

16. J. Pan, S. Lu, et al. *Adv. Funct. Mater*, 20 (2010) 312.

17. Y. Wu, C. Wu, F. Yu, T. Xu, Y. Fu, *J. Membr. Sci*, (2008) 28.

18. Y. Wan, K. Creber, B. Peppley, V. T. Bui, E. Halliop, *Polym. Int*. 54 (2005) 5.

19. Y. Wan, K. Creber, B. Peppley, V. T. Bui, *J. Membr. Sci.* 280 (2006) 666.

20. V. M. Nikolic, A. Krkljes, Z. Popovic, Z. Lausevic, S. Miljanic, *Electrochem. Commun.* 9 (2007) 2661.

21. G. Wu, S. Lin, C. Yang, *J. Membr. Sci*. 275 (2006) 127.

22. J. Varcoe, R. Slade, E. Yee, S. Poynton, D. Priscoll, D. Apperley, *Chem. Mater.* 19 (2007) 2686.

23. J. Varcoe, R. Slade, *Electrochem. Commun*. 8 (2006) 839.

24. H. Herman, R. Slade, J. Varcoe, *J. Membr. Sci*. 218 (2003) 147.

25. R. Slade, J. Varcoe, *Solid state Ionics*, 176 (2005) 585.

26. J. Varcoe, *Phy. Chem. Chem. Phys*. 9 (2007) 1479.

27. T. Danks, R. Slade, J. Varcoe, *J. Mater. Chem.* 13 (2003) 712.

28. G. Wang, Y. Weng, D. Chu, R. Chen, D. Xie, *J. Membr. Sci.* 333 (2009) 63.

29. S. Lu, J. Pan, A. Huang, L. Zhuang, J. Lu, *PNAS* 105 (2008) 20611.

30. J. Zhou, M. Unlu, J. A. Vega, P. A. Kohl, *J. Power Sources*, 190 (2009) 285.

31. Y. Xiong, Q. Liu, Q. Zeng, *J. Power sources*, 193 (2009) 541.

32. G. Wang, Y. Weng, J. Zhao, R. Chen, D. Xie, *J. Appl. Polym. Sci.* 112 (2009) 721.

33. L. Li, Y. Wang, *J. Membr. Sci*, 262 (2005) 1.

34. J. Fang, P. Shen, *J. Membr. Sci.* 285 (2006) 317.

35. L. Wu, T. Xu, D. Wu, X. Zheng, *J. Membr. Sci.* 310 (2008) 577.

36. M. R. Hibbs, C. H. Fujimoto, C.J. Cornelius, *Macromol.* 42 (2009) 8316.

37. E. Switzer, T. Olson, A. Datye, P. Atanassov, M. Hibbs, C. Fujimoto, C. Conelius, *Electrochimi. Acta* 55 (2010) 3404.

38. A. Huang, C. Xia, C. Xiao, L. Zhuang, *J. Appl. Polym. Sci.*,100 (2006) 2248 .

39. K. Matsuoka, S. Chiba, Y. iriyama, T. Abe, M. Matsuoka, K. Kikuchi, Z. ogumi, *Thin Solid Films*, 516 (2008) 3309.

40. E. Agel, J. Bouet, J. F. Fauvarque, *J. Power Sources*, 101 (2001) 267.

41. D. Stoica, L. ogier, L. Akrour, F. Alloin, J. Fauvarque, *Electrochimi. Acta*, 53 (2007) 1596.

42. B. Lin, L. Qiu, J. Lu, F. Yan, *Chem. Mater*. 22 (2010) 6718.

43. L. Wu, T. Xu, *J. Membr. Sci*. 322 (2008) 286.

44. Y. Wan, K. Creber, B. Peppley, V. Bui, *J. Membr. Sci*., 284 (2006) 331.

45. Y. Wan, B. Peppley, K. Creber, V. Bui, E. Halliop, *J. Power Sources*, 162 (2006) 105.

46. J. Wang, R. He, Q. Che, *J. Colloid Interface Sci*., 361 (2011) 219.

47. Y. Wan, B. Peppley, K. Creber, V. Bui, *J. Power Sources,* 195 (2010) 3785.

48. J. Qiao, J. Fu, R. Lin, J. Ma, J. Liu, *Polym.*, 51 (2010) 4850.

49. L. Lebrun, E. Silva, G. Pourcelly, M. Metayer, *J. Membr. Sci*., 227 (2003) 95.

50. E. Silva, L. Lebrun, M. Metayer, *Polym*. 43 (2002) 5311.

51. J. Qiao, J. Fu, L. Liu, Y. Liu, J. Sheng, *Int. J. Hydrogen Energy*, doi:10.1016/j.ijhydene.2011.06.038.

52. C. M'Bareck, M. Metayer, Q. Nquyen, S. Alexandre, J. Malandain, *J. Membr. Sci.* 221 (2003) 53.

53. J. Zhou, M. Unlu, I. Anestis-Richard, P. Kohl, *J. Membr. Sci*, 350 (2010) 286.

54. C. Sollogoub, A. Guinault, et al., *J. Membr. Sci.*, 335 (2009) 37.

55. S. Gu, R. Cai, et al., *Angew. Chem. Int*. ed. 48 (2009) 6499.

56.http://www.drillspot.com/products/341705/Dayton_4RR10_Professional_Air_Brush_Kit.

57. R. Chetty, K. Scott, *Electrochimi. Acta*, 52(12)(2006)4073.

58. Arbin Instrumnts, *FCTS Testing System User Manual*, 2006.

59. Gamry Instruments, *Application Note Review 1.0*, 2010

60. http://www.scribner.com/bt-112-membrane-conductivity-cell.html.

61. (1)P. Painter, M. Coleman, *Fundamentals of polymer science, 2nd, Edition*, CRC Press, 1997; (2)Odian, George. *Principles of Polymerization (4th ed.).* New York: Wiley-Inter science 2004. (3) S. Harrisson, S. Mackenzie, D. Haddleton, *Chem. Commun*, (2002) 2850.

62. E. Nicol, J. Habib-Jiwan, A. Jonas, *Langmuir*, 19 (2003) 6178.

63. L. Nielsen, *Mechanical properties of polymers and composites volume 2*, Marcel Dekker Inc., New York, 1974.

64. J. F. Quinn, R. P. Chaplin, T. P. Davi, *J. Polym. Sci.: Part A: Polym. Chem*. 40 (2002) 2956.

65. R. Paris, J.Fuenta, *J. Polym. Sci.: Part A: Polym. Chem.* 45 (2007) 2538.

66. M. A. Dube, A. Penlidis, *Polym.* 36 (1995) 587.

67. R. C. Beauchemin, M. A. Debe, *Polym. React. Eng.* 7 (1999) 485.

68. Z. Pan, *Polymer Chemistry 3rd Ed*, Chemical Industry Press, Beijing, 2003.

69. M. Satterfield, P. Majsztrik, H. Ota, J. Benziger, A. Bocarsly, *J. Polym. Sci.: Part B: Polym. Phys.* 44 (2006) 2327.

70. Y. Luo, J. Guo, C. Wang, D. Chu, *J. Power Sources* 195 (2010) 3765.

71. H. Xu, J. Fang, M. Guo, X. Lu, X. Wei, S. Tu, *J. Membr. Sci.* 354 (2010) 206.

72. L. Domiguez, J. Economy, K. Benak, C. Mangun, *Polym. Adv. Technol.* 14 (2007) 632.

73. J. Reimrs, F. J. Schork, *J. Appl. Polym. Sci.* 59 (1996) 1833.

74. F. J. Schork, J. Guo, *Macromol. React. Eng*. 2 (2008) 287.

75. J. Guo, F. J. Schork, *Macromol. React. Eng.*, 2 (2008) 265.

76. Y. Luo, I. Chou, W. Chiu, C. Lee, J. *Polym. Sci., Part A: Polym. Chem.* 47 (2009) 4435.

77. J. Brandrup, E. Immergut, E. Grulke, *Polymer hand book*, fourth edition, Wiley-Interscience 1999.

78. J. E. Mark, Adi eisenber, W. W. Graessley, L. Mandelkern, E. T. Samulski, J. L. Koenig, G. D. Wignall, *Physical Properties of Polymers*, AM. CHEM. SOC., Washington, DC, 1993, pp. 87.

79. G. Hwang, H. Ohya, *J. Membr. Sci.* 140 (1998) 195.

80. S. Gamburzev, A. J. Appleby, *J. Power Sources* 107 (2002) 5.

81. R. O'Hayre, S. Cha, W. Colella, F. B. Prinz, *Fuel Cell Fundamentals*, WILEY, New York, 2006, pp. 204-224.

82. E. E. Switzer, T. S. Olson, A. K. Datye, P. Atanassov, M. R. Hibbs, C. Fujimoto, C. J. Cornelius, *Electrochimi. Acta* 55 (2010) 3404.

83. A. Park, P. Pintauro, *Electrochem. Solid-State Lett.* 15(2011) B27.

84. K. Matsuoka, Y. Iriyama, T. Abe, M. Matsuoka, Z. Ogumi, *J. Power Sources* 150 (2005) 27.

85. J. Varcoe, R. Slade, *Electrochem. Commun.* 8 (2006) 839.

86. D. Seo, A. Hossain, D. Lee, Y. Lim, S. Lee, H. Lee, T. Hong, W. Kim, *Electrochim. Acta.*, (2012) http://dx.doi.org/10.1016/j.electacta.2012.04.065.

87. J. E. Mark, A. Eisenberg, W. W. Graessley, L. Mandelkern, E. T. Samulski, J. L. Koenig, G. D. Wignall, *Physical Properties of Polymers*, United Book Press, Baltimore, MD, 1993.

88. Y. Luo, J. Guo, C. Wang, K. Y. Choi, D. Chu, *ECS Transactions*, 33(2010)1893.

89. A. Ziegler, K. Landfester, A. Musyanovych, *Colloid Polym. Sci.*, 287 (2009) 261.

90. G. Wang, Y. Weng, D. Chu, D. Xie, R. Chen, *J. Membr. Sci*., 326 (2009) 4.

91. Y. Xiong, Q. Liu, Q. Zeng, *J. Power Sources*, 193 (2009) 541.

92. S. Gu, R. Cai, T. Luo, K. Jensen, C. Contreras, Y. Yan, *ChemSusChem*, 3 (2010) 555.

93. L. Wu, T. Xu, D. Wu, X. Zheng, *J. Membr. Sci.*, 310 (2008) 577.

94. S. Lu, J. Pan, A. Huang, L. Zhuang, J. Lu, *PNAS*, 105 (2008) 20611.

95. Y. Wu, C. Wu, J. R. Varcoe, S. D. Poynton, T. Xu., Y. Fu, *J. Power Sources*, 195 **(**2010) 3069.

96. J. R. Varcoe, *Phy. Chem. Chem. Phys.*, 9 (2007) 1479.

97. A. Kucernak, F. Bidault, G. Smith, *Electrochim. Acta.*, 82 (2012) 284.

98. G. Wang, Y. Weng, J. Zhao, R. Chen, D. Xie, *J. Appl. Polym. Sci.*, 112 (2009) 721.

99. J. Pan, S. Lu, Y. Li, A. Huang, L. Zhuang, J. Lu. *Adv. Funct. Mater*, 20 (2010) 312

100. A. Bhattacharya, J. Rawlins, P. Ray, *Polymer Grafting and Crosslinking*, John Wiley & Sons, Inc. Hoboken, NJ, 2009.

101. P. Painter, M. Coleman, *Fundamentals of Polymer Science*, second edition, CRC Press LLC, 1997, pp107.

102. Y. Luo, J. Guo, C. Wang, D. Chu, *ChemSusChem*, 11 (2011) 1557.

103. S. Feng, Y. Shang, G. Liu, W. Dong, X. Xie, J. Xu, V. Mathur, *J. Power Sources*, 195 (2010) 6450.

104. J. Zhou, M. Unlu, J. Vega, P. Kohl, *J. Power Sources*, 190 (2009) 285.

105. J. Zhou, M. Unlu, I. Anestis-Richard, P. Kohl, *J. Membr. Sci*, 350 (2010) 286.

106. R. Paris, J. Fuente, *J. Polym. Sci. Part A: Polym. Chem.*, 45 (2007) 3538.

107. K. Wang, C. Luo, Xiao, Zhou, *Modern Instrumental Analysis of Polymer*, 2nd edition, Tsinghua University Press, 2000.

108. Y. Choi, M. Kang, S. Moon, *J. Appl. Polym. Sci.*, 88 (2003) 1488.

109. C. Yang,*J. Appl. Electrochem*, 42 (2012) 305.

110. R. Vinodh, D. Sangeetha, *J. Appl. Polym. Sci.*, (2012) DOI: 10.1002 / APP. 38266.

111. X. Wu, K. Scott, *J. Power Sources* 214 (2012) 124.

112. X. Lin, L. Wu, Y. Liu, a. Ong, S. Poynton, J. Varcoe, T. Xu, *J. Power Sources* 217 (2012) 373.

113. B. Qiu, B. Lin, Z. Si, L. Qiu, F. Chu, J. Zhao, F. Yan, *J. Power Sources* 217 (2012) 329.

114. M. Mamlouk, K. Scott, *J. Power Sources* 211 (2012) 140.

115. C. Yang, S. Chiu, S. Kuo, T. Liou, *J. Power Sources* 199 (2012) 37.

116. H. Bahrami, A. Faghri, *J. Power Sources* 218 (2012) 286.

117. Z. Zhao, F. Gong, S. Zhang, S. Li, *J. Power Sources* 218 (2012) 368.

118. S. Xu, G. Zhang, Y. Zhang, C. Zhao, W. Ma, H. Sun, N. Zhang, L. Zhang, H. Jiang, H. Na, *J. Power Sources* 209 (2012) 228.

119. A. Bartrom, J. Haan, *J. Power Sources*, 214 (2012) 68.

120. Y. Cao, X. Wang, K. Scott, *J. Power Sources,* 201 (2012) 226.

121. Y. Luo, J. Guo, Y. Liu, Q. Shao, C. Wang, D. Chu, *J. Membr. Sci.* 423-424 (2012) 209.

122. J. Ran, L. Wu, J. Varcoe, A. Ong, S. Poynton, T. Xu, *J. Membr. Sci.* 415-416 (2012) 242.

123. H. Zarrin, J. Wu, M. Fowler, Z. Chen *J. Membr. Sci.* 394-395 (2012) 193.

124. H. Luo, P. Xu, P. Jenkins, Z. Ren, *J. Membr. Sci.* 409-410 (2012) 16.

125. G. Merle, S. Hosseiny, M. Wessling, K. Nijmeijer, *J. Membr. Sci.* 409-410 (2012) 191.

126. Z. Xia, S. Yuan, G. Jiang, X. Guo, J. Fang, L. Liu, J. Qiao, J. Yin, *J. Membr. Sci.* 390-391 (2012) 152.

127. Y. Zhao, H. Yu, D. Xing, W. Lu, Z. Shao, B. Yi, *J. Membr. Sci.* 421-422 (2012) 311.

128. J. Wang, J. Wang, S. Zhang, *J. Membr. Sci.* 415-416 (2012) 205.

129. M. Zhiani, H. Rostami, S. Majidi, K. Karami, *Int. J. Hydrogen Energ.* (2012) j.ij hydene.2012.09. 001.

130. L. An, T. Zhao, Q. Wu, L. Zeng, *Int. J. Hydrogen Energ.* 37 (2012) 14536.

131. J. Fang, Y. Yang, X. Lu, M. Ye, W. Li, Y. Zhang, *Int. J. Hydrogen Energ.* 37 (2012) 5894.

132. J. Qiao, J. Fu, L. Liu , Y. Liu, J. Sheng, *Int. J. Hydrogen Energ.* 37 (2012) 4580.

133. M. Faraj, M. Boccia, H. Miller, F. Martini, S. Borsacchi, M. Geppi, A. Pucci, *Int. J. Hydrogen Energ.* 37 (2012) 14992.

134. Q. Hu, Y. Shang, Y. Wang, M. Xu, S. Wang, X. Xie, Y. Liu, H. Zhang, J. Wang, Z. Mao, *Int. J. Hydrogen Energ.* 37 (2012) 12659.

135. M. Mamlouk, J. Horsfall, C. Williams, K. Scott, *Int. J. Hydrogen Energ.* 37 (2012) 11912.

136. H. Sun, G. Zhang, Z. Liu, N. Zhang, L. Zhang, W. Na, C. Zhao, D. Qi, G. Li, H. Na *Int. J. Hydrogen Energ.* 37 (2012) 9873.

137. Z. Zhang, L. Xin, W. Li, *Int. J. Hydrogen Energ.* 37 (2012) 9393.

138. G. Liu, Y. Shang, X. Xie, S. Wang, J. Wang, Y. Wang, Z. Mao, *Int. J. Hydrogen Energ.* 37 (2012) 848.

139. S. Huo, H. Deng, Y. Chang, K. Jiao, *Int. J. Hydrogen Energ.* (2012) j.ij hydene.2012.09. 074.

140. C. Qu, H. Zhang, F. Zhang, B. Liu, *J. Mater. Chem.* 22 (2012) 8203.

141. B. Qiu, B. Lin, L. Qiu, F. Yan, *J. Mater. Chem.* 22 (2012) 1040.

142. C. Arges, J. Parrondo, G. Johnson, A. Nadhan, V. Ramani, *J. Mater. Chem.* 22 (2012) 3733.

143. D. Henkensmeier, H. Cho, H. Kim, C. Kirchner, J. Leppin, A. Dyck, J. Jang, E. Cho, S. Nam, T. Lim, *Polym. Degrad. Stabil.* 97 (2012) 264.

144. O. Deavin, S. Murphy, A. Ong, S. Poynton, R. Zeng, H. Herman, J. Varcoe, *Energy Environ. Sci.* 5 (2012) 8584.

145. E. Yu, X. Wang, U. Krewer, L. Li, K. Scott, *Energy Environ. Sci.* 5 (2012) 5668.

146. J. Ran, L. Wu, X. Lin, L. Jiang, T. Xu, *RSC Advances*, 2 (2012) 4250.

147. Y. Zha, M. Disabb-Miller, Z. Johnson, M. Hickner, G. Tew, *J. Am. Chem. Soc.* 134 (2012) 4493.

148. Y. Leng, G. Chen, A. Mendoza, T. Tighe, M. Hickner, C. Wang, *J. Am. Chem. Soc.* 134 (2012) 9054.

149. B. Lin, L. Qiu, B. Qiu, Y. Peng, F. Yan, *Macromolecules* 44 (2011) 9642.

150. N. Li, Q. Zhang, C. Wang, Y. Lee, M. Guiver, *Macromolecules* 45 (2012) 2411.

151. B. Ko, J. Sohn, J. Shin, Polymer 53 (2012) 4652.

152. X. Li, Y. Yu, Q. Liu, Y. Meng, *ACS Appl. Mater. Interfaces*, 4 (2012) 3627.

153. R. Souzy, B. ameduri, *Prog. Polym. Sci.* 30 (2005) 644.

154. T. Danks, R. Slade, J. Varcoe, *J. Mater. Chem.* 13 (2003) 712.

155. J. Varcoe, R. Slade, *Electrochem. Commun*. 8 (2006) 839.

156. R. Slade, J. Varcoe, *Solid State Ionics* 176 (2005) 585.

157. H. Herman, R. Slade, *J. Membr. Sci.* 218 (2003) 147.

158. Y. Kim, D. Lee, K. Lee, J. Kim, *Eur. Polym.* J. 44 (2008) 932.

159. E. Yu, U. Krewer, K. Scott, *Energies*, 3 (2010) 1499.

160.K. Matsuoka, Y. Iriyama, T. Abe, M. Matsuoka, Z. Ogumi, *J. Power Sources*, 150 (2005)27.

161. G. Merle, M. Wessling, K. Nijmeijer, *J. Membr. Sci*. 377 (2011) 1.

162. K. Fukuta, talk presentation, Electrolyte Materials for AMFCs and AMFC Performance, AMFC Workshop, DC, May 2011.

163. R. Schwesinger, R. Link, P. Wenzl, S. Kossek, M. Keller, *Chem. Eur. J.*, 12 (2006) 429.

164. M. Tomoi, K. Yamaguchi, R. Ando, Y. Kantake, Y. Aosaki, H. Kubota, *J. Appl. Polym. Sci*, 64 (1997) 1161.

165. M. Disaman, L. Alvarado, D. Larner, P. Wang, B. Garg and K. Littau, *Energy Environ. Sci.* 4 (2011) 1319.

166. X. Wang, M. Li, B. Golding, M. Sadeghi, Y. Cao, E. Yu, K. Scott, *Int. J. Hydrogen. Energ.*, 36 (2011) 10022.

167. J. O'Dea, S. Buratto, *J. Phys. Chem*, B 115(2011) 1014.

168. N. Takimoto, L. Wu, A. Ohira, Y. Takeoka, M. Rikukawa, *Polym.*, 50(2009) 534.

169. N. Takimoto, A. Ohira, Y. Takeoka, M. Rikukawa, *Chem. Lett.* 37(2008) 164.

170. H. Hertz, J. Reine, *Angew. Math.* 92 (1982) 156.

171. E. Franceschini, H. Corti, *J. Power Sources* 188(2009) 379.